Front. Phys. 10, 108101 (2015)
DOI 10.1007/s11467-014-0422-4

REVIEW ARTICLE

Self-assembly of InAs quantum dots on GaAs(001) by molecular beam epitaxy

Ju Wu[†], **Peng Jin**

Key Laboratory of Semiconductor Materials Science and Beijing Key Laboratory of Low-dimensional Semiconductor Materials and Devices, Institute of Semiconductors, Chinese Academy of Sciences, Beijing 100083, China

Corresponding author. E-mail: [†]*wuju@semi.ac.cn*

Received August 6, 2013; accepted March 12, 2014

Frontiers of Physics

Currently, the nature of self-assembly of three-dimensional epitaxial islands or quantum dots (QDs) in a lattice-mismatched heteroepitaxial growth system, such as InAs/GaAs(001) and Ge/Si(001) as fabricated by molecular beam epitaxy (MBE), is still puzzling. The purpose of this article is to discuss how the self-assembly of InAs QDs in MBE InAs/GaAs(001) should be properly understood in atomic scale. First, the conventional kinetic theories that have traditionally been used to interpret QD self-assembly in heteroepitaxial growth with a significant lattice mismatch are reviewed briefly by examining the literature of the past two decades. Second, based on their own experimental data, the authors point out that InAs QD self-assembly can proceed in distinctly different kinetic ways depending on the growth conditions and so cannot be framed within a universal kinetic theory, and, furthermore, that the process may be transient, or the time required for a QD to grow to maturity may be significantly short, which is obviously inconsistent with conventional kinetic theories. Third, the authors point out that, in all of these conventional theories, two well-established experimental observations have been overlooked: i) A large number of "floating" indium atoms are present on the growing surface in MBE InAs/GaAs(001); ii) an elastically strained InAs film on the GaAs(001) substrate should be mechanically unstable. These two well-established experimental facts may be highly relevant and should be taken into account in interpreting InAs QD formation. Finally, the authors speculate that the formation of an InAs QD is more likely to be a collective event involving a large number of both indium and arsenic atoms simultaneously or, alternatively, a morphological/structural transformation in which a single atomic InAs sheet is transformed into a three-dimensional InAs island, accompanied by the rehybridization from the sp^2-bonded to sp^3-bonded atomic configuration of both indium and arsenic elements in the heteroepitaxial growth system.

Keywords molecular beam epitaxy, InAs quantum dots

PACS numbers 81.07.-b, 81.05.Ea, 81.07.Ta

Contents

1 Introduction 2
2 General description 3
2.1 MBE growth of InAs QDs on GaAs(001) 3
2.2 Formation of InAs QDs is difficult to understand 4
3 Theoretical models of the QD formation process in heteroepitaxial growth 6
3.1 Surface morphological relaxation of an elastically strained film on a substrate 6
3.1.1 Asaro–Tiller–Grinfeld–Srolovitz instability 6
3.1.2 First-order phase transformation 7
3.2 Adatom aggregation 8
3.2.1 Physical scenario in the submonolayer regime of homoepitaxial growth 8
3.2.2 Mean-field rate equations (MFREs) 9
3.2.3 Scaling invariance ansatz 10
3.2.4 Fitting experimental data on the density and size distribution of InAs QDs with the MFREs and the scaling

© The Author(s) 2015. This article is published with open access at link.springer.com

invariance ansatz 12
3.2.5 MFREs tailored to QD formation in heteroepitaxial growth 12
3.3 Reaction kinetic model 13
3.4 Kinetic Monte Carlo simulation 14
3.5 Building a QD 16
3.5.1 Surface morphological relaxation 16
3.5.2 Uphill mass transfer and 3D epitaxial island growth 17
3.5.2.1 Kinetic roughening 17
3.5.2.2 Formation of growth mounds and huts in homoepitaxial growth 18
3.5.2.3 Super-epitaxial growth 19
3.5.3 Nanocrystal growth 19
3.6 Timescale and nature of QD formation 20
3.6.1 Surface relaxation processes 20
3.6.2 Adatom aggregation 21
3.6.3 Structural phase transformation 22
3.6.4 Experimental observations of the timescale of InAs QD growth 23
3.7 Wetting layer (WL) 23
3.8 Size limitation on the growth of InAs QDs 24
4 Experimental observations of MBE InAs/GaAs(001) 25
4.1 A large variety of experimental data in the literature on the formation of InAs QDs 25
4.2 Progressive epitaxial growth mode of InAs QDs 27
4.3 Instantaneous epitaxial growth mode of InAs QDs 29
5 "Floating" indium on the growth surface and mechanical instability of an epitaxially strained InAs film on the GaAs(001) substrate 31
5.1 Floating indium on the growth surface 31
5.1.1 Indium floating 31
5.1.2 Structures that may result from floating indium 32
5.2 Mechanical instability of a coherently strained InAs film on the GaAs(001) substrate 33
6 Structural transformation model of InAs QD formation 34
6.1 Formation of InAs WL on GaAs(001) 35
6.2 Structural transformation from a single InAs layer to an InAs QD on the growth surface 36
6.2.1 Structural transformation from a 2D InAs atomic sheet to a 3D epitaxial InAs island on the growth surface 36
6.2.2 Structural transformation from an epitaxial thin film to a 3D growth morphology in materials isoelectronics to InAs 37
6.3 Self-limitation mechanisms resulting in the uniform size of InAs QDs 38
6.3.1 Critical size for the structural transformation on the nanoscale 38
6.3.2 Mechanical mechanism 39
Acknowledgments 39
References and notes 39

1 Introduction

Since the first half of the 20th century, the epitaxial growth technique has been developed to fabricate atomically flat thin films on a solid substrate (see, for example, Ref. [1]); it involves simply depositing atoms or molecules from ballistic particle beams, the vapor phase, or the liquid phase on a solid surface. With significant developments in both the ultrahigh vacuum technique and surface science during the last decades, the thickness of an epitaxial film that is smooth at the atomic scale can now be precisely controlled down to the submonolayer regime in modern epitaxial growth techniques such as molecular beam epitaxy (MBE). In addition, in the last two decades, an increasing number of three-dimensional (3D) nanostructures [e.g., clusters, wires, and quantum dots (QDs)] have been experimentally observed to self-assemble themselves when a few atomic layers of a metal or semiconductor are epitaxially deposited onto a planar substrate. However, much of both the energetics and kinetics of the mechanism underlying the spontaneous formation or self-assembly of these surface nanostructures remains a puzzle. Here, the word *self-assembly* implies that the formation of these self-assembled nanostructures cannot be controlled by just adjusting the growth parameters, such as the substrate temperature T and epitaxial flux rate F.

The self-assembly of QDs in heteroepitaxial growth is a very fundamental and important phenomenon in many basic research fields, such as nanoscience, solid-state physics, surface science, growth phenomena, and two-dimensional (2D) physical systems. In addition, owing to the quantum confinement effect in them, these 3D nanostructures have great potential in nanotechnology for possible use in next-generation nanodevices in technological fields such as catalysis, optoelectronics, and data storage. For example, InAs QDs fabricated on the GaAs(001) substrate by MBE may be used in mid- and far-infrared detectors (see, for example, Refs. [2, 3]), terahertz emitters [4, 5], vertical-external-cavity surface-emitting lasers (see review article, Ref. [6]), and single-photon emitters (see review article, Ref. [7]). These QD-based nanodevices are expected to outperform those based on tradi-

tional materials, such as semiconductor quantum wells. However, at present, the structural parameters of epitaxial QDs (e.g., their size, shape, and chemical composition) cannot be properly controlled during epitaxial growth, and these structural parameters are expected to significantly influence the QDs' physical properties and, in consequence, greatly affect the nanodevice performance. To realize greater control over the epitaxial growth of self-assembled QDs to improve the device performance, an adequate theoretical understanding of the process or underlying physical mechanism is necessary.

InAs QDs in MBE InAs/GaAs(001) may serve as a model system or paradigm for self-assembled semiconductor QDs. In the last two decades, a number of kinetic theories have been proposed, and a huge amount of experimental data have been accumulated on the InAs QD formation process in the literature. However, the mechanism underlying the phenomenon remains a hard challenge. The purpose of this article is to discuss *how an InAs QD self-assembles* itself during MBE heteroepitaxial growth of InAs/GaAs. This article contains six sections. Section 2 presents a general description of the phenomenon. Section 3 briefly reviews the current conventional kinetic theories for heteroepitaxial growth of QDs in the literature. Section 4 summarizes the experimental observations made by the authors. Section 5 briefly reviews and discusses two well-established experimental facts in the literature: the presence of a relatively large amount of "floating" indium on the growth surface during the epitaxial growth of InAs/GaAs(001), and the mechanical instability of an elastically strained InAs film on the GaAs(001) substrate. In addition, it is pointed out that these two well-known phenomena may be highly relevant to the self-assembly of InAs QDs and should be properly taken into account in the interpretation of InAs QD formation. Finally, in Section 6, by considering these experimental facts, which should be relevant to the topic but have been overlooked in the conventional kinetic theories, the authors speculate that InAs QD formation should be a collective event involving a large number of atoms simultaneously on the growth surface or, alternatively, a morphological/structural phase transformation in which a single atomic InAs sheet is transformed into a 3D compact InAs island or a QD, accompanied by simultaneous rehybridization from the sp^2 to the sp^3 atomic configuration in both the indium and arsenic elements in the system.

2 General description

In this section, a general description of InAs QD formation in the MBE InAs/GaAs(001) system is presented.

2.1 MBE growth of InAs QDs on GaAs(001)

More than two decades ago, the spontaneous formation of dislocation-free epitaxial 3D islands at the nanoscale was experimentally observed in the lattice-mismatched heteroepitaxial growth of Ge/Si(001) [8, 9] and InAs/GaAs(001) [10–13]. These epitaxial 3D islands, after being capped by a Si or GaAs capping layer, effectively confine excitations, electrons, or holes, and have since been called QDs. The epitaxial growth of these QDs was traditionally classified as the Stranski–Krastonov (SK) growth mode, in which the formation of a wetting layer (WL) of a few atomic layers in thickness is followed by the epitaxial growth of 3D islands. The SK growth and the classification of the epitaxial growth modes are currently explained in terms of energetics and thermodynamics. However, up to the date, the atomistic details of QD growth or the physical mechanism underlying the dynamical growth process remains a puzzle.

In the epitaxial growth of InAs QDs on the GaAs(001) substrate, the substrate temperature T is generally kept within 480–530°C, and the As pressures P_{As} are kept within (2–8) $\times 10^{-6}$ Torr. Before indium deposition, the clean GaAs(001) surface exhibits $c(4\times4)$ or (2×4) reconstruction depending on the substrate temperature and arsenic flux, as revealed by the *in-situ* streaky reflection of high-energy electron diffraction (RHEED) pattern. With an indium deposition flux F of 0.01–1 monolayer per second (ML/s), a flat or 2D InAs WL of about 1.5 ML forms first. With additional InAs deposition, an ensemble of QDs develops progressively on the surface of the InAs WL [10–13]. Leonard *et al.* [13] performed an MBE growth experiment on InAs/GaAs(001) under the conditions of $T = 530$°C, $P_{\mathrm{As}} = 7\times10^{-6}$ Torr, and $F = 0.01$ ML/s. They found that InAs QDs begin to appear on the WL around a critical InAs coverage θ_c of ∼1.5 ML, and the QDs' areal density N_{dot} increased sharply from zero to more than $1\times10^{10}/\mathrm{cm}^2$ with increasing InAs coverage θ. The experimental data can be fitted well to the curve represented by the power law $N_{\mathrm{dot}} = N_0(\theta-\theta_c)^{1.76}$, where N_0 is a constant independent of θ. In addition, the InAs QDs grew in size at a remarkably rapid rate, and with an additional coverage of $\Delta\theta \sim 0.01$, their average height increased by about 9 nm or 30 monolayers, which is 1000 times more than the increment in θ. At 1.6 ML, the QDs' average base diameter as measured by atomic force microscopy (AFM) was about 30 nm, and the average height was about 9 nm. Hereafter, this rapid growth behavior of InAs QDs is called "super-epitaxial growth" and will be further dis-

cussed in Section 3.5.2.3. The QDs' size distribution was significantly narrow, and the standard deviations in the histograms of the island height and base diameter were 7% and 10%, respectively. This uniformity in QD size was rather amazing, and some unknown physical mechanism is expected to underlie this self-limited growth or self-organization phenomenon. More amazingly, both the average QD diameter and height varied in a rather odd way: As θ increased further above 1.6 ML, both the average diameter and average height decreased instead of increasing. At θ = 1.85 ML, the average diameter decreased from 30 nm to less than 20 nm, and the average height decreased from 9 nm to less than 8 nm. Above a coverage of θ = 1.85 ML and a QD density $N_{\mathrm{dot}} = 4 \times 10^{10}/\mathrm{cm}^2$, these dislocation-free QDs were converted into dislocated 3D islands.

Since these pioneering experimental investigations of epitaxial growth of InAs QDs on the GaAs(001) substrate by the MBE method, a huge amount of experimental data have been accumulated in the literature; these investigations demonstrated that the evolution of an ensemble of InAs QDs with increasing InAs coverage depends sensitively on the experimental conditions in MBE growth. For example, Zorozaryov *et al.* [14] performed their MBE growth experiment on InAs/GaAs(001) at T = 500°C and F = 0.2 ML/s, and they observed that the QD density increases linearly with increasing InAs coverage, in contrast to the power law obtained by Leonard *et al.* [13]. A linear increase in the QD density was also experimentally observed by Wu *et al.* [15] in their InAs QD sample fabricated by the so-called mobility-enhanced epitaxy method. In addition, Wu *et al.* [16, 17] found that their experimental data on the QD density can be fitted well by the exponential expression $N_{\mathrm{dot}} = N_0 \exp[k(\theta - \theta_c)]$ in a given range of θ, where their MBE growth conditions were T = 520°C and F = 1.0 ML/s.

2.2 Formation of InAs QDs is difficult to understand

To further describe the nature of the problems relevant to the QD formation process, we divide all the scientific problems that a researcher may encounter in nature or in the laboratory into two types: "easy" and "complex." At least in principle, it is relatively easy to find a universal law or build a generic model for a large number of phenomena that are apparently distinct from each other in some details but are the same in some fundamental characteristics, such as symmetry and dimensionality. The conventional scientific method for theoretically understanding these distinct phenomena with a fundamentally important characteristic in common is to construct a simple model by concentrating on only a small number of presumably important factors and disregarding other details, which are thought to be trifles. In doing so, the researcher usually manages to make the model as simple as possible so that the fundamental concepts and sophisticated mathematical technical theories well-established in elementary textbooks can be used or applied directly to the problem. Undoubtedly, such a strategy is usually successful for many problems in physics as well as materials science (e.g., to describe the thermodynamic equilibrium state of a rare gas contained in a sealed container of a certain volume at room temperature, to analytically describe the spinodal decomposition processes occurring in a binary solid alloy, to find a power-law function for an equilibrium or self-organized critical phenomenon, or to numerically simulate homoepitaxial growth of a simple metal film on a solid surface at a relatively low substrate temperature). Here, problems of this type are defined as "easy" or "simple." In contrast, it is usually much more difficult to theoretically describe a realistic process or phenomenon in a practical physical system, which may proceed in several distinct stages successively, involves a large number of constituents or particles interacting with each other in some delicate or subtle ways, and is highly sensitive to or susceptible to a variety of external or environmental factors. Frequently, in dealing with problems of the latter sort, the task should be to understand their particularities, specificities, or exclusive characteristics, instead of abstracting a law universal to many others. In contrast to the easy problems defined above, these latter problems are called "difficult" or "complex" hereafter. These complex problems, which are encountered in a variety of scientific and technical fields, seem to be very perplexing and usually remain a hard challenge for many decades.

A theoretical understanding of the physical nature of InAs QD formation in MBE InAs/GaAs(001) should undoubtedly be a paradigm for the complex problems. The difficulties in interpreting the phenomenon are both experimental and theoretical. The experimental difficulties arise mainly from two facts: i) To date, no microscopy technique has been available for direct *in situ* observation of the InAs QD growth process; as Grosse and Gyure [18] commented, the experimental atomistic microscopy techniques available to observe epitaxial growth, such as scanning tunneling microscopy (STM) and AFM, are incompatible with the InAs MBE process on the GaAs(001) substrate. To use these techniques to measure the growth morphology in MBE InAs/GaAs(001), the sample has to be transferred to the STM characterization chamber, and its temperature must be reduced. The measured surface morphology is therefore

not necessarily identical to the real growth surface. ii) In a subtle way, the outcome of epitaxial growth of MBE InAs/GaAs(001) is highly sensitive to the experimental conditions such as the growth temperature and deposition rate. For example, Leonard *et al.* [13] found that at a substrate temperature $T = 530°\mathrm{C}$ and an indium flux $F = 0.01$ ML/s under sufficiently arsenic-rich conditions, even in the earliest InAs QD growth stage after the critical InAs thickness for the transition from the 2D growth mode to the 3D growth mode ($\theta_{\mathrm{InAs}} \sim 1.6$ ML) was reached, both the average height and base diameter of InAs QDs stopped increasing with increasing θ_{InAs}, as observed in an AFM measurement. In contrast, on the basis of their experimental observations under growth conditions of $T = 465°\mathrm{C}$ and $F = 0.0088$ ML/s, Takahasi *et al.* [19] concluded from X-ray diffraction (XRD) measurements that the average InAs QD height increases continuously with increasing θ_{InAs} up to 2.7 ML. Theoretically, the formation of InAs QDs seems to be a highly nonlinear process under the conditions far from equilibrium; it is notoriously difficult to obtain an analytical formula and solution of the problem. Furthermore, instead of one or a small number of well-defined dynamical variables, a myriad of dynamical issues or questions must be addressed to understand InAs QD formation, e.g., the physical origin of the InAs WL, the nucleation and nanocrystal growth processes of an individual InAs QD, the self-limited growth or self-organization mechanism, and the dynamic evolution of the size distribution of InAs QDs in the ensemble. Moreover, each of these questions seems to have its own subquestions. For example, for the nucleation and growth of an individual QD as a nanocrystallite on the growth surface, one has to consider how uphill mass transport occurs for the QD to grow in the vertical direction, how nucleation of a new atomic layer occurs on nanocrystalline facets, the kinetics of adatom attachment to the step edges, and so on.

The experimental data currently available in the literature for InAs QD formation are puzzling as well as divergent, rather than tending toward some consensus, and a variety of difficulties are encountered in theoretically handling the formation of InAs QDs. However, to the eye of both the theoretical and experimental communities working on the topic, the physical nature of InAs QD formation seems to be rather plain and “easy” and can be understood in terms of some universal law or a generic model describing the motion of individual atoms on the growth surface (see, for example, Refs. [20–24]). From this viewpoint, the formation of QDs should be an ordinary epitaxial growth process as implemented via individual atomistic events (deposition, adatom diffusion and attachment to step edges) on the growth surface. The process of QD formation is currently modeled as a well-known physical scenario, e.g., aggregation of randomly diffusing adatoms on the growing surface, or nanocrystal growth via the classical step-flow growth mode, or a first-order phase transformation from a uniformly flat strained InAs film into a rough surface, or a surface morphological relaxation process initially induced by the well-known Asaro–Tiller–Grinfeld instability. Nevertheless, there seems to be no sound reason to regard such a complicated problem as the formation of InAs QDs in a heteroepitaxial growth system as one of these well-known simple physical processes *a priori*. The popularity of these conventional theories and simple physical scenarios among the researchers concerned with the formation of InAs QDs might be due simply to the fact that these theories and scenarios are well-known or well-established in the literature and textbooks, and the dynamics of the QD formation process can be expressed in terms of them as a set of linear or nonlinear partial differential equations or simulated numerically as a series of random atomistic events that can be approximated as a Markovian chain, which is an ideal task for kinetic Monte Carlo (KMC) computer simulations. In addition, by using these conventional concepts and theoretical frameworks, all the difficulties that are encountered could be reduced to the mathematical complexities of the formulation and solution [25] and the limited computational power of computers [26, 27].

Note that in the all of the conventional theoretical models currently used to understand the InAs QD formation process, three significant, well-established experimental facts have been omitted: i) A relatively large amount of “floating” indium exists on the growth surface at the moment when the InAs QDs are self-assembling; ii) an epitaxially or coherently strained InAs film on the GaAs(001) substrate should be mechanically unstable due to the lattice compression caused by the lattice mismatch between the film and the substrate, which is about 7%; iii) the formation process of an InAs QD is transient or remarkably rapid, which is obviously inconsistent with the conventional kinetic theories based on single atomic events on solid surfaces. It should be emphasized that these three experimental facts may be significant and key to the formation process of InAs QDs during MBE growth; however, if they are incorporated into a theoretical understanding of the phenomenon, the traditional theoretical framework suitable for ordinary epitaxial growth of an epitaxial film should obviously be inapplicable to the formation of InAs QDs. In the conventional theoretical interpretation of QD formation, neglecting these three phenomena that are highly relevant to the issue may be, on deliberation, seen as a wise

strategy for dealing with "simple" phenomena, as these three experimental observations cannot be embraced by the conventional kinetic theories, or taking them into account would make the task too complex for conventional theoretical or numerical methods. Another reason for this neglect may be unconscious. It is well known that the literature contains a huge amount of data on apparently separate topics such as QD formation, many complex phenomena in epitaxial growth occurring in apparently different materials systems, the physical behavior of a 2D system supported by a solid surface, the behavior of a crystalline solid under a relatively high pressure, the relationship between the size and the atomic configuration of a nanocrystallite, and so on. These data in different fields may be highly relevant and shed light on each other; however, it seems to be inevitable to be unknown each other, sometimes among different research communities, owing to the diversity of modern scientific research. The situation of disregarding other data in presenting one's own experimental results can occur even when the investigators are working on the same topic. For example, in the homoepitaxial growth on the GaAs(001) substrate, as pointed out by Tiedje and Ballestad [28], Cho [29] had experimentally demonstrated that the homoepitaxial growth of GaAs(001) with a planar growing surface is highly stable in the early 1970s, while Johnson *et al.* [30–32] interpreted their experimental results on the GaAs(001) homoepitaxial growth in terms of the growth instability due to the kinetic roughening effect in the 1990s. Cho's result is currently regarded as classical, whereas the work of Johnson et al. has frequently been cited positively in the GaAs(001) homoepitaxy community to date. In addition, Martini *et al.* [33, 34] experimentally confirmed that the strong decay of the oscillation in the RHEED intensity during growth of an InGaAs film on the GaAs(001) substrate arises from floating indium resulting from indium surface segregation; alternatively, many other research groups have persistently interpreted the phenomenon in the literature as progressive roughening of the growing surface due to the lattice misfit.

3 Theoretical models of the QD formation process in heteroepitaxial growth

In the literature, as mentioned above, it has long been a convention to theoretically interpret QD formation in lattice-mismatched heteroepitaxial growth in terms of individual atomistic events on the growth surface. These events include deposition of atoms or molecules on the surface from a mass flux, surface diffusion of adatoms, and their attachment to step edges. This section briefly reviews these conventional theoretical descriptions, which are classified as three different surface processes or phenomena: i) the morphological instability of an elastically strained flat film on the substrate, ii) adatom aggregation, and iii) nanocrystal growth. In addition, the timescale consistent with these theoretical processes, the physical nature of the WL in heteroepitaxial growth, and size selection in QD growth are described.

3.1 Surface morphological relaxation of an elastically strained film on a substrate

It is well known that if the surface or interface morphology of a thin epitaxial film on a substrate has been driven out of thermodynamic equilibrium or into a metastable state by an external force or an agent such as surface tension or elastic strain, it will spontaneously relax toward its equilibrium state through a quasi-spinodal process or a first-order phase transformation, and the mechanism for mass transfer is drift surface diffusion driven by the capillary effect and/or a gradient in the surface stress field. In the literature, QD formation has frequently been modeled either as a surface relaxation process driven by the Asaro–Tiller–Grinfeld–Srolovitz (ATGS) instability of an elastically strained film or as the kinetics of the first-order phase transformation from an atomically flat elastically strained film to an ensemble of 3D islands on the growth surface. The two types of kinetic theory are briefly described in Sections 3.1.1 and 3.1.2, respectively.

3.1.1 Asaro–Tiller–Grinfeld–Srolovitz instability

According to the ATGS instability theory [35–38], the planar surface of an elastically strained solid is unstable to morphological perturbations at certain wavelengths as specified by the stress level and surface tension. Similarly, a flat elastically strained thin film in mismatched heteroepitaxial growth is also unstable because of the same effect. By taking account of the wetting effect of the film, it can be theoretically demonstrated that an elastically strained atomically flat film that is unstable as a result of the ATGS instability should relax, reaching a thermally stable state with a regular array of 3D epitaxial islands, which are identified as self-assembled QDs in the literature [39–58].

The QD formation theory in terms of the ATGS instability can be described in a way similar to that formulated by Herring [59] and Mullins [60] for surface relaxation driven by the capillary effect. If the unstable planar film is slightly perturbed and becomes inhomogeneous in both the surface morphology and surface stress, the surface begins to roughen according to the dynamic

law

$$\frac{\partial h}{\partial t} = D(1 + |\nabla_s h|^2)^{1/2}\nabla_s^2\mu, \tag{3.1.1.1}$$

where h is the surface height, t is the time, ∇_s^2 is the surface Laplacian operator, and D is a parameter determined by the surface adatom diffusivity, adatom density, adatom volume, and absolute surface temperature T. The surface chemical potential μ of an adatom or atom on the surface in Eq. (3.1.1.1) can be written in the simplest form as [38]

$$\mu = \mu_0 + \omega - \kappa\gamma, \tag{3.1.1.2}$$

where μ_0 is the reference chemical potential (the reference state is the planar geometry of an epitaxially strained film), $\omega = \sigma_{ij}\varepsilon_{ij}/2$ is the density of the strain energy (σ_{ij} is the stress tensor, and ε_{ij} is the strain tensor), and κ and γ are the mean surface curvature and surface free energy, respectively. However, with the surface chemical potential defined in Eq. (3.1.1.2), Ostwald ripening will occur among 3D epitaxial islands induced to form by the ATGS instability. Therefore, to theoretically establish a thermally stable or metastable ensemble of regular QDs via Eqs. (3.1.1.1) and (3.1.1.2), other additional ingredients and contributions to the chemical potential μ have to be considered, such as the anisotropy in the surface energy $\gamma(\theta)$, and the wetting interaction between the film and the substrate. If these two additional terms are considered, the chemical potential should have the form [58]

$$\mu(\boldsymbol{r}) = \mu_0 + \left[\omega - (g(h) + \gamma(\theta))\kappa + \frac{\partial g}{\partial z}n_z + \nabla\cdot\frac{\partial\gamma}{\partial\boldsymbol{n}}\right], \tag{3.1.1.3}$$

where $g(h)$ is the wetting interaction between the thin film and the substrate, $\boldsymbol{n}$ is the surface orientation, and $\gamma(\theta)$ is the orientation-dependent surface tension. By using the chemical potential $\mu(\boldsymbol{r})$ expressed in Eq. (3.1.1.3), the time evolution equation (3.1.1.1) can be solved numerically to produce a regular array of 3D islands stable against Ostwald ripening out of the originally planar epitaxially strained film.

3.1.2 First-order phase transformation

In general, dynamically evolving phenomena in materials science or condensed matter physics are hard to investigate theoretically, as these problems are very difficult to model using simple physical arguments and to analytically formulate in the language of mathematics. One of several exceptional cases is the classical nucleation and growth theory (CNGT) for the kinetics of the first-order phase transformation, which occurs in a large variety of material systems, for example, condensation from vapor; boiling of a liquid; and crystallization, melting, and formation of a new phase in binary solid or liquid solutions. Since the 1920s–1930s, a systematic kinetic theory of classical nucleation and growth has been developed on the basis of thermodynamics theory [61]. To date, the CNGT is most frequently employed in understanding kinetic phenomena in materials science and condensed matter physics (see, for example, Ref. [62]).

In the CNGT, the kinetics of a first-order phase transformation occurring in a system is divided into three successive stages: i) nucleation, ii) steady-state growth, and iii) coarsening or Ostwald ripening. In the first stage, a nucleation event is a spatial local atomic event in which a new stable phase forms locally from the pristine metastable phase through thermal fluctuations. Many of these nuclei that form may be converted back into the thermodynamic state of the original phase. However, if a nucleus of the new phase as formed via the nucleation event is larger than a critical size, it will become stable against this conversion and grow into a larger size; the driving force for a successful nucleation event and its subsequent growth is the difference in the Gibbs free energy between the metastable and stable phases. One of the central issues for the theoretical description of nucleation events is the critical nucleus of the new phase, which defines the free energy barrier that has to be surmounted by thermal fluctuation for the nucleation event to occur. The most important dynamical variable in the CNGT for the nucleation regime is the number of stable-phase nuclei that form per unit volume and per unit time, or the nucleation rate of the stable phase, which is given by the Zeldovich equation [63, 64]. In the second stage, steady-state growth, the predominant kinetic event is the growth of the new-phase nuclei into clusters of various sizes by local consumption of the surrounding material in the old metastable phase. The dynamical behavior of this regime is generally described in terms of $n(s,t)$, the cluster size distribution as a function of time t and the number of atoms s contained in a cluster. In general, the time evolution of $n(s,t)$ is controlled by the discrete Becker–Doring equations [65] or continuum Fokker–Planck equation [66]. In the third stage, the coarsening stage, all the material in the old phase has been consumed by the formation of the new phase, and the system now consists entirely of an ensemble of stable-state clusters of various sizes. Now, the system evolves in time, driven by the capillary effect via Ostwald ripening. According to the Gibbs–Thomson relation, $\Delta\mu \propto 2\gamma/r$ (where $\Delta\mu$ is the increment in chemical potential due to surface curvature

of a cluster, γ is the surface tension of the cluster material, and r is its curvature radius), a smaller cluster has a larger chemical potential than a larger cluster. Driven by this difference in μ, atoms will detach progressively from smaller clusters, migrate thermally via surface diffusion, and become attached to clusters larger than a characteristic size of the cluster ensemble, as characterized by a characteristic chemical potential $\bar{\mu}$. The dynamics of the Ostwald ripening process can be described by the classical theory by Lifshitz and Slyozov [67] and Wagner [68] (LSW theory). Ostwald ripening or coarsening is a significantly slower process than the two earlier stages, nucleation and steady-state growth, as it is controlled by the $\bar{\mu}$ value of the system and proceeds via surface diffusion driven by the capillary effect, which is much weaker.

Osipov *et al.* [69, 70] and Dubrovskii *et al.* [71–73] systematically applied the CNGT, as outlined above, to explain QD formation in lattice-mismatched heteroepitaxy. These authors assumed that an elastically strained epitaxial flat film forms first as the metastable phase with a thickness h significantly exceeding a critical value $h_{\rm eq}$, below which the film is thermodynamically stable; the corresponding "supersaturation" or superstress is defined in terms of $\zeta \equiv h/h_{eq} - 1$. QD formation, as a first-order phase transformation, starts from the metastable strained film, and the new stable phase (the QDs) nucleates by thermal fluctuations. The nucleation event of a QD nucleus is a local competition between the strain energy and surface energy of the epitaxially strained film [74], in which a stable 3D island having a size s larger than the critical nucleus s_c is formed. For example, with the application of materials parameters suitable for MBE InAs/GaAs(001) and according to the Zeldovich equation, the nucleation rate of InAs QDs can be expressed as [75]

$$J_\theta = 2 \times 10^{19} \exp[-G(s_c)/(kT)], \tag{3.1.2.1}$$

where $G(s_c)$ represents the energy barrier that has to be overcome for an InAs QD to form via the nucleation event. In the steady growth regime, QD nuclei grow deterministically according to the Becker–Doring equations or the Fokker–Planck equation, as mentioned above. Finally, these InAs QDs become coarsened in the asymptotic time limit.

In the above two kinetic theories for QD formation, on the basis of the physical concepts associated with the ATGS surface morphology instability and the first-order phase transformation, it has to be assumed that an unstable or metastable elastically strained flat thin film must form before QD formation. This situation can occur only when the latter process is significantly slower than the incident flux during heteroepitaxial growth. If this were the situation, QD formation would apparently be similar or equivalent to the de-wetting of an unstable solid metal [76] or semiconductor film [77, 78] from a solid surface to form nanocrystallites, which is currently under intensive investigation in materials science, microelectronics, and nanotechnology; see, for example, Refs. [79, 80].

3.2 Adatom aggregation

In the literature, there are two distinct theories for nucleation and growth phenomena occurring in both nature and a laboratory or an industrial process. Section 3.1.2 briefly described one of them as the CNGT, which is based on the macroscopic concepts of thermodynamics. In contrast, the other NGT is based entirely on microscopic kinetic concepts such as random particle diffusion, collision, capture, and emission by a cluster of particles. To distinguish the two different NGTs, the latter theory based entirely on the kinetic concepts of particle (atom or molecule) motion is usually termed the standard nucleation and growth theory in the literature. Hereafter, for a homoepitaxial growth in the submonolayer regime, the theoretical process described by the standard NGT is called adatom aggregation on the substrate surface, where an adatom is defined as an isolated atom chemically adsorbed on the growth surface in epitaxial growth. As an alternative to the theories involving a relaxation process, during which an unstable or a metastable material system enters a thermodynamically stable state, as described in the last two subsections, the QD formation process is more often modeled or theoretically described in the literature as adatom aggregation driven by epitaxial deposition. This section describes the adatom aggregation theory of the QD formation process during heteroepitaxial growth.

3.2.1 Physical scenario in the submonolayer regime of homoepitaxial growth

The formation of QDs in lattice-mismatched heteroepitaxial growth is frequently interpreted as an adatom aggregation process on a growth surface [81–92], which is very similar to the well-known physical scenario for epitaxial growth of 2D islands in the submonolayer stage in homoepitaxial growth. In the conventional description of homoepitaxial growth in the submonolayer regime, the growth process of 2D epitaxial islands is divided into three distinct regimes: nucleation, steady growth, and coalescence; this is very similar to the kinetic theory of first-order phase transformations. It is generally as-

sumed that atoms from vapor, once they land on the growing surface, immediately become adatoms and then diffuse randomly from site to site. These adatoms interact with each other only via the short-range chemical interaction. Upon meeting each other on collision, these adatoms aggregate into 2D islands and settle down the surface. These adatom clusters or 2D epitaxial islands grow further by capturing more adatoms. In the very early stage, because few 2D islands exist, the probability that an adatom will find an adatom counterpart is much larger than that of being captured by a 2D island nucleus; thus, nucleation events should be much more frequent than growth events in which an adatom is captured by a pre-existing 2D island. This early stage is called the nucleation stage. As deposition continues, more and more 2D islands nucleate; finally, their number density becomes so large that almost all adatoms landing on the surface are captured by growing 2D islands, and nucleation events happen very seldom. This growth regime is called the steady-state growth stage. As these 2D epitaxial islands grow further, they come into contact with each other and coalesce into much larger ones; this regime is called the coalescence stage in the submonolayer range of epitaxial growth.

In the submonolayer regime in homoepitaxial growth, the most interesting and extensively investigated issues are the total number density of 2D islands $n_{\mathrm{tot}}(F,T)$ as a function of the flux F and temperature T, and the temporal evolution of their size distribution with increasing coverage in the steady growth regime. With some simplifying assumptions, the total 2D epitaxial island density in the steady growth regime can be analytically obtained by the mean-field rate equations (MFREs), which are further expounded in Section 3.2.2. Physical intuition suggests that the 2D epitaxial island size distribution (ISD) in the steady growth regime can be expressed as a function of the coverage θ (or time t) and the number of atoms s contained in a 2D island, $n_{\mathrm{isl}}(s,t)$, which is generally believed to determine the quality of an epitaxial film in the multilayer stage of homoepitaxial growth. Unlike the total density of 2D islands $n_{\mathrm{tot}}(F,T)$, the ISD cannot be deduced from the MFREs. However, there is a well-known assumption that the time evolution of the 2D island size distribution in the steady growth stage with increasing θ should be consistent with the well-established scaling invariance ansatz in the theoretical investigation of aggregation phenomena. Both the MFREs and the scaling invariance ansatz are an important theoretical tool for investigation of the nucleation and growth of 2D epitaxial islands in the submonolayer regime in epitaxial growth, and they will be briefly described in Sections 3.2.2 and 3.2.3, respectively.

3.2.2 Mean-field rate equations (MFREs)

The mean-field (MF) approximation is made by neglecting both the local effect in the area around individual 2D islands and the effect of the spatial correlation among these 2D islands on their nucleation and growth processes. According to the MF approximation and the simple physical scenario described in Section 3.2.1, the dynamical behavior of the average density $n_{\mathrm{isl}}(s,t)$ of 2D epitaxial islands with size s and the adatom density n_1 can be described by a set of the coupled MFREs (see the review articles [93–95]):

$$\frac{\mathrm{d}n_1(t)}{\mathrm{d}t} = F - 2D\sigma_1 n_1^2 - Dn_1 \sum_{s>1} \sigma_s n_{\mathrm{isl}}(s,t), \quad (3.2.2.1)$$

$$\frac{\mathrm{d}n_{\mathrm{isl}}(s,t)}{\mathrm{d}t} = Dn_1[\sigma_{s-1} n(s-1,t) - \sigma_s n_{\mathrm{isl}}(s,t)], \quad (3.2.2.2)$$

where σ_s is the capture coefficient of islands of size s, and D is the adatom diffusion coefficient. Both Eqs. (3.2.2.1) and (3.2.2.2) are appropriate only when the total deposition amount is very small and the total area covered by 2D epitaxial islands is negligible compared with the entire surface area. The first term F in Eq. (3.2.2.1) represents the increase in n_1 due to the deposition flux F, the second term represents the collision event of two adatoms to form an ad-dimer, and the third term represents the fact that all the 2D islands in the ensemble capture adatoms and cause n_1 to decrease. The first term in Eq. (3.2.2.2) represents the event in which a 2D island of size $s-1$ becomes an island of size s by capturing one additional adatom, and the second term is the event in which an island of size s grows into size $s+1$ at the moment t by capturing an additional adatom. Furthermore, adatom aggregation is assumed to be an irreversible process, and therefore, in Eqs. (3.2.2.1) and (3.2.2.2), the detachment of an atom from a 2D island to become an adatom again is neglected. In principle, the entire set of MFREs can simply be integrated to obtain all the densities for adatoms and 2D islands of various sizes at any moment t during epitaxial growth. However, the number of dynamical equations in the MFREs is infinite; in addition, the σ_s variables should have a complicated physical meaning and a remarkably complex mathematical expression. Therefore, no satisfactory analytical expressions for the adatom and 2D island densities have ever been found by direct integration of the MFREs expressed by Eqs. (3.2.2.1) and (3.2.2.2) [96–98].

For a more qualitative discussion of epitaxial growth of 2D islands in the submonolayer steady growth stage in terms of the MFREs, these dynamical equations must be further simplified. If only the total number island density $n_{\mathrm{tot}}(t) = \sum_{s\geqslant 2} n_{\mathrm{isl}}(s,t)$ and the adatom density n_1 are

considered, the unit of the density is per adsorption site on the surface, and $\sigma_s = \sigma_1 = 1$, the number of MFREs, as expressed by Eqs. (3.2.2.1) and (3.2.2.2.), can be reduced to the following two equations in simpler form:

$$\frac{\mathrm{d}n_1(\theta)}{\mathrm{d}\theta} = 1 - 2Rn_1^2 - Rn_1N_{\mathrm{tot}}, \tag{3.2.2.3}$$

$$\frac{\mathrm{d}n_{\mathrm{tot}}(\theta)}{\mathrm{d}\theta} = Rn_1^2, \tag{3.2.2.4}$$

where $\theta = Ft$ is the coverage amount at time t, and $R = D/F$. By directly integrating Eqs. (3.2.2.3) and (3.2.2.4), the expressions for n_{tot} and n_1, respectively, can be obtained in the nucleation and steady growth submonolayer regimes [99]. In the first regime, where the deposition amount θ is very small, $n_{\mathrm{tot}} \ll 1$ and $n_1 \ll 1$. The last two terms in Eq. (3.2.2.3) can be neglected; thus, we have, by integration

$$n_1(\theta) = \theta, \tag{3.2.2.5}$$

$$n_{\mathrm{tot}}(\theta) \sim \theta^3. \tag{3.2.2.6}$$

In the second regime, nucleation of a 2D island has occurred many times, and the inequality $n_1 \ll n_{\mathrm{tot}}$ is satisfied. The island density n_{tot} and adatom density n_1 are obtained as follows:

$$n_1(\theta) = \theta^{-1/3}, \tag{3.2.2.7}$$

$$n_{\mathrm{tot}}(\theta) \sim \theta^{1/3}, \tag{3.2.2.8}$$

respectively. In the above description, it was assumed that the smallest stable 2D islands on the surface during epitaxial growth are ad-dimers. This may be appropriate only when the substrate temperature T is relatively low. As T increases, the relatively small islands may dissociate into isolated adatoms again, and only sufficiently large 2D islands are kinetically stable and can grow irreversibly in size. Therefore, in a more refined description, it is necessary to define the critical size for 2D epitaxial islands, $i^* = s_i - 1$, where s_i is the size of the smallest kinetically stable island. For $s_i > 1$, Frankl and Venables [100] deduced the expression for the total number density of stable 2D epitaxial islands in the steady growth stage on the basis of the MFREs:

$$n_{\mathrm{tot}} \propto (F/\nu)^{(i^*+1)/(i^*+3)} \times \exp\{(E_{i^*}+(i^*+1)E_{diff})/(i^*+3)k_{\mathrm{B}}T\}, \tag{3.2.2.9}$$

where E_{i^*} is the binding energy of a 2D critical nucleus with i^* atoms, i.e., the energy required to decompose a 2D critical island into a number of single adatoms, and E_{diff} is the energy barrier for adatom diffusion. In general, Eq. (3.2.2.9) is in agreement with experimental observations of homoepitaxial growth of some metals without surface reconstruction at relatively low substrate temperatures [95].

3.2.3 *Scaling invariance ansatz*

Irreversible aggregation of a large number of moving isolated single particles into particle clusters of various sizes is a dynamic process that occurs in a variety of systems under conditions far from thermodynamic equilibrium, as the case of adatom aggregation in the submonolayer regime in the homoepitaxial growth. The similar phenomena have long been a fundamental issue in many traditional scientific fields and practical technologies, such as physics, chemistry, astronomy, biology, materials science, surface science, and metallurgy. In particular, the topic is currently paramount in nanotechnology and nanoscience. In these irreversible aggregation processes, the average size $S(t)$ of the aggregates or clusters is expected to increase with the time t in accordance with the power law

$$S(t) \sim t^z, \tag{3.2.3.1}$$

where z is generally called the growth exponent and depends on the mass transport mechanism in the system. Earlier studies on the adatom aggregation processes focused on the growth morphologies of these aggregates. In diffusion-limited aggregation models in two dimensions, in which individual Brownian particles on a solid surface irreversibly stick together without any restructuring processes, the aggregates are highly ramified and scale-invariant in geometry or structure (fractal shape or geometry), and these fractal structures possess the relatively low fractal dimension $D \sim 1.4$–1.5 [101–104]. Since 1983 [105, 106], the size distribution function of the aggregates of particles (which is a function of the time and average cluster size) began to appear as an important topic in the investigation of aggregation processes. The time evolution of the size distribution of these aggregating clusters became the main dynamic characteristic of great interest; however, it remains theoretically challenging for many aggregation processes to date. Although no systematic theory is available for investigation of this topic yet, the well-known *scaling invariance ansatz* is appropriate and is universally applicable to many practical situations. In the ansatz, it is presumably assumed that, in the long time limit, the cluster size distribution can be expressed as a function of time t and size that is invariant in form with increasing time t when the cluster sizes in the system are rescaled by a characteristic length, which varies with time t according to a power law with t^z (see, for example, Ref. [107]). This section briefly describes the scale invariance ansatz.

In general, it is hard to theoretically analyze the time

evolution of the cluster size distribution in a given system. However, an exceptional case exists in which the mathematical expression for the cluster size distribution as a function of time has been obtained analytically. When a solid binary mixture is quenched from the disordered phase into the coexistence region in the phase diagram, the minority component condenses into spherical droplets of various sizes in the matrix of the majority component. Ostwald ripening occurs among these droplets, in which larger droplets grow at the expense of smaller ones via diffusion and/or evaporation–condensation. The classic theory for the dynamical evolution of the droplet size distribution in the long-time limit was theoretically established by Lifshitz and Slyozov [67] and Wagner [68] (LSW theory) using the analytical method. It was found that in the long-time limit, the dynamical evolution of the droplet size distribution $f(R,t)$ obeys the scaling invariant form:

$$f(R,t)=g\left(\frac{R}{\overline{R}}\right)/\overline{R}^4, \tag{3.2.3.2}$$

where g is the scaling function, R represents the diameter of a spherical droplet if atomic diffusion is the rate-limiting process, $\overline{R}=(Kt)^{1/3}$ is the characteristic length for Ostwald ripening, and K is the asymptotic growth rate of the droplets.

The scale-invariant form of the cluster size distribution has been observed in many Monte Carlo simulations and relevant experimental observations. For example, using the KMC simulation method, Family *et al.* [108, 109] proposed the following dynamic scaling relation for the droplet size distribution formed by diffusion-limited growth in vapor-deposited thin films:

$$n(s,t)\sim s^{-\theta}f(s/S(t)), \tag{3.2.3.3}$$

where $n(s,t)$ is the number of droplets of size s at instant t, $S(t)\sim t^z$ is the average droplet size, and f is the scaling function. The exponents $\theta(=5/3)$ and $z(=3)$ describe the scaling and growth law. On the experimental side, as reviewed in Ref. [110], it was practically observed that in the coarsening processes of spherical clusters of several metals and semiconductors on the Si surface, the cluster size distribution on long timescales approaches the scaling invariant form f_s:

$$f(r,t)\to f_s(r/r_c(t)), \tag{3.2.3.4}$$

where $r_c(t)\propto t^{1/n}$ is the characteristic cluster radius, and the exponent n depends on the rate-limiting factors for the growth and the dimensionality of the system; e.g., $n=4$ for 3D clusters on a surface where surface diffusion is the rate-limiting factor for the aggregation process. In addition, Vicsek and Family [106] performed a KMC simulation of an aggregation process occurring on a solid surface. In their simulation model, initially a finite number of single particles randomly hop across the surface lattice sites. On meeting with each other or with a cluster of particles, the single particles permanently stick together to form a cluster that continues to move randomly. In this simulated dynamic system, the cluster size distribution $n(s,t)$ evolves according to the scaling law after a long time t elapses:

$$n(s,t)\sim t^{-w}s^{-\tau}f(s/r_c(t)), \tag{3.2.3.5}$$

where $r_c(t)\sim t^z$ is the characteristic size of the clusters, and the power law t^{-w} describes the decay of $n_s(t)$ with time t for every cluster size s; τ is a constant called the static exponent. The three examples above demonstrate that the scaling invariance ansatz should be universal for a variety of irreversible aggregation processes of individual particles.

In particular, in the irreversible aggregation process as represented by the nucleation and growth of 2D epitaxial islands in the submonolayer regime, the island size distribution should be consistent with the scaling invariance ansatz in the steady-state growth stage. If the average 2D island linear size $s_{\mathrm{av}}\sim t^z$ is taken as the characteristic length of the system, it can be deduced that the scaling law for the island size distribution $n(s,\theta)$ of 2D epitaxial islands should have the form [111, 112]

$$n(s,\theta)=(\theta/s_{\mathrm{av}}^2)f(s/s_{\mathrm{av}}), \tag{3.2.3.6}$$

where $\theta=Ft$ is the amount of coverage; the scaling function $f(s/s_{\mathrm{av}})$ depends on the ratio R of the adatom diffusion constant D to the deposition flux F, $R=D/F\sim 10^4$–10^8, and $s_{\mathrm{av}}=\theta^{2/3}(D/F)^{1/3}$ according to the scaling analysis [113, 114]. The scaling law (3.2.3.6) has been confirmed by experimental observations of 2D island homoepitaxial growth of Fe/Fe(001) [115] and 2D InAs islands in the submonolayer regime on GaAs(001) [116, 117], as well as KMC simulations [118, 119]. Note that the scaling function $f(s/s_{\mathrm{av}})$, which depends on the growth parameters, such as θ and F as well as T, enters Eq. (3.2.3.6) only through s_{av}.

The scale invariance, Eq. (3.2.3.6), is a fundamental hypothesis for stochastic aggregation phenomena of randomly moving adatoms. Although its validity in some homoepitaxial growth systems has been demonstrated by both experimental observations [115–117] and computer simulations [118, 119], its physical nature or origin is not properly understood yet. A number of investigators attempted to provide a physical explanation or meaning and to fix the scaling function $f(s/s_{\mathrm{av}})$ in Eq. (3.2.3.6). For example, Mulheran and Blackman [120, 121] suggested a geometrical model based on the concept of the

capture zone of an epitaxial island. In their model, an island nucleus is formed via a collision event involving a number of adatoms in dynamical Brownian motion, and it grows further by capturing more adatoms deposited in its capture zone, which is defined as the regions closer to that island than to any others. Hence, the island growth rate and its volume are proportional to its capture zone, where the size distribution of the capture zones is in accordance with the scale-invariant form. Fanfoni *et al.* [89] and Ratto *et al.* [122] proposed that all the epitaxial islands can be nucleated simultaneously or within a very short period. Therefore, the entire growth surface can be statistically subdivided into Voronoi cells according to the principle of Voronoi tessellation on the basis of the islands' distribution: The Voronoi cell of one reference island represents the fraction of the surface closer to that island than to any other and is constructed by drawing the axes of the segments joining that island's center of mass to its neighbors' mass centers (see, for example, Ref. [91]). It can be proved that the areal size distribution of Voronoi cells, which are equivalent to the capture zones of epitaxial islands, is consistent with the scaling invariance ansatz [89], which should be the physical origin of the scale-invariant island size distribution given by Eq. (3.2.3.6).

3.2.4 Fitting experimental data on the density and size distribution of the InAs QDs with the MFREs and the scaling invariance ansatz

In the effort to understand the spontaneous formation of InAs QDs, it has long been customary to assume that the process should be essentially similar to adatom aggregation in the submonolayer regime during epitaxial growth, as described in Section 3.2.1. Therefore, the experimental data on the InAs QD number density and size distribution should be well fitted by the two universal laws for the adatom aggregation processes, Eqs. (3.2.2.9) and (3.2.3.6), respectively. In the literature, some authors [123–126] have claimed that their experimental data on InAs QD number density are fitted well by the Arrhenius law, Eq. (3.2.2.9). Moreover, by such a fitting, Shiramine *et al.* [125] even obtained a critical island size of 1–10 atoms for InAs QD formation via adatom aggregation and a thermal activation energy of 2.0 eV for the corresponding Arrhenius behavior. Even further, some authors [127, 128] have successfully fitted their experimental observations of the InAs QD size distribution with the scale invariance ansatz, Eq. (3.2.3.6), even though InAs QD formation is generally regarded as a self-limited growth phenomenon from the experimental viewpoint, which will be further discussed in the remainder of this section.

In the literature, the above experimental observations [89, 123–128] have often been taken as strong experimental evidence to support the view that InAs QD formation should be a surface process remarkably similar to adatom aggregation in homoepitaxial growth in the submonolayer regime. However, it will be further demonstrated in Section 4 that the outcome of practical epitaxial growth of InAs QDs depends sensitively on the growth parameters, such as the flux rate F and temperature T; although some experimental data in the literature obtained under certain growth conditions seem to be consistent with Eqs. (3.2.2.9) and (3.2.3.6), these two famous laws for adatom aggregation are obviously not universally applicable to a number of distinct situations involving InAs QDs obtained under various experimental conditions. In addition, Eqs. (3.2.2.9) and (3.2.3.6) are appropriate only in the steady growth regime when a saturated 2D island density is well defined. However, for InAs QDs, no such a saturated island density has been well-defined experimentally [13]. Furthermore, for the scale-invariant form, Eq. (3.2.3.6), to be appropriate, it has to be assumed that adatom aggregation proceeds exclusively via random adatom diffusion, and the average size s_{av} of the ensemble of adatom aggregates grows with increasing amount of deposition θ according to the power law $s_{\mathrm{av}} \propto \theta^z$. In contrast, from the experimental viewpoint, InAs QD formation is definitely a self-limited growth process, and the growth power law $s_{\mathrm{av}} \propto \theta^z$ for an aggregation process makes no sense for InAs QD growth behavior. Therefore, the apparent fitting of the experimental data reported in these references [89, 123–128] may only demonstrate that both the universal laws, Eqs. (3.2.2.9) and (3.2.3.6), are very versatile and flexible in fitting experimental data obtained in a large number of cases, and may provide little insight into the nature of the InAs QD formation process.

3.2.5 MFREs tailored to QD formation in heteroepitaxial growth

In the conventional MFREs, the nucleation and growth of a 2D epitaxial island during epitaxial growth are assumed to proceed via the atomic events of adatom diffusion and adatom attachment to the island edges, and the possible restructuring of a 2D island after an adatom sticks to it irreversibly is not considered. By taking account of the additional atomic events by which a 2D epitaxial island is transformed into a 3D island in the atomic aggregation model of QD formation, Dobbs *et al.* [81] extended the MFREs to describe 3D epitaxial island growth or QD formation in heteroepitaxial growth. By

defining a critical island size i^*, Dobbs *et al.* [81] divided all the 2D epitaxial islands initially formed into two categories: stable and unstable. A stable 2D island, with a size larger than i^*, grows by capturing more adatoms at its step edges; simultaneously, the edge atoms may detach from the step edge and become mobile again, and the detachment rate would increase with increasing 2D island diameter r. Adatoms detached from the 2D island edge may drift away as an adatom, or hop upward to nucleate a new 2D island atop the original 2D island. Once a second atomic sheet or a smaller 2D island nucleates on top of a pre-existing 2D island, it is said that a 3D island has nucleated and, from then on, all the atoms detaching from the original 2D island edges climb up to the higher-level atomic layers of the 3D island instead of migrating away. Given the foregoing, the MFREs that are applicable to the densities of adatoms n_1, 2D islands n_{2D}, and 3D islands n_{3D} are given as follows:

$$\begin{aligned} \frac{\mathrm{d}n_1}{\mathrm{d}t} &= F - D[(i^*+1)\sigma_{i^*}n_{i^*} + \sigma_{2D}n_{2D} + \sigma_{3D}n_{3D}]n_1 \\ &\quad + \frac{n_{2D}}{\tau}, \\ \frac{\mathrm{d}n_{2D}}{\mathrm{d}t} &= D\sigma_{i^*}n_{i^*}n_1 - \gamma n_{2D}, \\ \frac{\mathrm{d}n_{3D}}{\mathrm{d}t} &= \gamma n_{2D}, \end{aligned} \tag{3.2.5.1}$$

where σ_{i^*}, σ_{2D}, and σ_{3D} are the capture numbers of the critical 2D island, 2D island, and 3D island, respectively; γ is the transition rate from 2D to 3D islands. By properly choosing the kinetic parameters in the rate equations, Eq. (3.2.5.1) can be solved numerically to obtain the variation in n_{3D} as a function of the coverage θ, which shows a "dog-leg" curve in the $n_{3D} - \theta$ diagram [81].

In Dobbs' MFREs for QD formation, Eq. (3.2.5.1), there are only three dynamical variables, n_1, n_{2D}, and n_{3D}. Furthermore, as an island's base diameter grows, its lateral growth rate is progressively reduced. However, atoms detaching from the edges of the island base hop up the island, which should make it grow increasingly faster vertically. Obviously, in the model, there is no self-limited growth mechanism and no information about the island size distribution. To address these two shortcomings, the MFREs formulated for QD formation by Dobbs *et al.* [81], or QD-MFREs, were extended further by Heyn [92] and Nevalainen *et al.* [90]. In these further extended QD-MFREs, a growing QD is assumed to have a truncated pyramid shape, and its growth rate R is assumed to be in accordance with the expression

$$R \propto 1 - V_s/V_p, \tag{3.2.5.2}$$

where V_s is the volume of the growing truncated pyramid, and V_p is the volume of a fully pyramidal island. Artificially imposing such a relationship between the growth rate and the volume of a growing QD ensures that after a QD grows into a full pyramid, its growth stops automatically. With these assumptions, the QD-MFREs can be solved numerically. The results show that the island size distribution of QDs evolves naturally from an initially quite broad one into a sharp peak at the size fixed by the pyramid [90, 92].

3.3 Reaction kinetic model

In Section 3.2, QD formation in heteroepitaxial growth is assumed to be entirely mediated by random adatom diffusion and irreversible attachment upon direct contact between a diffusing adatom and the step edges of a growing epitaxial island, and the atomic events should be independent of the energetics and the size of the island besides Section 3.2.5. Alternatively, in the reaction kinetic model, as described in this subsection for the nucleation and growth of a QD, the probability that an epitaxial island will capture an adatom and grow in size depends on the energetic factors, which can be given as an explicit analytical expression in terms of the island size. In addition, the capture of an adatom by a growing island of any size is reversible, and the adatom located on the edge of a growing island can detach from it at any moment with a certain probability.

In the reaction kinetic model [129–135], the growth of a QD via individual adatom events of atomic attachment to and detachment from the epitaxial island can be expressed in the form of a chemical reaction,

$$\mathrm{A}_1 + \mathrm{A}_s \leftrightarrow \mathrm{A}_{s+1}, \tag{3.3.1}$$

where A_1 and A_s are identified as an adatom and a cluster of size s in the ensemble of QDs, respectively. The chemical reaction (3.3.1) indicates that an adatom may attach to an island of size s to convert it into an island of size $(s+1)$; inversely, an island of size $(s+1)$ can be decomposed into an island of size s and an isolated adatom. This reaction kinetic model is also mean-field in nature, and the time evolution of the densities n_s of epitaxial islands of different sizes s induced by the reaction in (3.3.1) can be expressed by the MFREs as follows:

$$\frac{\mathrm{d}n_1}{\mathrm{d}t} = F - 2\sigma_1 n_1^2 - n_1 \sum_{s\geqslant 2} \sigma_s n_s + \kappa\gamma_2 n_2 + \kappa \sum_{s\geqslant 2} \gamma_s n_s, \tag{3.3.2}$$

$$\frac{\mathrm{d}n_s}{\mathrm{d}t} = \sigma_{s-1}n_{s-1}n_1 - \sigma_s n_s n_1 + \kappa\gamma_{s+1}n_{s+1} - \kappa\gamma_s n_s. \tag{3.3.3}$$

In these MFREs for the reaction kinetic model, F is the atomic flux, and κ is a parameter defined as the ratio between the attachment and detachment rates σ_s and γ_s. These two sets of kinetic parameters are size-dependent, and their analytical expressions can be obtained by the principle of detailed balance and the self-consistent scheme of Bales and Zangwill [133]:

$$\sigma_s = s^q/(1 + \mathrm{e}^{\frac{\Delta_s}{kT}}), \tag{3.3.4}$$

$$\gamma_s = s^q/(1 + \mathrm{e}^{-\frac{\beta\Delta_{s-1}}{kT}}), \tag{3.3.5}$$

where $\Delta_s = E_{s+1} - E_s$, and E_s is the formation energy of an island of size s.

Together, Eqs. (3.3.2) and (3.3.3) can be reduced to the Becker–Doring equation [70] of the form

$$\frac{\mathrm{d}n_s}{\mathrm{d}t} = \sigma_{s-1}n_{s-1} - (\sigma_s + \gamma_s)n_s + \gamma_{s+1}n_{s+1} + (n_1 - 1)(\sigma_s n_s - \gamma_{s-1}n_{s-1}), \tag{3.3.6}$$

which can be further reduced to a continuum equation when the island size s becomes so large that it can be treated as a continuous variable x. This continuum equation is a Fokker–Planck equation of the form

$$\frac{\partial n(x,t)}{\partial t} = -\frac{\partial}{\partial x}[J(x,t)], \tag{3.3.7}$$

$$J(x,t) = v(x,t)n(x,t) - \frac{\partial}{\partial x}[D(x,t)n(x,t)], \tag{3.3.8}$$

where $J(x,t)$ is the flux in the configurational space of the cluster sizes. The first term in Eq. (3.3.8) is called the drift term, whereas the second term is called the diffusive term, where $v(x,t)$ and $D(x,t)$ are the time- and size-dependent drift and diffusion coefficients, respectively. The Fokker–Planck equation (3.3.8) is also generally regarded in the literature as a standard approach to studying time-dependent nucleation, growth, and evolution of an ensemble of nanostructures [136, 137]. By using some further mathematical tricks and physical assumptions, Eq. (3.3.8) can be solved by numerical methods to obtain the time evolution of the QD size distribution $n(x,t)$ [135, 136].

To describe the time evolution of an ensemble of QDs taking into account the island growth energetics, Ross *et al.* [83] adopted an alternative approach that is simpler than that used by Bales and Zangwill [133]. Ross *et al.* [83] expressed the formation energy of a 3D island in terms of its volume V in the dimensionless formula

$$E = V^{2/3}\alpha^{4/3} - V\alpha, \tag{3.3.9}$$

$$\mu = \partial E/\partial V = 2V^{-1/3}\alpha^{4/3}/3 - \alpha, \tag{3.3.10}$$

where α is a constant determined by the facet angle of a 3D island. In addition to the growth in the mean-field island size driven by the deposition flux F, a coarsening process occurs in which islands with a smaller chemical potential μ than the mean-field value $\bar{\mu}$ grow at the expense of those islands with a larger μ than $\bar{\mu}$. With an appropriate scaling of the units of time, island growth is governed by the dimensionless equation

$$\mathrm{d}V/\mathrm{d}\tau = V^{1/3}(\bar{\mu} - \mu). \tag{3.3.11}$$

The mean-field chemical potential $\bar{\mu}$ is determined by the constraint that the rate of volume change integrated over all the QDs must equal the total flux incident on the surface. Again, the time evolution of the island size distribution of a QD ensemble governed by Eqs. (3.3.9), (3.3.10), and (3.3.11) can be expressed by the Fokker–Planck equation (3.3.7) and Eq. (3.3.8). In addition, the approach developed by Ross *et al.* [83] was also adopted by Bimberg *et al.* [138, 139] and Bergamaschini *et al.* [140] to identify a metastable state with a narrow Gaussian-type QD size distribution established by an anomalous coarsening process in an ensemble of QDs during growth or annealing.

Note that in the conventional kinetic growth theories (as described in Sections 3.2 and 3.3), only some statistical average quantities such as the total island density, average size of islands, and island size distribution in an ensemble of QDs can be provided. In addition, it is implicitly assumed in these theories that once an adatom is captured by a growing QD, the QD instantaneously restructures itself and accommodates the newly incorporated adatom to a proper position in the growing 3D island or nanocrystallite with a geometrically compact shape. This seems to be inappropriate and inconsistent with the well-established experimental fact that the rate of adatom diffusion along a step edge and around a step corner, as well as that of migration up a 3D epitaxial island, should be much slower than that of adatom diffusion on a smooth terrace [20]; in the former diffusion events, an adatom has more nearest neighbors to break off than an isolated adatom on a terrace. Without restructuring after aggregation of a large number of adatoms on the surface, the aggregate of adatoms should be dendritic or fractal in geometrical shape or structure, similar to the situation in diffusion-limited growth (see the review in [141]) or diffusion-limited aggregation [142]. Therefore, without considering how an atomic aggregate restructures itself or relaxes from a fractal object to a compact 3D epitaxial island, modeling the formation of a QD as just an adatom aggregation phenomenon differs significantly from the realistic situation for the formation of a compact 3D epitaxial island or a QD during epitaxial growth.

3.4 Kinetic Monte Carlo simulation

As mentioned above, in the theoretical community investigating epitaxial growth from the vapor phase, it is com-

monly believed that the time evolution of the growth surface morphology is due to atom deposition and random adatom diffusion, as well as the attachment of adatoms to step edges on the growth surface. One important reason for the popularity of this dynamic growth scenario may be that it can be fully implemented by a KMC simulation [143–148], in addition to being expressible in analytical form on the basis of the surface diffusion equation and MFREs. At present, the KMC simulation is generally regarded as the only method capable of describing surface evolution with atomistic details on experimentally relevant time and length scales. In KMC simulations of homoepitaxial growth, the fundamental atomistic processes are deposition and individual adatom diffusion, whose kinetics is approximated by thermal hopping from site to site on the surface, and the temporal resolution is in the range of 10^{-4}–10^{-6} s. The stochastic and discrete nature of adatom motion and their thermal fluctuations are fully taken into account, and the KMC simulation method is currently regarded as the most atomistically detailed, faithful, useful, and promising way to describe the dynamics of epitaxial growth of both a thin film and an ensemble of 3D islands. At each numerical step during the KMC simulation of an epitaxial growth system, all the atomistic events on the $M \times M$ lattice sites (e.g., with cubic symmetry and an M value of a few hundreds) are listed, and a periodic boundary condition is imposed; then the occurrence probability of each of these atomic events is calculated. In homoepitaxial growth, the hopping rate p_i of the adatom on lattice site i is expressed by the Arrhenius law

$$p_i = v \exp\left(-\frac{E_s + n_i E_n}{k_\mathrm{B} T}\right), \tag{3.4.1}$$

where v is the relevant pre-factor (typically 10^{12}–10^{13}/s), E_s is the binding energy to the growth surface, E_n is the binding energy to a single nearest neighbor, n_i gives the number of nearest neighbors to the adatom, and k_B and T are the Boltzmann constant and absolute temperature, respectively. Among all the listed atomistic events, one is randomly chosen to occur in each simulation step according to its relative probability. The probability for deposition of an adatom on a lattice site at a given moment is expressed as

$$P_d = \frac{F}{F + \sum_{j=1}^{M^2} p_j}, \tag{3.4.2}$$

and the probability of the adatom on the lattice site i making a hop is

$$P_i = \frac{p_i}{F + \sum_{j=1}^{M^2} p_j}. \tag{3.4.3}$$

The generic KMC model based on these three expressions has been successful in revealing some qualitative trends in epitaxial growth, such as a scaling law for island size distributions, and quantitative predictions, such as the occurrence and decay of the RHEED signal (see, for example, Ref. [148]).

In KMC simulations of QD formation in heteroepitaxial growth, such as MBE InAs/GaAs(001), in addition to the chemical bonding energy, the elastic strain energy caused by lattice mismatch has to be taken into account in determining the adatom hopping probability, and the Arrhenius law, Eq. (3.4.1), for the probability of adatom diffusion is transformed into the form [149–151]

$$p_i = v \exp\left(-\frac{E_s + n_i E_n + E_c(x, y)}{kT}\right), \tag{3.4.4}$$

where $E_c(x, y)$ is the local strain energy at the plane position of (x, y) and is a long-range field, instead of being local like the effects of E_s and $n_i E_n$ [152–155]. The elastic strain is expected to affect adatom diffusion by reducing the binding energy of an adatom to the surface and to other surface atoms, and the value of $E_c(x, y)$ is always negative in Eq. (3.4.4). Therefore, an adatom should move more rapidly in places where the absolute value of $E_c(x, y)$ is relatively large, which causes more adatoms to drift from the highly strained surface regions toward regions where the lattice is less strained. On the basis of physical intuition, it is well known that the top of a 3D island is more elastically relaxed than the regions at its base. In consequence, in the KMC simulation of QD growth, adatoms are driven uphill a 3D island by the gradient in the elastic strain field, and the 3D island grows in height as well as lateral size. Indeed, Eq. (3.4.4) seems to be versatile in describing the formation of 3D growth morphologies in the SK growth mode. Moreover, by adding a wetting energy to the numerator in Eq. (3.4.4), the formation of a WL with a certain critical thickness can be observed [156, 157] in the KMC simulation. Furthermore, by taking account of the anisotropy in the surface free energy and surface diffusion [158], the faceting of the side wall of a 3D island or QD is also realized in the KMC simulation.

Note that although the atomistic model used in KMC simulations of QD formation is very simple in its physical concepts, it is somewhat computationally expensive in numerical simulation. In taking account of the local strain energy $E_c(x, y)$ in Eq. (3.4.4), it has to solve the elastic equations at every numerical time step; the result is the inverse of the diffusion constant and often $O(10^{-6}\mathrm{s})$ or smaller. Therefore, when the KMC method is applied to heteroepitaxial growth, the system must be rather small [159, 160] compared with the system size when it is applied to homoepitaxial growth.

In combination with the use of density functional theory to calculate the microscopic parameters obtained from first-principles calculations, KMC simulation of an epitaxial growth system describes the physical scenario on the growth surface in terms of an ensemble of atomic deposition and diffusion events. The KMC method seems to reliably account for the lattice discreteness, non-equilibrium condition, and stochastic nature of each atomistic event. Therefore, a KMC simulation is generally expected to faithfully reproduce the surface morphological evolution and 3D epitaxial island growth in lattice-mismatched heteroepitaxial growth. This expectation for the KMC method seems to be successfully realized in some simple metallic systems without lattice mismatch [161–164]. However, it is well known that a growth process that can be simulated by the KMC method is Markovian, so the consequence of one step of the process has no influence on the next step. In addition, the movement of individual adatoms is regarded as the only thermally activated motion in a KMC simulation. Therefore, in a KMC simulation, any form of collective motion simultaneously involving a large number of adatoms and any possible correlation in adatom motion in both the temporal and spatial range are completely ignored. More importantly, the epitaxial growth that can be simulated by the KMC method has to be a very time-lengthy process in practice (this topic will be further explored in Section 3.5 and Section 3.6), which is obviously inconsistent with experimental observation of InAs QD formation, as demonstrated in Section 4.

3.5 Building a QD

Although the literature contains many theoretical investigations of QD formation, as described in the last four subsections, the fundamental concepts of the phenomenon still seem to be rather confused. According to the surface relaxation theory in Section 3.1, QD formation should result from a morphological relaxation process of an elastically strained thin film on a lattice-mismatched substrate. In Sections 3.2 and 3.3, QD formation is described as an adatom aggregation process via adatom diffusion and attachment to the step edges of epitaxial islands. In KMC simulations, as described in Section 3.4, QD formation is a 3D growth process driven by both atom deposition and lattice mismatch, with mass transfer via surface diffusion. In fact, each of these different theoretical descriptions should be appropriate to a different physical scenario. However, in the literature, they have all been regarded, implicitly or explicitly, as alternative and effective approaches to interpret the QD formation. From these theories, it is still not clear whether the QD formation process should be morphological relaxation, adatom aggregation, or nanocrystal growth driven by deposition, which differ distinctly from each other in their physical nature. Moreover, the theories listed above provide no or little information on how a compact crystalline QD is built from individual atoms, or how nanocrystal growth proceeds on the surface. The purpose of this section is to describe how a QD can be constructed in the framework of traditional kinetic theories.

3.5.1 Surface morphological relaxation

From the viewpoints of Sections 3.1 and 3.2, QD formation has to undergo a relaxation process driven by elastic strain and surface tension. In Section 3.1, QD formation is simply described as a surface morphological relaxation process from a 2D flat film into a 3D surface morphology, and the relaxation process is driven by the gradients of both the elastic strain and the capillary effect, whereas in Section 3.2, QD formation is described as an aggregation process in which a large number of adatoms aggregate into an ensemble of QDs. In the latter case, the formation of a compact 3D epitaxial island has to exhibit two successive distinct stages owing to the well-known fact that adatom diffusion on a smooth terrace is much faster than atomic motion either along a step edge or upward on a 3D epitaxial island. Because of the difference in the surface diffusion behaviors in the formation of a QD, as described at the end of Section 3.3, first a large number of adatoms aggregate into an epitaxial island via terrace diffusion, which should be fractal or dendritic in geometry, and then a morphological relaxation process follows, during which the adatom aggregate restructures itself and transforms from a fractal object or dendrite to a compact 3D epitaxial island to further reduce the associated strain energy and surface free energy.

Before the morphological relaxation process occurring during QD formation is described, the concept of thermal roughening of a crystalline surface of a solid should be recalled. It is well known that the roughening temperature T_{R} of the crystalline atomic plane is defined as the temperature at which it transforms from a flat (or faceted) morphology to a rough one at the atomic scale in thermodynamic equilibrium. Whether the crystalline surface is atomically rough or faceted has an important impact on the kinetics of the surface morphological relaxation as well as the crystal growth process. If the temperature is above T_{R} and the surface is microscopically rough, there should be a large number of binding or adsorption sites on the surface lattice for adatoms to settle down, and the rate of the surface morphological change

is determined only by adatom diffusion. In this case, the surface relaxation process occurring on a relatively large object can be described by the mathematical continuum theory established by Herring [59] and Mullins [60]. An important conclusion of this continuum theory is that the time $t_{\rm eq}$ required for the system to reach the equilibrium morphological state scales with the fourth power of its linear dimension. This result is consistent with the common experience that a macroscopic solid maintains its non-equilibrium shape indefinitely. In contrast to macroscopic solid bulk objects, nanocrystallites can rapidly change their shape by means of surface diffusion, and their behavior resembles that of a liquid droplet [165]. The topics related to the timescale of the relaxation process associated with crystalline surface morphology will be further discussed in Section 3.6.

Below their $T_{\rm R}$, the sidewall facets of a crystallite are all faceted and atomically flat. During the surface relaxation process, diffusing adatoms on these crystalline facets have to find a step edge to settle down, and the rate of the surface relaxation process depends on the probability of the nucleation of a new 2D atomic layer on a flat facet, which may encounter a quite large energy barrier for the formation of the step. Therefore, the morphological change or surface relaxation of a faceted 3D island proceeds via events such as nucleation of new atomic layers and advancing or receding of the atomic steps on a singular crystalline plane [166], and the continuum theory, which is appropriate to a thermally roughened crystalline surface when $T > T_{\rm R}$, can no longer be applied. Herring [167] pointed out that in the absence of screw dislocations or surface catalysts, nucleation of a new atomic monolayer on a flat crystalline facet is likely to constitute an insuperable barrier to any surface-tension-motivated morphological change that requires the growth of low-crystalline-index planes. This argument was further emphasized by Mullins and Rohrer [168, 169]. For this reason, at temperatures below $T_{\rm R}$, nanocrystallites can be trapped for a relatively long time in a sequence of metastable configurations before finally reaching the equilibrium morphology. Therefore, the timescale for a morphological change process occurring in a small crystallite should be much longer below $T_{\rm R}$ than above $T_{\rm R}$, and this has been well confirmed by both experiments and KMC simulations [170, 171].

The surface morphological relaxation theory described in Section 3.1 for QD formation is currently popular in the literature. However, it has a very obvious drawback that has been overlooked by researchers who favor the theory: The surface morphological relaxation should be, in essence, an annealing process driven by the capillary effect and/or strain energy, instead of a crystal growth process driven by the deposition flux. The former process requires much more time than the latter. However, as will be shown in Sections 3.6 and 4, experimental InAs QD formation is practically a much more rapid process than the deposition flux. Therefore, the morphological relaxation theory for the QD formation process should be simply unreasonable in terms of the relevant experimental timescale.

3.5.2 Uphill mass transfer and 3D epitaxial island growth

In describing epitaxial growth of 2D islands in the submonolayer regime of an epitaxial growth system, only the lateral mass transfer on the flat terrace needs to be considered. In contrast, if a 3D epitaxial island develops out of the growth plane with a growth rate significantly faster than the deposition flux (as in InAs QD formation), an effective uphill mass transfer or flux along the island sidewall has to occur at a much more rapid rate than the deposition flux. In this subsection, a few of the various mechanisms suggested in the conventional theories for uphill mass transfer and the associated 3D growth morphology are described briefly.

3.5.2.1 Kinetic roughening

In MBE growth, if an adatom's movement is limited to the neighborhood nearest its landing site by some geometrical mechanism (i.e., the trapping effect of the local lowest atomic positions), the growth surface will become increasingly rougher, resulting in an irregular 3D surface morphology due to the stochastic nature of both the deposition flux and adatom diffusion. This phenomenon is called kinetic roughening and has been extensively studied, mainly theoretically and by numerical simulation, in the past three decades as a topic interesting in both fundamental research and a large number of practical systems [172–174]. In the theory, to quantitatively express the growth surface morphology, the growth surface width is defined as

$$W(L,t) = \langle 1/L^2 \rangle \sum_i^{L^2} (h_i^2 - \bar{h}^2)^{1/2}, \quad \bar{h} = \langle 1/L^2 \rangle \sum_i^{L^2} h_i, \tag{3.5.2.1.1}$$

where h_i is the height of the atomic column at site i of a growth surface lattice of dimensions L. According to the solid-on-solid model, where no overhangs or vacancies exist inside the growing lattice structure, the dynamic evolution of $W(L,t)$ is described by the coarse-grained continuity equation:

$$\frac{\partial h}{\partial t} + \nabla \cdot \boldsymbol{j} = F\Omega + \eta(\boldsymbol{x}, t), \tag{3.5.2.1.2}$$

where $\boldsymbol{j}$ is the local surface current, F is the incoming flux, Ω is the surface cell volume, and $\eta(\boldsymbol{x},t)$ is a Gaussian-uncorrelated white noise. With some simplifying assumptions, Eq. (3.5.2.1.2) can be solved numerically [172–174], which demonstrates that, in the early growth period, $W(L,t)$ increases with time t according to the power law

$$W(L,t)=t^{\beta}, \tag{3.5.2.1.3}$$

where β is called the growth exponent. It was theoretically confirmed that the maximum value of the growth exponent, $\beta=1/2$, occurs when surface diffusion is completely suppressed and a deposited adatom remains at the site where it initially landed. The situation with $\beta=1/2$ is called Poisson growth in the literature. The situation is also referred to in the literature as the statistical growth or random deposition limit (see the review article Ref. [177] and references therein). This period of time in epitaxial growth is called the growth regime when Eq. (3.5.2.1.3) holds. For a long limit or an asymptotic time, the growth phenomenon approaches the steady state, at which the surface width remains constant and is characterized by the power law

$$W(L,t)=L^{\alpha}, \tag{3.5.2.1.4}$$

where α is the roughness exponent.

More generally, both Eqs. (3.5.2.1.3) and (3.5.2.1.4) satisfy the dynamic scaling form as proposed by Family and Vicsek [175]

$$W(L,t)=t^{\beta}f(L/t^{1/z}), \tag{3.5.2.1.5}$$

where $\beta=\alpha/z$ in Eq. (3.5.2.1.5) is a growth exponent that describes the short-term growth behavior, and the scaling function $f(u)$ has asymptotic properties such that $f(u)\sim$ const for $u\to 0$ and $f(u)\sim u^{\alpha}$ for $u\to\infty$. The roughness exponent α and dynamic exponent z describe the asymptotic behavior of the growing interface on the large length scale and long timescale, respectively. In theory, all dynamically evolving interfaces controlled by stochastic and random deposition and diffusion and satisfying Eq. (3.5.2.1.2) can be classified into a limited number of different universality classes according to the values of the exponents α and β. The classification is determined mainly by the structural symmetry and space dimensionality of a growth system, independent of its particular microscopic details.

3.5.2.2 Formation of growth mounds and huts in homoepitaxial growth

According to conventional kinetic theory of epitaxial growth of a film on a substrate, if there is no additional restriction preventing an adatom on the upper terrace from crossing a step downward to the lower terrace via diffusion, the film will grow via the 2D or layer-by-layer growth mode, and no 3D features or islands will develop on the growth surface. This is because, in atomic kinetic theory, the average adatom diffusion length on a terrace is intrinsically assumed to always be larger than the maximum lateral size of the 2D islands before they coalesce into a complete atomic layer across the entire growth surface. This guarantees that an adatom atop a 2D island can always step down and be incorporated into the atomic step edges bounding the 2D island, rather than forming a new nucleus with its counterparts on the top of the 2D island [176, 177]. The layer-by-layer growth mode can usually be achieved by controlling the experimental parameters such as the temperature $T$and incident flux F. If some intrinsic physical mechanism becomes dominant over the effect of T and F so that the layer-by-layer growth mode becomes out of control, a growth instability is said to occur; this generally results in 3D growth features or morphologies at the nanoscale [178]. This subsection focuses on the growth instability induced by the additional energy barrier an adatom meets when it steps down a step edge on the growth surface.

During epitaxial growth, if the adatom movement of stepping down an atomic step is hindered to some extent by an additional energy barrier induced by the presence of the step, nominal uphill mass transport occurs, and 3D mounds will develop with a regular geometrical shape; these 3D growth mounds are often called "wedding cakes" in the literature. In practice, a wedding cake typically occurs in homoepitaxial growth of metals at a relatively low substrate temperature and has been systematically investigated both theoretically and experimentally (see, for example, Refs. [179, 180]). In this case, a step-edge energy (SE) barrier that prevents an adatom from stepping down a terrace at its edges is usually encountered, and the adatom tends to be reflected by the downward step at one side of the terrace toward the upward step on its other side. Therefore, the effect of the SE barrier produces a nominal uphill current of adatoms $J_{\rm up}$ [181–183]. In addition, an equivalent mechanism leading to the formation of growth mounds during MBE growth was also proposed by Amar and Family (AF) [184], in which adatoms on terraces are attracted toward the base of a step because of a short-range attractive force. Similar to the SE barrier, the AF mechanism causes atoms on terraces to preferentially collect at up-steps rather than down-steps, leading to the mounded morphology or wedding cakes.

In their numerical simulations of QD formation in heteroepitaxial growth using the KMC simulation, Brunev

et al. [185] interpreted QD formation in terms of the upward adatom current J_{up} induced by the SE energy barrier. They defined the ratio of J_{up} to the downward current J_{down}, $R = J_{\mathrm{up}}/J_{\mathrm{down}}$, and their result shows that QDs can form only when the value of R is sufficiently large [186]. However, it has been proven that, even when the SE barrier is infinitely large, the step-down motion of an adatom is completely prohibited; i.e., at $R = \infty$, a 3D growth mound grows to a height h, which is equivalent to the surface width $W(L,t)$ defined in Eq. (3.5.2.1.1), with a deposition amount θ (monolayer) according to the Poisson growth law, as defined in the last subsection (see, for example, Refs. [177, 187, 188]). This is obviously a remarkably inefficient mass transport mechanism for the self-assembly of QDs, at least in the MBE InAs/GaAs(001) system.

3.5.2.3 Super-epitaxial growth

In the conventional kinetic theories, the mass transfer necessary for the formation of 3D growth morphologies in epitaxial growth occurs via adatom diffusion, and the height of a 3D epitaxial growth feature should increase progressively with increasing deposition amount θ. As demonstrated in the last subsection, if there is no genuine uphill mass transport during epitaxial growth, and the 3D growth morphologies on the surface are simply induced by the combined effect of the stochastic nature inherent to both the deposition flux and adatom diffusion, as well as the effect of an infinitely large SE barrier at the step edges, the surface width W increases with increasing θ according to the Poisson growth mode, $W(L,t) \propto \theta^{1/2}$. If a practical or genuine upward mass transport is caused by some mechanism other than the stochastic nature of the deposition/diffusion or the SE effect, the growth width of the surface will also increase with increasing θ according to the power law $W(L,T) = \theta^{\beta}$ with a growth exponent $\beta > 1/2$. Hereafter, the growth behavior with a growth exponent $\beta > 1/2$ is called "super-epitaxial growth behavior." In the conventional kinetic theory, QDs are generally considered to grow via uphill mass transport of adatoms driven by the lattice-mismatch strain [189], which can be implemented well in KMC simulations [190–194]. In their KMC simulation of the heteroepitaxial growth (with the elastic property of the system similar to semiconductors) at a lattice mismatch of 5%, Ratsch *et al.* [192] observed the formation of 3D islands that grow according to the super-epitaxial growth law

$$h \propto \theta^{0.7}. \qquad (3.5.2.3.1)$$

This simulated result demonstrates that the elastic strain is slightly more efficient in driving uphill mass transport than the stochastic nature of the deposition and diffusion as well as the SE barrier in the Poisson growth. However, it has been experimentally shown that an InAs QD can rapidly grow into a mature height of more than 30 ML with an additional deposition of about 0.01 ML of InAs, with the former being about 3000 times larger than the latter [13]. This super-epitaxial growth behavior is indeed astonishing and extraordinary from the viewpoint of the conventional kinetic theory.

In fact, super-epitaxial growth behavior has reportedly occurred in many experimental studies of epitaxial growth. For example, Buatier de Mongeot *et al.* [195] observed super-epitaxial growth of Al huts on the Al(110) substrate due to the faceting instability of an unstable or metastable smooth crystallographic plane. These regular 3D Al islands have precise slope selection with the major and minor sidewalls terminated by the {111} and {100} planes or facets, and are 10 times taller than the Al deposition amount of 10 ML. The discovery of the formation of Al huts of unusual height is claimed and applauded as a significant step toward self-assembly of nanostructures during epitaxial growth by Fichthorn and Scheffler [196], and cannot be attributed purely to insufficient downward adatom diffusion induced by the SE barrier; in this situation, more significantly massive uphill adatom transport is obviously required [197, 198].

Incidentally, the super-epitaxial growth phenomenon defined above has also been experimentally observed in metal/semiconductor heteroepitaxial systems, where 3D epitaxial metal islands form with a preferred height because of quantum size effects (QSEs) or electronic growth [199, 200]. Among these systems that exhibit a QSE-induced height, 3D Pb islands in the Pb/Si(111) system stand out for their remarkably efficient super-epitaxial growth [201]. It was observed that during epitaxial growth of Pb on the Si(111)-(7×7) substrate with a slow deposition rate of 0.025 ML/min and a substrate temperature of 240 K [202], 3D Pb islands of 4–6 ML formed at a deposition coverage of $\theta = 1.5$ ML. When the Pb coverage increased by $\Delta\theta = 0.25$ ML, these 3D Pb islands grew by several monolayers. Furthermore, these Pb islands also exhibit an unanticipated fast lateral expansion on the Si(111) substrate. These behaviors are obviously inconsistent with the conventional kinetic growth theory based on adatom diffusion. On the basis of experimental observations [200, 201], it was suggested that the mass transfer for such super-epitaxial growth at a low temperature proceeds via continuous spreading of the Pb WL across the growth surface [201, 202].

3.5.3 Nanocrystal growth

From the viewpoints of both simple physical intuition

Frontiers of Physics

and conventional growth kinetic theories, building a QD on a growth surface in heteroepitaxial growth should be very similar to the construction of a skyscraper on the ground. The entire job can be divided into two parts, transporting building materials (adatoms) to the construction site and putting them into position. The first job can be conventionally described by adatom aggregation, as mentioned in Section 3.2; the second job can be traditionally described as nanocrystal growth in terms of the classic step-flow picture originally proposed by Burton, Cabrera, and Frank [203]. In models of nanocrystal growth, the growth surface is regarded as having the well-known terrace-step-kink structure model for a vicinal crystalline surface, and the key atomic events are intralayer transport of adatoms and their attachment to the kink sites or step edges [204, 205]. Currently, two speculative simple physical scenarios are frequently referred to in the literature on nanocrystal growth during the self-assembly of a QD. One of them is the method used by ancient Egyptian farmers to build a pyramid for their Pharaohs by using a large number of pieces of stone. In the pyramid-building kinetic pathway for nanocrystal growth [206–211], a square atomic layer with its length determined by the misfit-epitaxial stress is laid down first; then a second atomic square with a smaller size is laid down upon it, followed by a third atomic square with a still smaller size, and so on. Although it is efficient for building a pyramid with a square base, the pyramid-building method cannot deal with a multifaceted QD. Another kinetic pathway is the so-called facet growth mode. In the facet growth kinetics, a very small 3D precursor, which may be a small mound surrounded by a set of atomic steps [212, 213], forms first, either as the result of a thermal fluctuation or as a stochastic perturbation. As its size increases, the 3D precursor somehow becomes a small faceted 3D island with a regular geometric shape, such as a pyramid bound by the {105} facets in a Ge/Si(001) system or by the {137} face facets in InAs/GaAs(001). Once the faceted sidewalls are fully formed around the 3D island, classical 2D layer-by-layer nucleation and growth occur on these sidewall facets [214–222]. As the 3D island increases in size by facet growth, at some critical point, steeper facets successively appear on its sidewalls. It was also suggested that a QD forms by a combination of these two types of growth kinetics [223, 224]: the 3D island first grows in the layer-by-layer mode along the direction normal to the surface of the substrate, and then sidewall facets with certain crystallographic orientations are formed on it, and layer-by-layer growth proceeds on these sidewall facets.

According to the above physical scenario or classical step-flow growth mode, the nucleation of a new atomic layer on the sidewall facets is neglected, and there must be a train of steps for growth to proceed continuously. However, it is well known that the geometrical shapes of QDs are highly faceted in both InAs/GaAs(001) and Ge/Si(001), and the layer-by-layer growth process occurring on the nanofacets in the conventional kinetics should involve the repeated nucleation of a new atomic layer on these sidewall facets. To date, this topic has not been systematically discussed. It can be speculated that, similar to the surface relaxation process of a small crystallite below the roughening temperature, as discussed in Section 3.5.1, these nucleation events may also encounter a quite large energy barrier in the nanocrystal growth process, which would make QD formation a much longer process; this is significantly inconsistent with the experimentally observed timescale of InAs QD formation, as will be discussed further in the next subsection.

3.6 Timescale and nature of QD formation

Experimentally estimating and discussing the timescale on which an InAs QD forms can illuminate the nature of the process. In this subsection, the timescales consistent with the kinetic pathways for QD formation suggested in the conventional kinetic theories are analyzed and discussed.

3.6.1 Surface relaxation processes

In theory, the timescale for a surface relaxation to proceed should be determined by the surface kinetic coefficients or parameters, such as the adatom diffusion coefficient D_s and adatom concentration, which depend on the material parameters and the substrate temperature T. For MBE InAs/GaAs(001), these relevant material parameters are mostly unknown at present. However, we can obtain a basic idea of the timescale by looking at two relevant experimental observations in the literature.

As experimentally observed by Watanabe *et al.* [225], the flat surface morphology in MBE $Si_{0.75}Ge_{0.25}$/Si(001) formed with a relatively rapid deposition flux ($\leqslant$ 1.9 ML/s) at $T = 600$°C progressively roughened with a characteristic length scale L_c owing to the ATGS instability after the fluxes were turned off. According to the ATGS instability theory in the linear regime [226, 227], the roughening rate ω_c can be expressed as

$$\omega_c = D_s n_0 \left(\frac{\sigma_0^2}{2MkT}\right) \Omega^2 L_c^3, \tag{3.6.1.1}$$

where D_s, n_0, and Ω are the diffusivity, concentration, and volume, respectively, of the adatoms responsible for

mass transport on the surface; M is the plane strain modulus. The timescale for 3D morphology to form with a characteristic length scale can be defined as $\tau_c = 1/\omega_c$. For $Si_{0.75}Ge_{0.25}$/Si(001) at the substrate temperature $T = 600°C$ and $L_c = 80$ nm, it is theoretically estimated that $\tau_c \approx 20$ s, whereas in an experimental measurement of the material system, $\tau_c \approx 80$ s [225]. It will be shown in Section 3.6.4 that this order of magnitude (20 s or 80 s) for the timescale is remarkably larger than that experimentally observed for InAs QD formation in MBE InAs/GaAs(001), which is usually smaller than a fraction of 1 s. In addition, in the conventional relaxation theory of the nature of the QD formation process, it has to be assumed that an unstable or a metastable epitaxially strained film much thicker than the critical thickness of the WL should be well developed before the appearance of QDs, and, therefore, the timescale for QD formation should be much longer than the incident flux F. This is also obviously inconsistent with practical situations for the material system.

In the above case of surface morphological relaxation, the surface morphology changes via adatom diffusion, and no nucleation of a new atomic layer on the singular crystalline facet is involved; this corresponds to the situation above the roughening temperature of the surface. However, it has been well established experimentally that most of the sidewalls of an InAs QD are faceted, and, in theory, the corresponding relaxation process as well as the nanocrystal growth process has to involve the nucleation of new atomic layers on these faceted sidewalls of the nanoscale, which is much more time-consuming than the relaxation process that proceeds only via adatom surface diffusion.

It can be experimentally demonstrated that if the nucleation of new atomic layers on the facet is involved in the surface morphological relaxation, the timescale of the process will increase tremendously [228]. For example, an ice film 1 nm in average thickness formed by vapor deposition on a Pt substrate at 140 K is unstable [229], and it de-wets to form ice nanoislands on the surface during annealing. Just after epitaxial growth at 140 K, epitaxial ice islands about 3 nm in height were embedded in the one-bilayer ice WL on the Pt substrate. These ice islands have a flat top facet. The epitaxial structure is unstable and de-wets further, and the epitaxial ice islands grow via the nucleation of new molecular layers on the flat top facets. After 1 h of annealing, these ice epitaxial islands grew by just a few molecular layers in height [229].

Another example that involves a surface morphological change via a relaxation process below T_R and the nucleation of new atomic layers is an epitaxial micrometer-sized Pb crystallite formed by vapor deposition on the Ru(0001) substrate [230]. A Pb crystallite about 1 μm in diameter with a stable morphology can be achieved by lengthy annealing at a relatively high temperature. If the temperature is quenched to a relatively low temperature T_L, the surface morphology will relax toward a new steady state. In this surface morphological relaxation process, according to the Wulff–Herring reconstruction [231, 232] and Andreev mapping [233], the radius of the top facet of the Pb crystallite increases; this can be achieved only by layer-by-layer peeling of the atomic layers, and no nucleation of a new atomic layer is necessary. Experimentally, one atomic layer can be peeled off within half an hour if the temperature is quenched from 300°C to 150°C. In contrast, if the temperature is increased from 110°C to 205°C, the radius of the top facet of a crystallite will decrease, and this change in the surface morphology can be brought about only by the nucleation of new atomic layers on the facet. Experimentally, within a few days, no new Pb atomic layer can be observed to nucleate after the temperature is increased, and the original shape of the crystallite is trapped for a significantly long time [166].

According to the theory of relaxation processes, the situation that is most apparently similar to the formation of InAs QDs is the de-wetting of a Si film a few nanometers in thickness from the SiO_2 substrate [234], the so-called silicon-on-insulator system. In the de-wetting process, it was experimentally observed by low-energy electron microscopy [234] that voids exposing the substrate surface in the Si film are formed by heterogeneous nucleation at defects in the Si film. The area of a void grows linearly with time, and the Si material expelled from the void is accumulated as a rim around the void. The rim is crystallographically faceted, and its top facet is in the (001) orientation. As de-wetting proceeds, the area of the void is enlarged, and the height of the rim increases. The growth of the rim proceeds through the nucleation and growth of atomic layers on the (001) top facet, and the rate-limiting step is the nucleation of a new atomic layer on the top facet [234, 235]. At 770°C, the time interval between two atomic layer nucleation events is about 100 s [234]. Incidentally, the rims break down into separate silicon nanocrystallites. From these examples of relaxation processes occurring in small crystallites below the roughening temperature, as illustrated above, it should be clear that the surface relaxation process below the roughening temperature should proceed at a very slow rate.

3.6.2 Adatom aggregation

As shown in Section 3.2, it has long been conventional to

speculate that QDs form in heteroepitaxial growth by an adatom irreversible aggregation process. However, it can easily be shown that this speculation makes no sense for QD formation, at least in MBE InAs/GaAs(001), when we consider the difference in timescale between the results estimated according to the concepts of adatom aggregation and those obtained in experimental observations. We can have some idea of the time required for an adatom aggregate to form by examining the case of noble-metal clusters formed in metal vapor [236]: The typical metal vapor temperature T_{v} and pressure p_{v} are on the order of 1000–1500 K and 1–10 mbar, respectively. From the kinetic theory of an ideal gas, the atomic flux onto the surface sites of a spherical metal cluster of 100–200 atoms is estimated to be $\Phi_v \sim 10^7$ s^{-1}. Thus, a cluster of 10^3 atoms is formed on a timescale of a fraction of a millisecond [21]. In contrast, if a QD is formed via an adatom-diffusion-mediated aggregation process on a substrate, its growth rate should be proportional to the total number of adatoms, which is directly related to the incident flux F. If F is in the range of 0.1–0.01 ML/s, which is usually the case in MBE InAs/GaAs(001), the timescale to provide a sufficient number of adatoms for an InAs QD to form should be on the order of minutes at least, which is obviously inconsistent with experimental observations, as will be shown in Section 3.6.4. Furthermore, in vapor or in free space, metal atoms migrate with the thermal speed, which can be as high as several hundred meters per second. In contrast, on the growth surface in MBE InAs/GaAs(001), adatoms are chemisorbed on the lattice sites, and their speed in random motion is much slower. Hence, the extra time required for adatom diffusion has to be considered, which makes it impossible to speculate that an InAs QD should form via adatom diffusion and aggregation.

In the standard nucleation and growth theory mentioned in Section 3.2.3 for the adatom aggregation process on a surface, the average size of the adatom clusters should be consistent with the power law in Eq. (3.2.3.1), which has been experimentally confirmed in the Pb/Cu(111) epitaxial growth system [237, 238]. This implies that the growth rate of an adatom cluster formed by aggregation should be relatively small in comparison to the deposition flux F. In addition, a KMC simulation can also be used to estimate the timescale if QD formation proceeds via the adatom aggregation process. In KMC simulations, QD formation is essentially described as a strain-biased stochastic surface diffusion during which adatoms aggregate, and they have to climb up atomic step edges on a 3D epitaxial island driven by epitaxial strain. The QD grows in height h with coverage θ according to the power law $h \propto \theta^{0.7}$ at a lattice misfit of 5% [192], which should require more time in comparison to the incident flux $F = \theta/t$. In their KMC simulation using kinetic parameters suitable for Ge/Si(001), Gaillard *et al.* [158] obtained similar results for the slow growth rate of Ge QDs considered as an adatom aggregation process.

3.6.3 Structural phase transformation

As illustrated in Sections 3.1–3.5, the conventional kinetic theories in terms of the individual atomic events of QD formation in heteroepitaxial growth have been extensively explored in the last two decades. Among these theoretical processes, the surface relaxation process above the roughening temperature T_{R} should be the most rapid, as it involves only surface diffusion and no nucleation of a new atomic layer on a crystallographic facet at the nanoscale. Another type of dynamical processes that has been extensively studied in condensed matter physics is structural phase transformations in solids or crystalline materials induced by variation in a thermodynamic parameter such as the temperature or pressure. In general, a structural transformation requires no long-distance atomic diffusive motion, and it proceeds very rapidly through the entire body via atomic rearrangement or atomic displacement within the unit cells or in a crystallographic plane in the material system. Therefore, a structural transformation is often called a collective phase transformation and is similar to a sort of the "military" action. Three examples are presented below to illustrate the rapidness of a structural phase transformation in solid matter.

The first example is the structural evolution of an aluminum film 20 nm in thickness as it underwent an ultrafast laser-induced solid–liquid phase transition [239]. Under normal conditions, a solid should melt through equilibrium fluctuations. However, by using short-pulsed lasers to deposit heat at a rate faster than the thermal expansion, it is possible to prepare extreme states of solid matter at temperatures well above the normal melting point, T_{m}, by exciting electron states in the matter [240]. The energy stored in electrons can be transferred to the lattice within a fraction of a picosecond [240]. Solid aluminum in such an extreme state can be transformed into the liquid state within 3.5 ps, which can be measured by the femtosecond-resolved electron diffraction technique (see the review article Ref. [241]).

The second example is the solidification of a metallic alloy from its undercooled liquid. In the usual physical scenario for the solidification of metallic or semiconducting materials, atoms in the liquid independently jump across an interface and join the solid structure [242].

At the interface, the atoms should be incorporated into the crystalline structure more easily and rapidly than the diffusive process in the liquid. Therefore, under a certain undercooling condition, the rate at which the solid–liquid interface in a metal material advances can be approximated by the diffusive speed $V_D = D_L/a_0$, where D_L is the liquid diffusive constant, and a_0 is an interatomic spacing. In general, for a metallic material, $D_L \sim 10^{-6}$ m^2/s and $a_0 \sim 10^{-10}$, and V_D can be as high as few tens of meters per second [219, 243]. Therefore, the timescale for solidification on the nanometer scale should be nanoseconds.

The third example is the bcc–hcp (body-centered cubic–hexagonal close-packed) structural phase transformation in iron. At room temperature and ambient pressure, the so-called α-iron is in the bcc lattice structure. It is well known that under increasing pressure, iron exhibits a structural phase transition at ∼13 GPa from the bcc to the hcp structure. The transformation occurs by a non-diffusive martensitic process and can be viewed as a combination of an anisotropic compression in the (100) direction of the bcc phase with a shuffle in the (011) plane [244]. Therefore, the bcc–hcp structural phase transformation can be propagated in iron at a speed as high as the sound velocity, 5×10^5 m/s [245, 246].

As shown in the next subsection and Section 4, it can be experimentally demonstrated that the timescale for the MBE InAs QD formation process on the GaAs(001) substrate is quite short, which is obviously inconsistent with the kinetic models based on surface relaxation, adatom aggregation, and nanocrystal growth described in the previous subsections of this section. The observed timescale suggests that QD formation in a heteroepitaxial growth system such as MBE InAs/GaAs(001) is more likely to be a sort of structural transformation.

3.6.4 Experimental observations of the timescale of InAs QD growth

Experimentally, direct observation of epitaxial growth on the atomic scale is very difficult because of limitations in both the spatial and temporal resolution. In MBE InAs/GaAs(001), the dynamic evolution of an ensemble of QDs was generally monitored *in situ* via either RHEED [247–251], the photoluminescence optical properties [252], or XRD [253]. From these experimental observations, a timescale of at least a few seconds for InAs QD growth was extracted; this was regarded as quite fast in comparison with the deposition rate (which is usually $\leqslant$ 0.1 ML/s). However, these experimental measurements were made on an ensemble of InAs QDs instead of an individual QD; therefore, in interpreting the results of these experiments, it has to be assumed artificially that a large number of InAs QDs nucleate randomly or statistically within a very brief nucleation stage, and then that all these QD precursors grow simultaneously in a later stage during epitaxial growth. It should be obvious that these assumptions are inconsistent with experimental practice for the MBE InAs/GaAs(001) system, which will be further demonstrated in Section 4.

To perform *in situ* experimental observations under realistic growth conditions without a quenching process, during which the temperature of a sample for STM imaging is lowered from the growth temperature to room temperature, Tsukamoto *et al.* [254, 255] placed the STM inside the MBE growth chamber; this technique was called STMBE. They observed that the local 2D–3D transition occurs at the critical InAs coverage on the WL very rapidly in comparison to an ultralow deposition flux, in which a 3D feature 1.45 nm in height and 7.5 nm in width is well developed within a coverage interval of 0.01 ML, corresponding to a time of a few seconds. However, the experimental observation of Tsukamoto *et al.* [254, 255] was performed at a very low F and a growth temperature of $T = 400$°C, which is considerably lower than the normal growth temperature (by about 100°C). Note that the substrate temperature significantly affects the growth dynamics in MBE InAs/GaAs(001). Hence, the dynamics of InAs QD formation may differ significantly between these two growth temperatures, 400°C and 500°C.

As will be demonstrated in Section 4, a QD in MBE InAs/GaAs(001) can self-assemble itself instantaneously or within a time less than 2×10^{-5} s under a given growth condition, which is remarkably inconsistent with the classical kinetic theories describing individual atomic movements according to the solid-on-solid model. In Section 6, a novel physical scenario will be presented for a reasonable interpretation of the instant formation of InAs QDs in the MBE InAs/GaAs(001) system.

3.7 Wetting layer (WL)

Although, like many other issues in the formation of InAs QDs, the physical nature of the InAs WL is still poorly understood [256], the basic physical picture of WL formation in the SK growth mode often seems to be rather clear and simple in many theoretical models as well as in the interpretation of experimental observations in the literature: A planar WL grows into a critical thickness via the layer-by-layer growth mode on the substrate before 3D epitaxial islands begin to form or the 2D-to-3D morphological transition occurs, and the WL thickness should be uniquely determined by either the energetics or

the thermodynamics [257–267]. Therefore, the main task in a theoretical investigation of the mechanism of WL formation in the SK growth mode should be to identify various contributions to the formation energy of the WL and the QDs by a technical theory such as first-principles calculations.

In experimental practice, it is well known that there are a large variety of heteroepitaxial growth systems that are traditionally classified as the SK growth mode: One or two flat atomic layers of the deposited material form first on the bare substrate, and the formation of 3D crystallites follows. However, each of these has its own particular physical or chemical mechanism for WL formation, which is determined exclusively by such factors as the lattice mismatch, chemical bonding (metallic versus covalent), surface reconstruction, and surface segregation effect. Therefore, there should be no common growth mode (such as layer by layer) or universal factor (such as energetics) suitable for all of the heteroepitaxial systems in which the so-called SK growth phenomenon occurs, as idealized by many theoreticians in the literature. For example, it is generally considered that group-III or group-V metals on a semiconductor substrate, such as Si(111)-(7×7), are typical systems for the SK growth mode. At a relatively high substrate temperature, it commonly occurs that when 1/3 ML of metal has been deposited, the surface reconstruction is transformed from Si(111)-(7×7) to the $(\sqrt{3}\times\sqrt{3})$R30° one [268, 269]. In each unit cell of this reconstruction, one metal atom is chemically bonded by three Si adatoms (each having one dangling bond) to form a metal–Si_3 unit, such as Ga–Si_3 on the Si(111) substrate [270]. As the metal coverage increases further up to one or two atomic layers, a large number of surface reconstruction phases or exotic surface structures occur in sequence before epitaxial 3D islands form at the 2D-to-3D growth mode transition with increasing coverage [271]. Another prototypical form of heteroepitaxial growth, in which the SK growth mode is considered to occur, is found in the bimetal epitaxial growth system Pb/Cu(111) [272–274]. It has been experimentally observed in this system that below 0.4 ML of Pb coverage, an ordered surface Pb–Cu alloy is formed; when the Pb coverage is increased further, the surface alloy decomposes or de-alloys, and 2D Pb islands are formed [273]. Increasing the Pb coverage further causes a Pb film in the (111) orientation to form with a lattice constant close to the Pb bulk value until a complete film is formed [272]. Upon further Pb deposition, atoms are initially squeezed into this first layer, compressing the film laterally by up to 3%. During the formation of the compressed Pb layer, its lattice constant increases smoothly with increasing coverage independent of the substrate, indicating that the film is incommensurate with the substrate and floating on it. Deposition of more Pb finally forms the second Pb layer. At high temperatures above 300 K, 3D Pb islands subsequently grow. There may be different reasons for compression of a monolayer; one of them is that the binding energy of the adatoms to the substrate is high, so as many adatoms as possible will try to bind [272]. This process for the formation of a WL, which proceeds via the alloying and de-alloying stages in sequence as the coverage is increased, is very common for metal–metal heteroepitaxy. Obviously, growth processes leading to WL formation that are as complicated as those encountered in the Ga/Si(111) and Pb/Cu(111) systems cannot be described by the relatively simple layer-by-layer growth mode.

For MBE InAs/GaAs(001), Yu and Tersoff [275] attributed WL formation to surface segregation of indium, and they estimated the InAs WL critical thickness h_c by considering the effect of segregation. Walther *et al.* [276] experimentally studied the crucial role played by In segregation in InGaAs/GaAs(001) and concluded that 3D island formation begins when the average concentration of indium segregated at the surface reaches a value of $\sim$85%. Belk *et al.* [277] and Krzyzewski *et al.* [278] found experimentally that during the growth of an InAs WL, a variety of surface reconstructions can be observed, including $c(4 \times 4)$, (1×3), and (2×4). Prohl *et al.* [279, 280] studied the evolution of the InAs WL with increasing InAs coverage during epitaxial growth in MBE InAs/GaAs(001)-$c(4 \times 4)$ using STM and observed that the WL growth behavior is much more complicated than the conventional layer-by-layer growth mode as which it is usually regarded. They observed that at an InAs coverage of less than 0.6 ML, indium signatures appear on the hollow sites of the unperturbed GaAs(001)-$c(4 \times 4)$ reconstruction. The number of these indium signatures increases proportionally with increasing InAs coverage. However, their atomic structure is not clear, and it is not known whether they are crystalline. When the indium coverage increases to 0.6 ML, the surface transforms into an atomic alloyed $In_{2/3}Ga_{1/3}As$ layer with (4×3) reconstruction, which was previously proposed on the basis of XRD data [281]. At an InAs coverage of 1.42 ML, the growing surface become an InAs(001)-(2×4) reconstructed surface. Subsequently, InAs QDs begin to form as the InAs coverage increases further.

In Section 6, a very simple "mechanical" mechanism will be proposed for the formation of the WL in the MBE InAs/GaAs(001) system.

3.8 Size limitation on the growth of InAs QDs

After growing to a certain volume, an InAs QD is ex-

perimentally stable against further growth and seems to have a "magic" size under ongoing deposition flux, as first noticed by Leonard *et al.* [13]. The phenomenon of self-limited growth or self-organization in InAs QD size cannot be properly explained by the conventional theoretical descriptions. Like many issues on the topic of the self-assembled QDs, the mechanism of the InAs QD stability against further growth remains a puzzle. An ensemble of QDs may have a global average size favored by thermodynamics, which may contribute to producing a uniform size distribution against Ostwald ripening; however, it cannot explain the island stability against further growth under an ongoing incident flux. Because the QD stability against further growth occurs uniquely in heteroepitaxial growth systems, such as InAs/GaAs, with an appreciable lattice misfit, it is tempting to interpret the stability in terms of the relaxation of the misfit strain [282], which can be theoretically proved for 1D and 2D systems [283, 284], such as atomic chains and disks, that are coherent to the substrate with a smaller lattice parameter. As noted by Tokar and Dresse [283], in these 1D and 2D cases, their free ends or edges relax outwardly, thus providing a mechanism for strain relief with an energetically favorable length or diameter. However, for InAs QDs, 3D epitaxial islands grow in the vertical direction, and the strain relaxation mechanism is no longer applicable. This subsection describes the interpretations of the self-limited growth and stability against the growth mechanisms for InAs QD formation.

The QDs' stability against further growth under an incident flux may call to mind atomic clusters of metals or inert gases containing a magic number of atoms owing to electronic or atomic shell effects in the gas phase [285, 286] or magic metal clusters supported on a surface, which are either induced by QSE [287, 288] or mediated by surface reconstruction [289, 290]. However, these magic metal clusters are much smaller than an InAs QD containing more than 10^4 atoms, as they are usually composed of a number of atoms ranging from a few up to several hundreds, or have a height of a few atomic layers. Furthermore, the stability of these magic clusters is relatively weak, and there may be peaks of several sizes simultaneously representing magic clusters of different sizes in the system. In contrast, the "magic" size of the InAs QDs in an ensemble is unique.

To explain the narrow QD size distribution, Priester and Lannoo [291] suggested a model of QD formation in terms of thermodynamic concepts, via which an ensemble of 2D islands forms first with a narrow peak in the island size distribution, as the islands have a thermodynamically favored size. Then, a morphological transformation occurs somehow in which these 2D epitaxial islands spontaneously transform into 3D islands, and the number of atoms in each epitaxial island remains unchanged. Alternatively, Heyn [92] suggested a more simplified mechanism for the QD stability against further growth; he simply formulated the growth rate R of a 3D island in the form $R \propto (1 - V_s/V_p)$ (where V_s is the volume of the growing island, and V_p is a pre-fixed volume). It can easily be seen that the QD growth rate decreases as its volume increases during its growth, and the growth automatically stops at the mature volume V_p. In discussing their experimental results, Leonard *et al.* [13] suggested that the stability of the InAs QDs against further growth is associated with a very high energy barrier for the formation of misfit dislocations in the interface area underlying an InAs QD. Alternatively, Kudo *et al.* [292] supposed that the stability of a mature QD results from its stable faceted sidewalls, which do not incorporate additional atoms after formation.

The stability of 3D epitaxial islands of a certain size against further growth with ongoing deposition in heteroepitaxial growth seems to be unique to group-IV, III-V, and II-VI semiconductors. In contrast, epitaxial metal islands in epitaxial growth usually exhibit unlimited grow with increasing deposition. For example, 3D epitaxial metal islands (e.g., Au/NaCl(001) [293] and Pd/TiO_2(110) [294]) obtained in Volmer–Weber growth may be uniform in size [295, 296]; however, these metal epitaxial islands always grow continuously with increasing coverage.

4 Experimental observations of MBE InAs/GaAs(001)

In this section, a remark is first made on the diverse nature of the experimental data accumulated to date for InAs QD formation in MBE InAs/GaAs(001) in the literature. Next, the experimental observations on this topic made by the authors themselves are summarized to show more clearly the diversity of InAs QD formation under different growth conditions, and to demonstrate that an InAs QD can form within a time as short as $< 10^{-5}$ s under a certain growth condition.

4.1 A large variety of experimental data in the literature on the formation of InAs QDs

We can divide all the phenomena of scientific and technological interest into two categories: static or equilibrium phenomena and evolving or dynamic ones. The phenomena in the first category are usually simpler and more uniquely defined; in contrast, dynamic phenomena usu-

ally depend on the initial conditions and proceed by a large variety of different pathways, as noted by Levi and Kotrla in an article on the simulation and theory of crystal growth [297]. Sometimes, via these different paths, an evolving system may arrive at an equilibrium state independent of both the initial conditions and the pathway it has taken. More frequently, the evolving system may be locked into one of the kinetically limited states in the middle of the pathway it has taken by a very large kinetic energy barrier; alternatively, the temporally evolving system is highly sensitive and susceptible to a number of external factors that significantly affect the evolution process. In consequence, when a dynamical process is investigated, a large variety of distinct phenomena may be observed in practice.

The epitaxial growth of InAs QDs is a very complex experimental phenomenon, as it is highly delicate and sensitive to slight variations in the MBE growth conditions. In other words, the process seems to be chaotic, and slight variations in the initial conditions and environment during the process may cause an enormously large change in the outcome [298]. Therefore, the experimental data accumulated on the topic to date in the literature provide only a kaleidoscope through which a large variety of QD growth behavior can be observed, instead of suggesting some consensus that might be framed within one of the conventional kinetic theories that have been thought to be appropriate to epitaxial growth phenomena. For example, it was experimentally observed that the variation in the InAs QD density as a function of InAs coverage may be a power-law function [13, 299], a linear form [15], or an exponential function [16, 17], depending on the respective growth conditions, such as the substrate temperature, incident flux, and deposition method.

It seems that the experimentally observed diversity in InAs QD epitaxial growth makes the phenomenon remarkably flexible and benefits the theoreticians working with distinctly different technical theories in formulating the QD growth process, as each of them can always find some experimental evidence in the literature for their own theoretical models. To further illustrate this situation, some examples are listed below:

1) Zhang *et al.* [48] attributed the formation of QDs in heteroepitaxial growth to the ATGS instability and analyzed the kinetics of QD formation by numerically solving a nonlinear evolution equation for the film surface shape and morphology. They found that their calculated results were fitted well by the experimental observations made by Floro *et al.* [300] on the heteroepitaxial growth system of SiGe/Si(001).
2) Chen and Washburn [82] suggested that QD formation is similar to an adatom aggregation process for the formation of a 2D island. In their model, initially, a number of adatoms irreversibly aggregate into a 2D epitaxial island, which grows progressively in size. At a critical number of atoms N_c, as determined by the energetics, the 2D island spontaneously changes to a 3D island, which continues its progressive growth by collecting more adatoms. Hence, the evolution of the island size distribution with increasing coverage can be expressed by Eq. (3.2.3.6), $n(s,\theta) = (\theta/s_{\rm av}^2)f(s/s_{\rm av})$. By direct integration, $N_{\rm QD} = \int_{N_c}^{\infty} n(s,\theta){\rm d}s$, the QD density $N_{\rm QD}$ can be obtained using the scaling function $f(u) = 1.1\exp(-0.27u^{3.7})$ and $s_{\rm av} \propto \theta$ [119]. Chen and Washburn successfully fitted their calculated data with the experimental results of Leonard et al. on InAs/GaAs(001) [13].
3) Similar to Chen and Washburn [82], Dobbs *et al.* [81] also suggested that the QD formation process is equivalent to adatom aggregation that results in the formation of 2D epitaxial islands, which then, at a critical 2D island size, spontaneously become 3D ones. Dobbs *et al.* theoretically estimated the variation in the QD density with increasing coverage θ using the MFREs and obtained a dog-leg curve, which was experimentally supported by experimental data on metalorganic vapor phase epitaxy growth of InP islands on the GaP-stabilized GaAs(001) substrate.
4) In addition, Meixner *et al.* [301] simulated QD formation using the KMC simulation method and found rather good agreement between their simulation results for the island density and experimental results for both Ge/Si(001) and InAs/GaAs(001).
5) In comparison with the theoretical works of Chen and Washburn [82] and Dobbs *et al.* [81], Wang *et al.* [302, 303], suggested an entirely different scenario. They subdivided the QD formation process into three distinct stages. In the first stage, nucleation, a regular array of 3D island nuclei with a fixed number density is formed. In the second stage, growth, these 3D nuclei grow in size with increasing coverage θ. Finally, coarsening occurs in the island array. However, before the process arrives at the third stage, the growth stage can be trapped in a constrained thermodynamic equilibrium state in which both the 3D island shape and size are uniform. Wang *et al.* [302, 303] theoretically calculated the formation energy of a 3D island required to fix its shape and size by trapping it in the second stage

and found that their calculation results were confirmed by the experimental data of Moison *et al.* [12] and Polimeni *et al.* [304] on InAs/GaAs(001).

6) As described in Section 3.1.2, Osipov *et al.* [69, 70] suggested a kinetic model on the basis of the CNGT for QD formation in terms of the first-order phase transformations. It is intrinsically different in nature from either the adatom aggregation model used by Chen and Washburn [82] and Meixner *et al.* [301] and the model of Wang *et al.* [302, 303]; in the kinetic model of Osipov *et al.* [69, 70], QD nucleation occurs in a well-developed uniformly elastically strained film of thickness h trapped in a thermodynamic metastable state characterized by a "supersaturation" $\zeta \equiv h/h_{\mathrm{eq}} - 1$. In this model, the QD nucleation rate, QD growth rate, and evolution of the island size distribution with increasing coverage can be calculated theoretically using the mathematical formula established for the kinetics of the first-order phase transformation. Their calculation results for the average island size and island density were found to be consistent with the experimental data obtained from an InAs/GaAs(001) system [73].

In addition, many experimentalists have successfully managed to fit their own experimental observations on the QD formation without much difficulty on the QD formation with one of the theoretical approaches that have been formulated by theoreticians from different theoretical schools. For example, as mentioned in Section 3.2.4, Leon *et al.* [124] and Shiramine *et al.* [125] successfully fitted their experimental data for InGaAs/GaAs(001) to Venables' theoretical expression for the saturated density of 2D epitaxial islands [93], which was established originally for 2D epitaxial islands in the submonolayer regime of homoepitaxial growth. Furthermore, in general, InAs QDs are experimentally observed to be uniform in both size and shape; i.e., the island size distribution is quite narrow. Therefore, an underlying mechanism for self-limited QD growth is firmly believed to exist in the literature; however, both Ebiko *et al.* [127] and Fafoni *et al.* [89] experimentally found that the island size distribution of QDs is in accordance with the scale-invariant form $n(s, \theta) = (\theta/s_{\mathrm{av}}^2) f(s/s_{\mathrm{av}})$, which had been confirmed to be suitable only for diffusion-mediated atomic aggregation processes on a solid surface without any regulation or limitation on their size during epitaxial growth.

To comprehensively review these divergent experimental observations is very challenging and difficult. Hence, in the following, the authors simply summarize the experimental observations of InAs/GaAs(001) QD growth performed in their own lab to emphasize the divergence of the experimental observations and to further reveal the significant rapidness of InAs QD formation.

4.2 Progressive epitaxial growth mode of InAs QDs

Much of the condition in our experiments described here has been published previously [15–17]. For readers' convenience, they are described in detail as follows. A buffer layer was grown on a GaAs(001) substrate at $T = 580$°C; it consisted of 500 nm GaAs, 10 periods of an AlAs (2 nm)/GaAs (2 nm) superlattice, and 10 nm GaAs, in growth sequence. Subsequently, T was reduced to 500°C or 520°C in 5 min for deposition of 1.8 ML of InAs to fabricate InAs QDs under an As_4 atmosphere to maintain a $c(4 \times 4)$-reconstructed growth surface on the bare GaAs(001) substrate. At $T = 500$°C, the incident indium flux was 0.1 ML/s, whereas at $T = 520$°C, it was 1.0 ML/s. After the deposition of 1.8 ML of InAs, the grown sample was immediately quenched to room temperature. During InAs deposition, substrate rotation was stopped to obtain inhomogeneous InAs coverage ranging from 1.5 ML to 3.0 ML at 0.1 ML/s and 500°C and from 1.6 ML to 2.2 ML at 520°C across the 2-in. diameter of the GaAs(001) substrate. Morphological measurements using AFM were made step by step along the [110] direction; the steps were separated by 0.15 mm or 0.5 mm, which can be converted to the increment of $\Delta\theta = 0.004$ ML or $\Delta\theta = 0.006$ ML, respectively. The variation in the InAs coverage with the distance along the substrate diameter was assumed to be approximately linear.

Experimental observation of the variations in the areal density $N_{\mathrm{QD}}(\theta_{\mathrm{eff}})$ and the average size of the InAs QDs with increasing effective coverage $\theta_{\mathrm{eff}} = \theta - \theta_c$ is a simple and straightforward macroscopic way to study the evolution of an ensemble of InAs QDs, where θ is the nominal InAs deposition, and θ_c is the critical coverage at which the formation of the WL is completed and QD formation begins. Under the normal growth conditions ($T \sim 500$°C, $F \sim 0.1$–0.01 ML/s, As pressure 4×10^{-6} Torr), it is frequently observed that the QD formation process exhibits a progressive growth regime during which an InAs QD precursor progressively grows to mature height with increasing θ_{eff}. This progressive QD growth behavior is called the "progressive growth mode" hereafter. The authors have reported that under the MBE growth conditions of $T = 500$°C and $F = 0.1$ ML/s, the formation process of a QD ensemble exhibits two distinctive growth regimes characterized by different power laws, $N_{\mathrm{QD}}(\theta_{\mathrm{eff}}) \propto \theta_{\mathrm{eff}}^{1.8}$ and $N_{\mathrm{QD}}(\theta_{\mathrm{eff}}) \propto \theta_{\mathrm{eff}}^{0.6}$, respectively, as shown in Fig. 1 [299]. Note that the distinct InAs QD growth regimes characterized by these

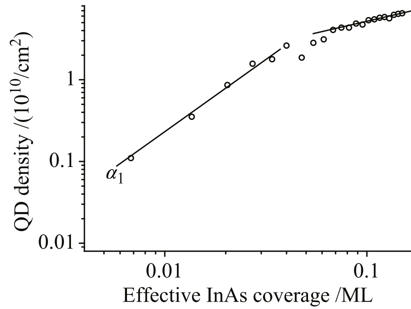

Fig. 1 Areal density of QDs N vs. effective InAs coverage θ_{eff}.

power laws are very analogous to the growth regimes characterized by $N_x \propto \theta^3$ and $N_x \propto \theta^{1/3}$, respectively, for the nucleation and growth of 2D epitaxial islands in the submonolayer growth regime in homoepitaxial growth, as described in Section 3.2.2. More generally, a rapid nucleation stage followed by a relatively long growth stage, each of which is characterized by a different power law, is a universal phenomenon in the nucleation–condensation processes that occur in a large variety of physical, chemical, and biological systems [305, 306].

The AFM snapshots and corresponding QD height histograms in Fig. 2 represent the two growth regimes characterized by the two power laws. At the moment when θ_{eff} is infinitely small in the first growth regime, there are only a few QD precursors, all shorter than 1 nm, as shown in the height histogram [Figs. 2(a) and (b)]. With slightly more InAs coverage, the height histogram evolves into a decreasing function of θ_{eff}, as shown in Figs. 2(c) and (d). These figures demonstrate that at the very beginning of QD formation, QD precursors of very low height begin to nucleate, and they grow in height progressively with increasing InAs coverage; as these first QD precursors grow in size, an increasing number of new QD precursors nucleate and grow in a temporal sequence, and the average height histogram shown in Fig. 2(d) is a

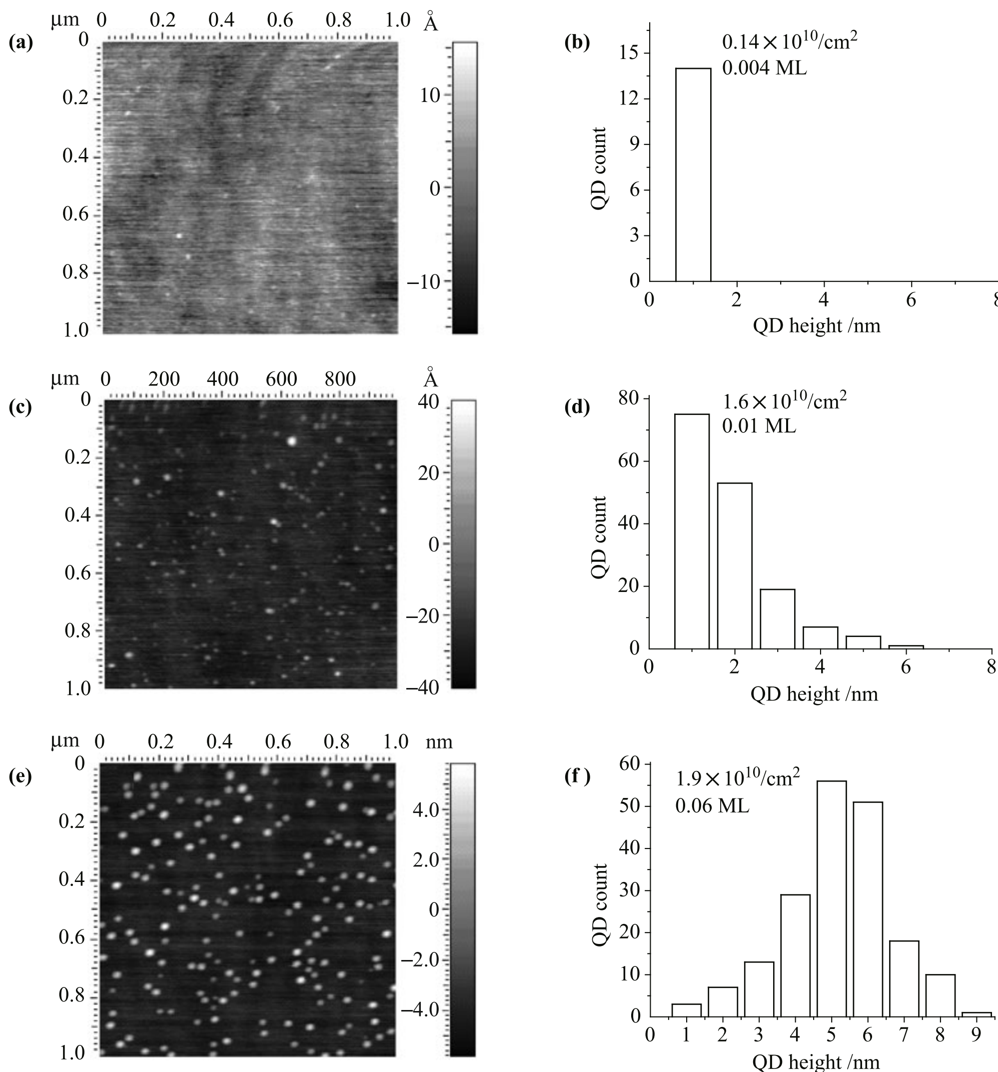

Fig. 2 **(a, c, e)** AFM images of QDs under $F = 0.1$ ML/s and $T = 500$°C; **(b, d, f)** corresponding height histograms.

monotonically decreasing function. At about $\theta_{\text{eff}} = 0.042$ ML, where the height histogram [Fig. 2(f)] has become a Gaussian type, the first growth regime, characterized by the power law $N(\theta_{\text{eff}}) \propto \theta_{\text{eff}}^{1.8}$, terminates, and the growth behavior crosses over into the second growth regime. In the second regime, characterized by $N(\theta_{\text{eff}}) \propto \theta_{\text{eff}}^{0.6}$, the QD number density increases with increasing InAs coverage at a much lower rate.

In the second growth regime, new QD precursors still nucleate but at a much slower rate than that in the first growth regime. As shown in Fig. 2(f), in the second regime, the height histogram of the InAs QDs is a Gaussian type centered around 5 nm, instead of a decreasing function of height as in the first growth regime, as shown in Fig. 2(d). This implies that the manner of QD growth in the second regime should differ significantly from that in the first regime. In the first growth regime, different QD precursors nucleate at different instants, and the QD height histogram has the form of a decreasing function [Fig. 2(d)]. In contrast, in the second growth regime, a QD may grow very quickly after nucleation instead of progressively with increasing coverage as in the first growth regime, and the rapid QD growth results in the Gaussian-type height histogram in Fig. 2(f). These experimental observations even suggest that these QDs are in the same ensemble and grow under the same experimental conditions; they grow in different growth modes only because their local environments, as determined by the local QD density, are different from each other.

The variations with increasing coverage in the average QD height and base diameter are also distinctly different in the two growth regimes. As shown in Fig. 3, the average QD height h and QD width w both increase with increasing coverage in the first growth regime. In contrast, at the beginning of the second growth regime at about 0.042 ML, h decreases rapidly from more than 5 nm to about 4.2 nm as the coverage increases from 0.042 ML to 0.044 ML; simultaneously, w decreases from 32 nm to 29.5 nm. Subsequently, w fluctuates at very small amplitudes, whereas h decreases continuously from 4.2 nm to 3.4 nm with increasing InAs coverage. The reduction in h with increasing InAs coverage and QD density has been experimentally observed [307], and the phenomenon was interpreted as a result of repulsive elastic interactions between these 3D islands [307].

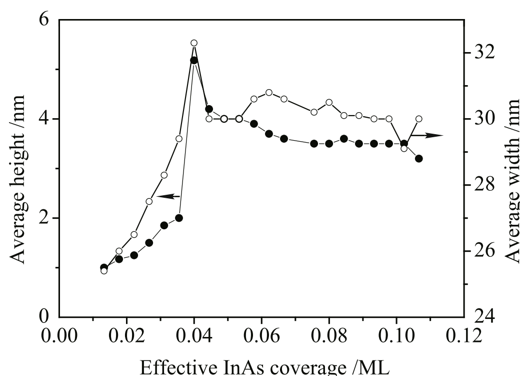

Fig. 3 Average height and width of QDs, h_{ave} and w_{ave}, vs. the effective InAs coverage for $F = 0.1$ ML/s.

In Section 3.6, it was mentioned that the timescale for QD growth completion was estimated by techniques such as RHEED [247–251], photoluminescence [252], and XRD [253]. A more direct and accurate measurement method for extracting the timescale is based on snapshots obtained in neighboring regions on the growth surface using STM and ATM. For example, at $T = 490°\text{C}$ and $F = 0.017$ ML/s [12], the first mature QD appears in the STM snapshot at $\theta_{\text{eff}} = 0.06$ ML InAs; on the basis of the experimental data and the expression $\theta = Ft$, the time an InAs QD requires to self-assemble itself into a mature state is estimated to be $0.06/0.017 = 3.5$ s, which is somewhat longer than the value (0.06 ML/0.1 ML/s = 0.6 s) estimated from the AFM snapshots in Fig. 2 in the first growth regime in the progressive growth of MBE InAs QDs.

4.3 Instantaneous epitaxial growth mode of InAs QDs

The authors found that, under the MBE growth conditions of $T = 520°\text{C}$, $F = 1.0$ ML/s, and $P_{\text{As}} = 6 \times 10^{-6}$ Torr, the epitaxial growth behavior of InAs QDs is obviously distinct from the progressive growth mode described in Section 4.2. In contrast to the progressive growth mode, the growth behavior described here is termed the "instantaneous growth mode," and the terminology will be further explained in the following. As shown in Figs. 4(a)–(f), even at the beginning of InAs QD formation when θ_{eff} is infinitely small, only a very few mature QDs 13 nm in height were observed at number densities below $10^7/\text{cm}^2$, and there was no sign of very short QD precursors as observed in the progressive growth mode described in Section 4.2. These experimental observations using AFM indicate that the InAs QDs shown in Fig. 4 have not undergone a progressive epitaxial growth process with increasing InAs coverage θ, and these QDs seemed to grow into maturity instantaneously or within a very short time after their nucleation. A similar instantaneous growth mode of InAs QDs was also reported by Guimard *et al.* [308] in metalorganic chemical vapor deposition growth with a low growth rate of 0.01 ML/s and $T = 520°\text{C}$. Similarly, the instantaneous growth mode has also been experimentally observed in MBE Ge/Si(001) [140]: only quite large and uniform Ge

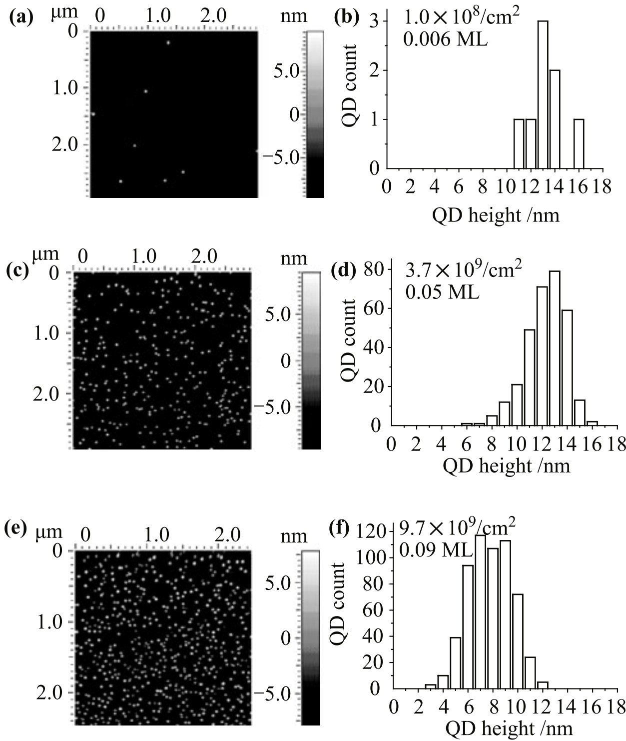

Fig. 4 **(a, c, e)** AFM images of QDs under $F = 1.0$ ML/s and $T = 520°$C; **(b, d, f)** corresponding height histograms.

QDs were observed to increase in number density with increasing Ge coverage, and no trace of Ge QD precursors appeared in a certain range of Ge coverage under the given growth conditions.

For the instantaneous InAs QD epitaxial growth mode, the upper limit of the timescale for a mature InAs QD to form can be estimated using sequential AFM snapshots, as shown in Fig. 4. These AFM images reveal that the QD density increases continuously with increasing $\theta_{\rm eff}$. The increment $\Delta\theta_{\rm eff}$ in the InAs coverage can be converted into the increment Δt in time via the relation $\Delta\theta_{\rm eff} = F\Delta t$. The increment in the QD density $\Delta N(\theta_{\rm eff})$ is easily discernible by comparing the two AFM images taken at two regions a few micrometers apart on the surface. Without substrate rotation, $\theta_{\rm eff}$ varies approximately linearly across a diameter (50 mm) of the GaAs(001) substrate, and the total variation is about 20% [309]. In our experiment, the nominal total InAs deposition is 1.8 ML. On the basis of these experimental data, the variation in $\theta_{\rm eff}$ across a distance of 5 μm should be $\sim 2\times10^{-5}$ ML, which can be converted to 2×10^{-5} s for $F = 1.0$ ML/s. Incidentally, such a short time is equivalent to the effective frequency of the diffusion hop of an adatom from site to site on a crystalline lattice in the normal growth condition for homoepitaxial growth on the GaAs(001) substrate [26]. The additional InAs QDs across a distance of 5 μm must grow into maturity within 2×10^{-5} s in the instantaneous growth mode. Such a remarkably rapid growth process for an InAs QD to form cannot be implemented via individual atomic events on a surface, such as atomic diffusion and adatom attachment to step edges one by one, as in a conventional kinetic theory of a nanocrystal growth process that takes at least more than a few seconds, as demonstrated in Section 3.4. Therefore, the self-assembly of an InAs QD in the instantaneous growth mode should be a collective atomic event involving more than 10^4 atoms simultaneously, more similar to a structural transformation in condensed matter, instead of conventional epitaxial growth or a surface relaxation process that can be properly described by the conventional kinetic theory described in Section 3. In Section 6, a novel physical scenario for the formation process of InAs QDs will be proposed to explain the rapidness of InAs QD formation.

As shown in Fig. 5, the experimental data for $N(\theta_{\rm eff})$ versus $\theta_{\rm eff}$ obtained from the AFM images in Fig. 4 are fitted well by the exponential function

$$N(\theta_{\rm eff}) = N_0 \exp(A\theta_{\rm eff}) \tag{4.3.1}$$

when $\theta_{\rm eff} \leqslant 0.05$ ML, where N_0 and A are constants independent of the effective coverage $\theta_{\rm eff}$. When the effective InAs coverage $\theta_{\rm eff} > 0.05$ ML, the QD number density $N(\theta_{\rm eff})$ tends to be saturated as $\theta_{\rm eff}$ increases further. These experimental observations indicate that in the instantaneous growth mode, InAs QDs are formed sequentially (which will be further explained in this subsection), instead of a large number of QD precursors randomly nucleating almost together at first and then growing simultaneously to maturity, as in the progressive growth mode. Figure 6 shows that initially, the average width and height of the mature QDs remain constant with increasing $\theta_{\rm eff}$. However, when $\theta_{\rm eff}$ increases above around 0.08 ML and the QD density is 6×10^9 cm^{-2}, the average height and diameter both decrease significantly. This experimental observation indicates that, similar to the situation in the progressive growth mode, a mature QD in the instantaneous growth mode is stable against further growth but unstable against a reduction

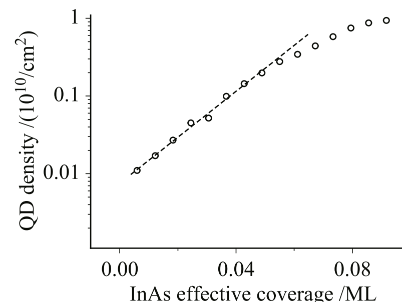

Fig. 5 Areal density of QDs N vs. effective InAs coverage $\theta_{\rm eff}$.

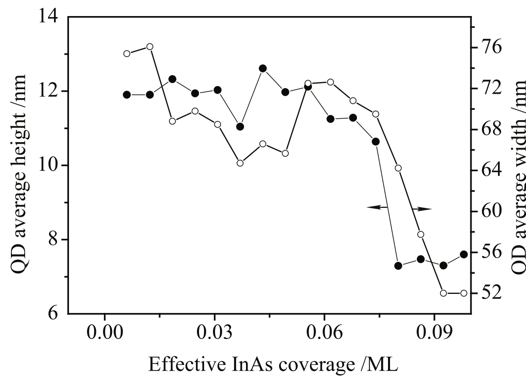

Fig. 6 Average height and width of QDs, $h_{\rm ave}$ and $w_{\rm ave}$, vs. the effective InAs coverage for $F = 1.0$ ML/s.

in size, probably because of elastic interactions among themselves when the QD areal density increases to a relatively large value [84, 307]. However, the progressive and instantaneous growth modes differ remarkably in the relationship between the InAs QD size and the InAs coverage. In the first growth mode, the average height and diameter of the InAs QDs decrease or vary monotonously with increasing InAs coverage or QD number density in a continuous way. In contrast, the average height and diameter of the InAs QDs in the instantaneous growth mode remain almost constant and decrease abruptly at a certain $\theta_{\rm eff}$ or QD number density with increasing InAs coverage.

The instantaneous growth of InAs QDs as well as the physical mechanism underlying Eq. (4.3.1) are described phenomenologically as follows. After the InAs WL is formed in the instantaneous growth mode, the first 3D island precursors appear spontaneously, and they grow instantaneously into mature QDs. Because there are only a few isolated QDs in a relatively large area on the surface at first, the formation of a single QD may use up all the indium material available in that region on the growth surface, which is perhaps as large as a few hundred square micrometers (as estimated from the QD density of $\sim 1 \times 10^7/{\rm cm}^2$). After the first QDs form, more of them are formed in the same way successively with as $\theta_{\rm eff}$ increases further. To explain the exponential relationship between the InAs QD density and the effective InAs coverage, Eq. (4.3.1), it seems necessary to assume that the production rate of QDs should be proportional to the additional $\theta_{\rm eff}$, that is, ${\rm d}N(\theta_{\rm eff})/{\rm d}\theta_{\rm eff} \propto \theta_{\rm eff}$. The effective InAs coverage, $\theta_{\rm eff}$, should have two sources. The first source is the direct impingement of atoms from the growth flux onto the unoccupied area on the surface, whereas the second source is lateral mass transport from the area occupied by mature QDs to the unoccupied area, where new QDs will be self-assembled. In consequence, $\theta_{\rm eff}$ may be expressed as the sum of the two terms: $\theta_{\rm eff} = A_1 F + A_2 N(\theta_{\rm eff})$, where A_1 and A_2 are proportional constants independent of $\theta_{\rm eff}$. If the number density $N(\theta_{\rm eff})$ of InAs QDs increases continuously and F is fixed, the effective area on the growth surface that can accommodate indium atoms and is available for the formation of new QDs is progressively diminished. In comparison with the rapid growth rate of an In As QD in the instantaneous growth mode, the flux F is very small and can be neglected. Then, we have a simple ordinary differential equation

$$\frac{{\rm d}N(\theta_{\rm eff})}{{\rm d}\theta_{\rm eff}} = A_2 N(\theta_{\rm eff}), \tag{4.3.2}$$

which is well-known for having a quite simple mathematical solution,

$$N(\theta_{\rm eff}) = N_0 \exp(A_2 \theta_{\rm eff}), \tag{4.3.3}$$

which has exactly the same form as Eq. (4.3.1).

5 "Floating" indium on the growth surface and mechanical instability of an epitaxially strained InAs film on the GaAs(001) substrate

In the conventional kinetic models of InAs QD formation in MBE InAs/GaAs(001), as described in Section 3, three important experimental phenomena are overlooked or ignored: i) the presence of a large amount of "floating" indium on the growth surface, ii) the mechanical instability of a coherently strained InAs film on the GaAs(001) substrate, and iii) the significantly short timescale for QD formation. To more properly interpret InAs QD formation, these three well-established experimental facts have to be taken into account. The rapidness of InAs QD formation has been described in Sections 3.6.4 and 4. In this section, both the presence of floating indium on the growth surface and the mechanical instability of the epitaxially strained InAs film are described.

5.1 Floating indium on the growth surface

In the literature, it is well known that, owing to surface segregation, a large number of indium atoms are floating or physisorbed on the growth surface in MBE $\mathrm{In}_x\mathrm{Ga}_{1-x}\mathrm{As}$/GaAs(001). To fully understand InAs QD formation, the role played by these floating indium atoms has to be considered.

5.1.1 Indium floating

The conventional theories of epitaxial growth of InAs on the GaAs(001) substrate generally assume, implicitly or explicitly, that once an indium or a gallium atom from

the ballistic beam lands on the growth surface, it immediately reacts and forms at least one chemical bond on the adsorption site with the surface lattice, becoming an adatom, and that its kinetic energy is dissipated quickly and it reaches thermal equilibrium with the surface within ~ 1 ps. However, this simple physical scenario may be plausible only for a limited range of epitaxial growth systems, such as homoepitaxy on a simple unreconstructed metal surface under a given growth condition.

For MBE InAs/GaAs(001), the lattice constant of InAs, a_{InAs}, is significantly larger than that of GaAs, a_{GaAs} $[(a_{\mathrm{InAs}} - a_{\mathrm{GaAs}})/a_{\mathrm{GaAs}} = 0.07]$, so an InAs film would be formed in perfect crystalline registry with the GaAs(001) substrate under a very large compressive strain. By physical intuition, the atoms in the elastically compressed InAs film on the GaAs(001) substrate will be squeezed toward each other in the lateral direction to a relatively large extent, and, owing to the Poisson effect, the chemical bonds will be extended in the direction normal to the surface; the chemical bond strength is expected to be significantly weaker than that in the unstrained bulk state. A chemical bond in a group-IV or group-III-V semiconductor in the diamond or zinc-blende structure is well known to be highly directional and very brittle. It is highly possible that the lattice mismatch between InAs and GaAs may cause these chemical bonds in the film to reach their limit for distortion and extension, and thus to break! Bond breaking may occur after the InAs WL is established (the formation of the WL will be explained in Section 6.1). This intuitive physical scenario implies that after the formation of the InAs WL, the growth surface may be forced to be "chemically" unreactive because of the epitaxial compression or strain to additional indium atoms and arsenic molecules from the incident flux, and they should be forced to float or become temporarily physisorbed on the growth surface, instead of being chemically incorporated instantaneously into the surface lattice structure. The scenario described above is apparently consistent with experimental observations [310] of the chemical properties of an epitaxially strained Ru(0001) film. The chemisorption of O atoms and CO molecules to the compressively strained Ru(0001) surface is experimentally observed to be remarkably reduced. In contrast, the chemisorption of O atoms and CO molecules to the surface is considerably enhanced by tensile strain on the same surface. These changes in the chemisorption property of a strained film, induced by epitaxial strain, can be explained by density functional calculations [311], which indicate that lattice compression (expansion) down- (up-) shifts the metal d bands, and that the overlap of electron clouds between the adsorbate and the film is significantly reduced (enhanced).

A considerable amount of experimental evidence for the existence of floating or physically adsorbed indium on the growth surface in MBE $\mathrm{In}_x\mathrm{Ga}_{1-x}\mathrm{As}$/GaAs(001) has been accumulated in the last two decades. In the literature, these floating indium atoms were generally assumed to be produced by surface segregation, which may result from three main driving forces: i) relative surface stress, ii) chemical interactions, and iii) size mismatch. For example, Muraki *et al.* [312] demonstrated that because of surface segregation of indium on the growth surface of an $\mathrm{In}_x\mathrm{Ga}_{1-x}\mathrm{As}$ alloy, the surface chemical composition may reach the point $x > 1$, which is possible only when excess indium is floating on the surface [313] instead of chemically bonded to it. Garcia *et al.* [314], by *in-situ* measurements of the epitaxial stress, experimentally demonstrated that only 50% of the indium could be incorporated into the lattice after 2.3 ML of InAs were deposited on the GaAs(001) substrate. Cullis *et al.* [315, 316] proposed that there should be a highly mobile indium population that was inhibited from being incorporated into lattice sites on the growth surface of MBE InAs/GaAs(001). By using *in-situ* STM, Honma *et al.* [317] directly observed that there is a large portion of indium atoms floating on the growth surface in MBE InAs/GaAs(001). In addition, the floating indium atoms have been referred to in the literature to explain the chemical composition of an InAs QD [315, 316] and as the agent of rapid surface mass transport [318].

5.1.2 Structures that may result from floating indium

As mentioned above, to these floating indium atoms, the strained InAs film under compression seems to be chemically inert or inactive. However, these floating indium atoms may interact strongly among themselves, and some novel atomic configuration may develop from them. For a long time, these floating indium atoms have been considered and intensively investigated as an impediment to the formation of a sharp interface in the InGaAs/GaAs system [319]. However, there have been almost no experimental data or systematic theoretical considerations in the literature on what type of possible atomic configurations may develop from floating indium. In this section, this issue is briefly discussed.

To have some idea of how floating indium atoms behave on the inert growth surface in the MBE InAs/GaAs(001), let us first look at the epitaxial growth of a number of metal or semiconductors elements on an inert substrate, such as highly oriented pyrolytic graphite (HOPG) and molybdenum disulphide (MoS_2)

[320–323]. In all of these cases, atoms of different elements are deposited and aggregate into nanoclusters or nano-crystallites on the inert substrates, and the process is generally portrayed as 3D island growth in the Volmer–Weber growth mode. However, the morphologies of these nanostructures on the inert substrate are case-dependent and associated with the experimental conditions. Here, the focus is on indium deposition on the HOPG and MoS_2 substrates [322], which should be the most similar to the topic discussed here. When 0.6 nm of indium is deposited on the HOPG substrate at room temperature under ultrahigh vacuum, triangular 3D indium islands with body-centered tetragonal lattice structure are formed with an average height of 5.6 nm, and they have no fixed orientation with respect to the substrate. On the MoS_2 substrate, the 3D epitaxial indium islands have an average height of 2.4 nm and are aligned in the crystalline orientation with respect to the substrate, indicating that the indium element has a significant tendency to wet the substrate. If floating indium atoms on the growth surface in MBE InAs/GaAs(001) aggregate into 3D indium liquid droplets or nanocrystallites, as occurs in both the In/HOPG and In/MoS_2 systems, they should be easy to observe experimentally using AFM or STM, as observed in the two latter cases. However, no such experimental evidence has been provided to date, and it can be concluded that the morphologies and structures of the nanostructure resulting from floating indium in InAs/GaAs(001) should differ from those of nanostructures on the HOPG and MoS_2 substrates. The difference may be attributed mainly to the fact that in the MBE InAs/GaAs(001) system, indium is deposited under an arsenic-rich condition as well as a relatively high substrate temperature.

It has been experimentally demonstrated that during MBE growth of InGaAs under As-deficient, Ga-rich conditions at about 350°C on a GaAs(001) substrate with a (4×2)-reconstructed surface, the excess indium floating on the growth surface of MBE GaAs(001) aggregates into liquid indium droplets nanometers in size, which can subsequently be transformed into InAs QDs when a sufficiently large As flux is introduced [324–328]. In the traditional MBE method, in which InAs QDs were commonly formed under As-rich conditions on a $c(4\times4)$-reconstructed bare GaAs(001) surface, the atomic configuration of the floating indium may differ remarkably from that under the indium-rich condition. To date, although the existence of floating indium on the surface is undeniable, no indium droplets have ever been experimentally observed under As-rich conditions in MBE InAs/GaAs(001). In Ref. [329], it was suggested that floating indium may form small indium atomic clusters (trimers, for instance), or floating indium atoms may be locally and temporarily stored on the In-terminated As-rich reconstructed InAs surface.

In discussing the behavior of floating indium on the growth surface, the presence of arsenic molecules from the arsenic flux under the arsenic-rich condition has to be taken into account. To discuss the possible configuration resulting from floating indium under the influence of arsenic molecules, investigations of the kinetics of the reaction of gallium atoms with arsenic molecules in homoepitaxial growth of GaAs(001) are briefly reviewed. In the 1960s and 1970s, Arthur [330–332] and Foxon and Joyce [339, 334] investigated MBE growth of GaAs(001) under various As fluxes; to properly interpret their results, it was suggested that As_2 or As_4 molecules from the arsenic flux are first deposited into a reservoir of arsenic precursors, denoted by As_2^*, and physisorbed on the surface [335, 336]. It was further assumed that gallium atoms and As_2^* precursors are independent of each other before they are incorporated into the surface lattice sites [337–342]. A similar situation was also suggested in KMC simulations of homoepitaxial growth of InAs(001) [18] and InGaAs [343], and growth of an InAs film on GaAs(001) [344]. However, it is not unreasonable to expect that gallium (indium) atoms may react chemically with As molecules before they are incorporated into the surface lattice sites.

As there is no experimental evidence for the formation of 3D indium nanostructures, as happens in the epitaxial growth systems of In/HOPG and In/MoS_2, as well as in the InAs/GaAs(001) system under the In-rich growth condition, it is reasonable to speculate that floating indium and physisorbed As should react chemically to form some 2D InAs structure [16, 345, 346]. Note that it is hard to directly probe a piece of such a 2D atomic InAs sheet with the STM or AFM methods in real space. In addition, if these 2D atomic InAs sheets shift and rotate randomly and rapidly or they are smaller than the coherent length of the electron beam, it also could not be detected by the RHEED pattern. The atomic configuration resulting from floating indium will be further discussed in Section 6.

5.2 Mechanical instability of a coherently strained InAs film on the GaAs(001) substrate

In the conventional theoretical discussion of QD formation in heteroepitaxial growth, the epitaxially strained film was almost always assumed to be mechanically stable, and its strain energy was discussed in terms of the continuum elasticity theory. However, in these classical theories, one important and significant possibility has

been overlooked or ignored. Both experimentally and theoretically, it is well known that all semiconductor materials with the diamond, zinc-blende, or wurtzite structure are mechanically unstable under a relatively high hydrostatic pressure. At atmospheric pressure, these materials tend to adopt an open and tetrahedrally covalently bonded crystal structure with a coordination number of 4. As the hydrostatic pressure increases remarkably, their crystalline structure is transformed from the open one to an increasingly close-packed structure, such as the rocksalt and hcp structures (see the review in Ref. [347]). InAs has the zinc-blende structure at ambient hydrostatic pressure, which is transformed to the rocksalt structure at a critical pressure p_c(InAs) at room temperature; p_c(InAs) is theoretically predicted to be in the range of 6.0–9.0 GPa [348–350] and experimentally determined to be 7.0 GPa [351].

If the pressure is applied uniaxially, instead of being hydrostatic, the value of the critical pressure at which the structural transformation occurs in these semiconductors is dramatically reduced [352–354]. For example, the diamond-to-β-tin phase transition under uniaxial compression in both Si and Ge was investigated with *ab initio* calculations, and the critical uniaxial compression at which the structural transition occurs was found to be markedly lower than those under hydrostatic compression, i.e., 3.9 and 2.5 GPa under uniaxial compression compared to 11.4 and 9.5 GPa under hydrostatic pressure for Si and Ge, respectively [355, 356]. The lowering of the structural transition pressure under asymmetric conditions should be associated with bond bending in the bulk material under the application of a uniaxial pressure. The biaxial compressive strain induced by the lattice mismatch in MBE InAs/GaAs(001) may also make the strained film in the zinc-blende structure mechanically unstable, and some structural transformation may occur in it before the formation of 3D epitaxial islands and/or the introduction of misfit dislocations. In other words, the strained film in registry with the substrate should have already collapsed or been transformed into a crystalline structure rather than the zinc-blende at an early stage before morphological changes or the introduction of misfit dislocations.

In MBE InAs/GaAs(001), the InAs film is under an elastic biaxial compression of $\varepsilon_{xx} = \varepsilon_{yy} = 7\%$ due to the lattice mismatch. This elastic deformation can be converted into the equivalent biaxial elastic stress and pressure $P$for the InAs film in the zinc-blende structure according to the relations

$$\sigma_{xx} = \sigma_{yy} = \frac{(c_{11} - c_{12})(c_{11} + 2c_{12})}{c_{12}}\varepsilon_{xx}, \tag{5.2.1}$$

$$P\delta_{ij} = \sigma_{xx} = \sigma_{yy}. \tag{5.2.2}$$

Using the values of the elastic constants c_{11}, c_{12}, and c_{44} in the literature [357], it can be deduced that the equivalent pressure $P \approx 4$ GPa. Therefore, it is highly possible that the thin pseudomorphic InAs film on the GaAs(001) substrate is mechanically unstable. It is well known that a relatively thick uniform epitaxial InAs film in the zinc-blende structure can exist only after the epitaxial strain is relaxed by the formation of a network of misfit dislocations on the interface between the InAs film and the GaAs(001) substrate. It is highly possible that, before 3D islands form on the growth surface and the dislocation network appears near the interface, a series of delicate structural transformations would have been induced by epitaxial strain, and InAs QD formation is only one of the nodes of the structural transformation process. From the viewpoint of mechanical instability under high pressure, a uniformly strained InAs film could not exist at all on the GaAs(001) substrate because the structural transformation due to mechanical instability of the solid structure is tremendously rapid compared to the morphological relaxation process. Based on their first-principles calculations, Pedesseau *et al.* [350] supposed that spherical InAs QDs in the GaAs matrix should be in the rocksalt crystalline structure, instead of the zinc-blende one as generally assumed, owing to the effect of hydrostatic pressure.

It is well known that hydrostatic pressure can significantly reduce the melting point of a semiconductor [358, 359]. Bottomly [360–362] demonstrated using thermodynamic calculations that the melting point T_m of an elastically strained InAs film on the GaAs(001) substrate should be well below 500°C ($T_m = 942$°C in the macroscopic bulk form), and the film should actually be in the liquid state. A similar theoretical computation for thin-layer melting in heteroepitaxial systems was performed on thin Ge layers on Si(001) and Si(111) by Rosei and Raiteri [363]. However, unlike the situation in pressure-induced bulk melting experiments, where hydrostatic pressure is externally applied, this hypothetical InAs liquid film on the GaAs substrate cannot be thermodynamically stable because it can no longer sustain the epitaxial strain after melting.

6 Structural transformation model of InAs QD formation

In Section 3, the conventional theoretical descriptions of QD formation based on individual adatom events on the growth surface were briefly reviewed. As discussed

in Sections 4 and 5, these conventional kinetic theories are obviously inconsistent with three important experimental observations in MBE InAs/GaAs(001): i) An InAs QD can grow to maturity within a transient time in the instantaneous growth mode; ii) a large amount of floating indium exists on the growth surface when the InAs QDs are formed; iii) the epitaxially strained InAs film on the GaAs(001) substrate should be mechanically unstable under compressive strain. In this section, a novel physical scenario that takes these three experimental facts into account is suggested for the formation of InAs QDs in MBE InAs/GaAs(001).

6.1 Formation of InAs WL on GaAs(001)

An excess surface stress generally exists on a free solid surface because of surface atom relaxation in position and/or surface reconstruction. In heteroepitaxial growth, a thin WL generally forms first on the substrate surface to reduce its surface free energy. In theoretical discussions, the WL is generally considered to form via the layer-by-layer growth mode, and the WL critical thickness should be simply determined by the energetics of the system. However, as discussed in Section 3.7, many experimental observations have shown that the particular mechanism of WL formation in heteroepitaxial growth and the WL thickness are determined by the system's specific chemical bonding at the interface and/or surface reconstruction.

At around 500°C under As-rich conditions, epitaxial growth of an InAs film usually starts from the bare GaAs(001) surface reconstructed in $c(4 \times 4)$ symmetry [279, 280, 364, 365], which is characterized by blocks of three As ad-dimers sitting on top of a complete surface As layer [366, 367]. These As ad-dimers at the topmost layer place the surface under tensile strain in both the [110] and [$1\bar{1}0$] crystalline directions [279, 280] because of stretching of the back-bonds of these ad-dimers, as well as the significantly short bond length between the two atoms in the ad-dimers. When epitaxial growth of the InAs film begins, indium atoms, with a larger atomic diameter, can be readily incorporated into the otherwise bare GaAs(001)-$c(4\times4)$ surface, which significantly compensates for the surface tensile strain induced by those ad-dimers. Such a tensile/compressive strain compensation mechanism may work efficiently up to about 1.4 ML of InAs, at which epitaxial growth of the InAs WL is experimentally observed to terminate, and the surface reconstruction is observed to change to $\beta2(2 \times 4)$ [254]. Subsequently, if the additional deposited indium atoms form chemical bonds with the surface atoms, these bonds must be remarkably distorted by the lattice mismatch. The chemical bonds in group-III-V semiconductors are well known to be very brittle and highly directional. Thus, it is highly possible that these additional indium atoms cannot be incorporated into the surface lattice and temporarily float freely on the growth surface or form a 2D atomic sheet together with arsenic atoms (as discussed in the next section), waiting to be assembled into InAs QDs or for some structural transformation to occur. The situation can be described more straightforwardly as follows: After the InAs WL has formed and the tensile/compressive strain compensation mechanism has been exhausted, additional indium atoms hereafter deposited on the surface cannot form a chemical bond with the surface, or else the chemical bonds with the growth surface are completely sheared off by lattice mismatch. Therefore, the thickness (1.5 ML) of the InAs WL is exactly tailored by epitaxial mismatch. The proposed mechanism for the formation of the InAs WL should be mechanical in nature, in contrast to the thermodynamic or kinetic mechanism usually assumed in the literature.

The mechanical mechanism suggested above for the formation of a WL in lattice-mismatched heteroepitaxial growth should be common to both the Ge/Si(001) and InAs/GaAs(001) systems. In fact, there is also some experimental evidence implying that in Ge/Si(001), mechanical shearing off of the chemical bonds between Ge adatoms and the growth surface occurs before a complete Ge WL is well established. It is well known that the free surfaces of both Ge(001) and Si(001) are (2×1)-reconstructed under the usual growth conditions. It was experimentally observed that, during epitaxial growth of Ge on Si(001) under the conventional growth conditions, the (2×1) reconstruction rapidly changes into the $(2 \times N)$ one at a Ge coverage of about 1 ML. In the $(2 \times N)$ reconstruction, every Nth line of Ge dimers in the first Ge atomic layer is removed to accommodate the lattice mismatch, and a $(2\times N)$ reconstruction is formed consisting of a periodic arrangement of dimer vacancy lines (DVLs) of the (2×1) dimer reconstruction (see, for example, [368–376]). The appearance of this reconstruction provides partial relief of the compressive strain originating in the 4.2% lattice mismatch in the Ge/Si(001) system. In other words, every Nth line of Ge dimers is sheared off by the epitaxial strain in excess of the tensile/compressive compensation. As deposition proceeds, the DVLs become closer together, and the value of N decreases from about 13 to a minimum value of ∼6–9, depending on the growth conditions. At a Ge thickness larger than 2.5–3 ML, the mismatch stress cannot be further relieved by additional dimer vacancies in the dimer rows, and additional stress relaxation is achieved by shearing off every Mth dimer row from the growth

surface to form dimer-row vacancies (see, for example, Ref. [372]). The resulting structure is called a patched structure or $(M \times N)$ reconstruction [373, 374]. It is reasonable to believe that at the completion of a critical Ge WL with the $(M \times N)$ reconstruction, all the Ge adatoms that have been sheared off of the surface are floating as quasi-free atoms on the surface, waiting to be incorporated into the crystalline lattice in the form of a Ge QD, similar to the situation speculated to occur in MBE InAs/GaAs(001) in the next section.

6.2 Structural transformation from a single InAs layer to an InAs QD on the growth surface

In the last section, it was suggested that the InAs WL may be formed by a "mechanical" mechanism, after which additionally deposited indium atoms are sheared off by the lattice mismatch of the growth surface and may float temporarily on the surface as quasi-free atoms. In this subsection, the fate of these floating indium atoms is further discussed, and a novel mechanism for the formation of InAs QDs is suggested.

6.2.1 Structural transformation from a 2D InAs atomic sheet to a 3D epitaxial InAs island on the growth surface

With their chemical bonds sheared off of the growth surface by compressive strain, as described above, the floating indium atoms may interact strongly among themselves via covalent chemical bonds and form a single atomic layer or a 2D atomic sheet on the surface. Such an atomic sheet on the growth surface should involve arsenic atoms from the arsenic incident flux, and hereafter the possible 2D structure is called a 2D InAs atomic sheet. InAs, a group-III-V binary compound, is isoelectronic to group-IV elements such as carbon and silicon. Therefore, it can be speculated that the lattice structure of the 2D InAs atomic sheet may be similar to that of a planar graphene sheet [375, 376] or low-puckered silicene sheet [377–380] fabricated in epitaxial growth on the chemically unreactive Ru(0001) or Ag(111) surface, respectively. Both the carbon and silicon atomic epitaxial sheets are interesting topics currently under intensive investigation in the fields of surface science and nanoscience; these two types of atomic sheets both have a 2D hexagonal honeycomb lattice structure in which nearest-neighbor carbon or silicon atoms are connected by an sp^2-hybridized chemical bond. It should be recalled that in the bulk form, InAs crystallizes in the zinc-blende lattice structure, in which nearest-neighbor indium and arsenic atoms are connected to each other by sp^3-hybridized chemical bonds. Although an epitaxial 2D InAs sheet connected by sp^2-hybridized chemical bonds among In and As atoms has never been experimentally demonstrated on a chemically unreactive substrate, it has been theoretically demonstrated to be an energetically stable 2D lattice by becoming low-puckered instead of planar in geometry with a chemically bonded configuration intermediate between the sp^2- and sp^3-hybridized ones [381].

It is further imagined that the low-puckered 2D InAs sheet may be either compact, fractal, or percolated in geometrical shape on the growth surface. As indium atoms continue to arrive from the flux, the size of the InAs atomic sheet might increase, or the atomic sheets might begin to overlap one another. At a critical point, the atomic InAs sheet becomes unstable, and a structural phase transformation occurs spontaneously, at which a sp^2–sp^3-hybridized bond rehybridizes to the full sp^3 bond at some specific surface sites, such as atomic step edges. Upon rehybridization, the atoms originally in the 2D InAs atomic sheet become chemically bonded with the growth surface again. Then, this local rehybridization event spreads quickly across the entire 2D InAs sheet, and all the atoms in the sheet are simultaneously folded into a more compact form, a 3D epitaxial island or an InAs QD, and become a portion of the crystalline lattice structure on the surface. This possible process involving rehybridization from sp^2/sp^3-type to the full sp^3-type orbital hybridization should be a series of electronic excitation and relaxation events accompanied by a process similar to the propagation of strain waves in a 2D solid, and should be much faster than the conventional epitaxial growth or adatom aggregation processes. In this way, an InAs QD may be assembled within a few nanoseconds. The rehybridization of chemical bonds in carbon from the sp^2 type to the sp^3 type during the transformation from the graphite phase to the diamond phase under high-pressure, high-temperature conditions can be completed within about 10^{-2} ps, as demonstrated by molecular dynamics simulations [382].

In accordance with the two growth modes for InAs QDs, progressive and instantaneous, as described in Section 4, the structural transformation from a piece of the 2D InAs atomic sheet to a compact InAs QD and the sp^2–sp^3 rehybridization proposed above could be either discontinuous or continuous. In the progressive growth mode under the specific condition of $F = 0.1$ ML and $T = 500°$C, as described in Section 4.2, the structural transition might start from a critical point similar to that in a second-order or continuous phase transformation, during which many QDs nucleate at first and then simultaneously grow progressively. In contrast, in the instantaneous growth mode under $F = 1.0$ ML and $T = 520°$C,

as described in Section 4.3, the phase transformation might occur on a point on the "coexistence curve" far from the critical point, and the structural transformation might be apparently discontinuous. In this discontinuous phase transformation, once an InAs sheet physically adsorbed on the surface exceeds a critical size or thickness, it instantaneously changes into a QD. The next QD to form has to wait for a sufficient amount of additional floating indium. Therefore, InAs QDs form sequentially in the instantaneous growth mode.

6.2.2 Structural transformation from an epitaxial thin film to a 3D growth morphology in materials isoelectronic to InAs

In the last subsection, InAs QD formation was speculated to be a structural transformation accompanied by sp^2–sp^3 rehybridization of chemical bonds induced by increasing InAs coverage. Indeed, similar structural transformations accompanied by the rehybridization of chemical bonds have been observed experimentally in some ultrathin epitaxial films (on an inert substrate) of materials with the zinc-blende or wurtzite structure, which are isoelectronic to InAs. This subsection presents three examples of this situation, which support the plausibility of the speculation regarding InAs QD formation via the structural transformation.

The first example is epitaxial growth of Sn on Si(111). Sn, a group-IV element, can exist in two distinct crystalline structures. The Sn diamond crystal structure (α-Sn) exists below 13.2°C, above which Sn switches to the body-centered-tetragonal structure (β-Sn). If 1/3 ML of Sn is deposited on Si(111) at a substrate temperature high enough to destroy the Si(111)-7×7 reconstruction, the well-known $(\sqrt{3}\times\sqrt{3})$R30° reconstruction occurs on the growth surface; at 1 ML of Sn, the $(2\sqrt{3}\times2\sqrt{3})$R30° reconstruction appears. With further deposition of Sn up to 3.5 ML at room temperature, the ultrathin Sn film seems to remain commensurate to the substrate and has an α-Sn-like crystalline structure. At 4 ML of deposited Sn, 3D β-Sn islands begin to appear [383–386]; the change in the growth morphology has to involve both the structural transformation and sp^2–sp^3 rehybridization, as speculated for InAs QD formation in the last subsection.

The second example involves a graphene sheet on an Ir(111) substrate [387–389]. The carbon atoms on the Ir(111) surface, which were produced by thermal decomposition of hydrocarbons, join to form a graphene layer physisorbed on the Ir(111) surface. Because the lattice constant of the graphene layer differs from that of the Ir(111) surface by 10%, the carbon atoms in the graphene sheet are located at three different positions with respect to the Ir atoms on the surface: hcp sites, face-centered-cubic hollow sites, and atop sites. This produces a moiré pattern of the hexagonal systems in the graphene/Ir(111) system, which corresponds to a 2D superstructure having a supercell with a (10×10) graphene lattice resting on top of a (9×9) Ir structure [390]. When about 0.01 ML of Ir is deposited on the graphene/Ir(111), Ir nanoclusters are formed on the graphene sheet at the locations where carbon atoms in the graphene sheet are in the atop positions, and sp^2–sp^3 rehybridization occurs simultaneously on the carbon atoms covered by the Ir clusters [366]. Upon sp^2–sp^3 rehybridization, the carbon atoms under an Ir cluster become sp^3-coordinated, and they are sp^3 chemically bonded alternately with an Ir atom above in the cluster and below in the Ir surface. The sp^2–sp^3 rehybridization in the graphene layer should also occur upon hydrogen adsorption on it [391].

The third example occurs in epitaxial growth of a ZnO film on a Ag(111) substrate. The group-II-VI binary compound is an ionic crystal to a large extent and exhibits three polymorphs, wurtzite, zinc-blende, and rocksalt. The wurtzite structure is the most stable and commonly observed under ambient conditions, whereas the latter two appear on a cubic surface under specific growth conditions and at pressures between 8–10 GPa, respectively. Theoretical investigation predicts that an ultrathin ZnO film on a substrate of a different material can be more thermally stable if it has a graphitic-like or hexagonal boron nitride- (BN-) like structure. In the BN-like structure, both the Zn and O atoms are in almost the same atomic plane and are connected via the sp^2 hybridized bonds; consequently, the polar moment is canceled. This theoretical prediction was experimentally confirmed by the deposition of ultrathin ZnO films on Ag(111) [392, 393]: Up to 2 ML, the ultrathin ZnO film is in the graphitic-like form with an atomically planar morphology; with further deposition, the ZnO film changes spontaneously in structure from graphite-like to bulk wurtzite, and simultaneously, the surface morphology becomes rougher and 3D islands appear. It should be mentioned that Ag(111) interacts with ZnO via the weak van der Waals forces, and the substrate simply acts as a mechanical support for the ZnO film. Therefore, the structural transformation with increments in the coverage should be simply induced by increasing the ZnO coverage. In addition, the transformation in the ZnO ultrathin films from the graphite-like structure to the bulk-type wurtzite structure was also experimentally observed in the epitaxial ZnO/Pd(111) system, in which the critical thickness for the structural transition is 4 ML [394].

6.3 Self-limitation mechanisms affecting the uniform size of InAs QDs

As discussed in Section 3.8, the mechanism for self-limited epitaxial growth of an InAs QD remains a puzzle. In the last subsection, it was speculated that an InAs QD might be produced by the structural transformation from a 2D atomic InAs sheet to a 3D InAs epitaxial island. This subsection discusses two possible size-selection mechanisms in the structural transformation.

6.3.1 Critical size for the structural transformation on the nanoscale

The first model proposed for the size-selection mechanism in the formation of an InAs QD may arise from the existence of a critical size for the structural transformation on the nanoscale, as speculated in Section 6.2.1. It can be imagined that at the moment just after the InAs WL is formed, there are quite a few floating indium atoms whose behavior should be similar to that of quasi-free particles on the surface. As their number increases, these indium atoms aggregate, together with As atoms, to form a piece of the InAs atomic honeycomb sheet. The size of a 2D InAs sheet increases with increasing number of floating indium atoms on the growth surface. At a critical size, the 2D InAs sheet is spontaneously transformed into a compact 3D island or an InAs QD, as suggested in Section 6.2. Therefore, all the InAs QDs resulting from the structural transformation should be calibrated according to the critical size for the structural transformation. The scenario in which QD formation proceeds via the transformation from a 2D atomic disk to a 3D island was suggested by Priester and Lannoo [291] to explain the QD size uniformity. They speculated that adatoms first aggregate into an ensemble of 2D atomic disks; on the basis of thermodynamic considerations, they found that these 2D atomic disks should have a minimal energy per atom for a given size, and they should have the same size. They further speculated that, at a critical coverage, these uniform 2D atomic disks of the given size can spontaneously change into 3D islands. In this way, the QD size is calibrated to be uniform.

At present, the speculated structural transformation together with sp^2/sp^3 rehybridization at a critical size in an InAs nanocluster cannot be proven either experimentally or theoretically. However, it has been well established that, at a critical size, some structural transformations, together with rehybridization of the chemical bonds, indeed occur in nanoclusters of both Si and C, both of which are isoelectronic to InAs. On the basis of experimental observations, it was concluded that three main structural transformations occur at different critical sizes in a Si cluster (in either free space or a polycrystalline film) in sequence as its size increases by incorporation of additional silicon atoms. The first occurs at the first critical size of $n_{\rm cri}^{\rm 1st} \sim 27$ atoms, at which the Si cluster is transformed from a prolate geometry to a near-spherical one or an endohedral fullerene [395–406]. At the second critical size of $n_{\rm cri}^{\rm 2nd}(\rm Si) \sim 60$, the silicon endohedral fullerene is transformed into a structure consisting of a number of subunits or magic clusters with sizes of $N = 6, 7, 9, 11$ [407, 408]. At the third critical size of $n_{\rm cri}^{\rm 3rd}(\rm Si) \sim 200$, the silicon cluster is transformed from a metal-like or amorphous type into the diamond structure [409–412].

There are some differences in the valence electronic properties of carbon and silicon. All the sp^1-, sp^2-, and sp^3-type bonds among the carbon atoms in a carbon cluster are significantly closer in energy than the situations in silicon. In addition, the sp^2-hybridized bond is more stable in carbon, whereas the sp^3-hybridized bond is more stable in silicon [413]. These differences in electronic structure between the two group-IV elements are reflected in the structural transformation behavior of an atomic cluster. According to both the experimental and theoretical data in the literature, a very small carbon cluster of a few atoms should be linear in structure; if more C atoms are added, it changes to a monocyclic or polycyclic structure at the first critical size, which is in the range of $4 \leqslant n_{\rm cri}^{\rm 1st}(C) \leqslant 8$ [414]. At the second critical size, which is in the range of $20 < n_{\rm cri}^{\rm 2nd}(C) \leqslant 30$, the C cluster changes to the fullerene form [415–419]. At the critical size of about $n_{\rm cri}^{\rm 3rd}(C) \sim 300$ carbon atoms (or a diameter of ~ 1.3 nm), the carbon cluster becomes an octahedral nanodiamond [420]. At a critical linear size ranging from 1.5 nm to 5 nm, the C cluster should be a spherical diamond; above this range, the cluster spreads into a graphene sheet or becomes a three-dimensional graphite crystallite [421]. InAs is isoelectronic to Si and C, and an InAs cluster may exhibit the same behavior as the atomic clusters of these elements. These structural transformations induced by increasing the size of both Si and C clusters support the plausibility of our speculation regarding an InAs cluster.

In addition, it is well known that in free space, the stable atomic configuration of a nanocluster of a material may differ significantly from the crystalline lattice of the bulk state because of the surface effect [422–425]. In Section 5.2, it was mentioned that an elastically strained and coherent InAs thin film with the zinc-blende lattice on the GaAs(001) substrate should be mechanically unstable. To interpret the formation of InAs QDs on the surface of the InAs WL on GaAs(001), it should be sup-

posed that the formation of InAs QDs with the zinc-blende structure may be possible because of the surface effect, as these 3D epitaxial islands on the nanoscale have a larger surface area than a 2D film, which may significantly suppresses the instability of the zinc-blende crystalline structure under the compressive strain due to lattice mismatch.

The epitaxial growth process of an InAs film proposed in Sections 6.1 and 6.2 can be summarized as follows: An ultrathin InAs film is formed first as the so-called WL, and its thickness cannot increase continuously with additional InAs deposition because of lattice compression due to lattice mismatch. Instead, additional InAs deposition results in floating indium atoms on the growth surface; these floating indium atoms, together with arsenic atoms, aggregate into a 2D InAs sheet. As its size increases, the 2D InAs sheet is spontaneously transformed into an ensemble of InAs QDs of a uniform size determined by a critical size, which should be stable because of the surface effect. As additional InAs is deposited, misfit dislocations develop at the interface, and the ensemble of QDs collapses; subsequently, with an array of misfit dislocations at the InAs/GaAs interface, the relatively smooth InAs film grows continuously in thickness with additional InAs deposition.

6.3.2 Mechanical mechanism

The second proposed size-limitation mechanism in the structural transformation yielding QD formation is "mechanical" in nature. As discussed in Section 6.1, the critical thickness of the InAs WL may be mechanically tailored by the epitaxial stress, and the chemical bonds between the adatoms and the surface of the WL should be sheared off at the critical thickness of the InAs WL. We suppose that a similar situation might also occur on the QD sidewalls. After growing to a given shape and size, an InAs QD could not incorporate any indium atoms into its lattice structure, and the possible chemical bonds should be sheared off owing to the effect of epitaxial strain. More simply, the size and shape of a QD are exactly tailored by the epitaxial strain. After the QD reaches its mature size, any atoms deposited on the QD from the flux would be rejected. Therefore, a uniform QD ensemble can be fabricated. We call this proposed mechanism for the formation of uniform QDs a mechanical one, in contrast to the kinetic self-limitation and thermodynamic ones that have been proposed in the literature. With further indium deposition, misfit dislocations begin to nucleate near the InAs/GaAs interface; the QDs become dislocated, and the InAs film continues its epitaxial growth in the traditional sense.

Acknowledgements The work was supported by the National Basic Research Program of China (Grant No. 2006CB604904) and the National Natural Science Foundation of China (Grant Nos. 61274072, 60976057, 60876086 and 60776037).

Open Access This article is distributed under the terms of the Creative Commons Attribution License which permits any use, distribution, and reproduction in any medium, provided the original author(s) and the source are credited.

References and notes

1. F. C. Frank and J. H. van der Merwe, One-dimensional dislocations (I): Static theory, *Proc. R. Soc. Lond. A* 198(1053), 205 (1949)
2. D. Pan, E. Towe, and S. Kennerly, A five-period normal-incidence (In, Ga)As/GaAs quantum-dot infrared photodetector, *Appl. Phys. Lett.* 75(18), 2719 (1999)
3. Z. Ye, J. C. Campbell, Z. Chen, E.T. Kim, and A. Madhukar, Voltage-controllable multiwavelength InAs quantum-dot infrared photodetectors for mid- and far-infrared detection, *J. Appl. Phys.* 92(7), 4141(2002)
4. H. C. Liu, B. Aslan, J. A. Gupta, Z. R. Wasilewski, G. C. Aers, A. J. SpringThorpe, and M. Buchanan, Quantum dots for terahertz generation, *J. Phys.: Condens. Matter* 20(38), 384211 (2008)
5. N. S. Daghestani, M. A. Cataluna, G. Berry, G. Ross, and M. J. Rose, Terahertz emission from InAs/GaAs quantum dot based photoconductive devices, *Appl. Phys. Lett.* 98(18), 181107 (2011)
6. G. Shan, X. Zhao, M. Hu, C. H. Shek, and W. Huang, Vertical-external-cavity surface-emitting lasers and quantum dot lasers, *Front. Optoelectron.* 5(2), 157 (2012)
7. G. C. Shan, Z. Q. Yin, C. H. Shek, and W. Huang, Single photon sources with single semiconductor quantum dots, *Front. Phys.* 9(2), 170 (2014)
8. D. J. Eaglesham and M. Cerullo, Dislocation-free Stranski-Krastanow growth of Ge on Si(100), *Phys. Rev. Lett.* 64(16), 1943 (1990)
9. Y. W. Mo, D. E. Savage, B. S. Swartzentruber, and M. G. Lagally, Kinetic pathway in Stranski–Krastanov growth of Ge on Si(001), *Phys. Rev. Lett.* 65(8), 1020 (1990)
10. C. W. Snyder, B. G. Orr, D. Kessler, and L. M. Sander, Effect of strain on surface morphology in highly strained InGaAs films, *Phys. Rev. Lett.* 66(23), 3032 (1991)
11. D. Leonard, M. Krishnamurthy, C. M. Reaves, S. P. Denbaars, and P. M. Petroff, Direct formation of quantum-sized dots from uniform coherent islands of InGaAs on GaAs surfaces, *Appl. Phys. Lett.* 63(23), 3203 (1993)
12. J. M. Moison, F. Houzay, F. Barthe, L. Leprince, E. André, and O. Vatel, Self-organized growth of regular nanometer-scale InAs dots on GaAs, *Appl. Phys. Lett.* 64(2), 196 (1994)
13. D. Leonard, K. Pond, and P. M. Petroff, Critical layer thickness for self-assembled InAs islands on GaAs, *Phys. Rev. B*

50(16), 11687 (1994)

14. A. Zolotaryov, A. Schramm, Ch. Heyn, and W. Hansen, InAs-coverage dependence of self-assembled quantum dot size, composition, and density, *Appl. Phys. Lett.* 91(8), 083107 (2007)
15. J. Wu, Y. H. Jiao, P. Jin, X. J. Lv, and Z. G. Wang, Effect of the growth mode on the two- to three-dimensional transition of InAs grown on vicinal GaAs(001) substrates, *Nanotechnology* 18(26), 265304 (2007)
16. J. Wu, Y. P. Zeng, B. Q. Wang, J. Peng, and Z. G. Wang, Self-Assembling of InAs Quantum Dots on GaAs(001) in Molecular Beam Epitaxy Advances in Nanotechnology, edited by E. J. Chen and N. Peng, Nova Science Publishers, 2009 ,Vol. 1, pp 209–222
17. J. Wu, Y. P. Zeng, B. Q. Wang, Z. P. Zhu, and Z. G. Wang, Growth of MBE InAs/GaAs(001) quantum dots by the rapid rate, *Micronanoelectronic Technology* 46, 79 (2009) (in Chinese)
18. F. Grosse and M. F. Gyure, Island and step morphology in InAs(001) homoepitaxy, *Phys. Status Solidi* (*b*) 234(1), 338 (2002)
19. M. Takahasi and J. Mizuki, X-ray diffraction study on self-organization of InAs islands on GaAs(001), *J. Phys. Conf. Ser.* 83, 012006 (2007)
20. H. Metiu, Building regulations, *Nature* 366(6451), 111 (1993)
21. Z. Zhang and M. G. Lagally, Atomistic processes in the early stages of thin-film growth, *Science* 276(5311), 377 (1997)
22. J. V. Barth, G. Costantini, and K. Kern, Engineering atomic and molecular nanostructures at surfaces, *Nature* 437(7059), 671 (2005)
23. J. A. Venables, Nucleation growth and pattern formation in heteroepitaxy, *Physica A* 239(1–3), 35 (1997)
24. A. K. Bhuiyan, S. K. Dew, and M. Stepanova, Controlled self-assembly of nanocrystalline arrays studied by 3D kinetic Monte Carlo modeling, *J. Phys. Chem. C* 115(40), 19557 (2011)
25. A. Madhukar, A unified atomistic and kinetic framework for growth front morphology evolution and defect initiation in strained epitaxy, *J. Cryst. Growth* 163(1–2), 149 (1996)
26. D. D. Vvedensky, Epitaxial phenomena across length and time scales, *Surf. Interface Anal.* 31(7), 627 (2001)
27. A. Voigt (Ed.), Multiscale Modeling in Epitaxial Growth, Birkhauser, 2005
28. T. Tiedje and A. Ballestad, Atomistic basis for continuum growth equation: Description of morphological evolution of GaAs during molecular beam epitaxy, *Thin Solid Films* 516(12), 3705 (2008)
29. A. Y. Cho, Film deposition by molecular-beam techniques, *J. Vac. Sci. Technol.* 8(5), S31 (1971)
30. M. D. Johnson, C. Orme, A. W. Hunt, D. Graff, J. Sudijono, L. Sander, and B. Orr, Stable and unstable growth in molecular beam epitaxy, *Phys. Rev. Lett.* 72(1), 116 (1994)
31. C. Orme, M. D. Johnson, K. T. Leung, B. G. Orr, P. Smilauer, and D. Vvedensky, Studies of large scale unstable growth formed during GaAs(001) homoepitaxy, *J. Cryst. Growth* 150, 128 (1995)
32. C. Orme, M. D. Johnson, J. L. Sudijono, K. T. Leung, and B. G. Orr, Large scale surface structure formed during GaAs (001) homoepitaxy, *Appl. Phys. Lett.* 64(7), 860 (1994)
33. S. Martini, A. A. Quivy, T. E. Lamas, M. J. da Silva, E. C. F. da Silva, and J. R. Leite, Influence of indium segregation on the RHEED oscillations during the growth of InGaAs layers on a GaAs(001) surface, *J. Cryst. Growth* 251(1–4), 101 (2003)
34. S. Martini, A. A. Quivy, T. E. Lamas, and E. da Silva, Real-time RHEED investigation of indium segregation in InGaAs layers grown on vicinal GaAs(001) substrates, *Phys. Rev. B* 72(15), 153304 (2005)
35. R. J. Asaro and W. A. Tiller, Interface morphology development during stress corrosion cracking (Part I): Via surface diffusion, *Metall. Trans.* 3(7), 1789 (1972)
36. M. A. Grinfeld, Instability of the Separation Boundary between a Nonhydrostatically Stressed Elastic Body and a Melt, *Dokl. Akad. Nauk. SSSR* 290(6), 1358 (1986)
37. D. J. Srolovitz, On the stability of surfaces of stressed solids, *Acta Metall.* 37(2), 621 (1989)
38. H. Gao and D. M. Nix, Surface roughening of heteroepitaxial thin films, *Annu. Rev. Mater. Sci.* 29(1), 173 (1999)
39. B. J. Spencer and J. Tersoff, Equilibrium shapes and properties of epitaxially strained islands, *Phys. Rev. Lett.* 79(24), 4858 (1997)
40. C. D. Rudin and B. J. Spencer, Equilibrium island ridge arrays in strained solid films, *J. Appl. Phys.* 86(10), 5530 (1999)
41. W. T. Tekalign and B. J. Spencer, Evolution equation for a thin epitaxial film on a deformable substrate, *J. Appl. Phys.* 96(10), 5505 (2004)
42. J. N. Aqua, T. Frisch, and A. Verga, Nonlinear evolution of a morphological instability in a strained epitaxial film, *Phys. Rev. B* 76(16), 165319 (2007)
43. B. J. Spencer, P. W. Voorhees, and S. H. Davis, Morphological instability in epitaxially strained dislocation-free solid films: Linear stability theory, *J. Appl. Phys.* 73(10), 4955 (1993)
44. J. E. Guyer and P. W. Voorhees, Morphological stability of alloy thin films, *Phys. Rev. B* 54, 11710 (1996)
45. C. H. Chiu, The self-assembly of uniform heteroepitaxial islands, *Appl. Phys. Lett.* 75(22), 3473 (1999)
46. C. H. Chiu and Z. Huang, Numerical simulation for the formation of nanostructures on the Stranski–Krastanow systems by surface undulation, *J. Appl. Phys.* 101(11), 113540 (2007)
47. M. Levine, A. Golovin, S. Davis, and P. Voorhees, Self-assembly of quantum dots in a thin epitaxial film wetting an elastic substrate, *Phys. Rev. B* 75(20), 205312 (2007)

48. Y. W. Zhang, Self-organization, shape transition, and stability of epitaxially strained islands, *Phys. Rev. B* 61(15), 10388 (2000)

49. J. Müller and M. Grant, Model of surface instabilities induced by stress, *Phys. Rev. Lett.* 82(8), 1736 (1999)

50. Z. Suo and Z. Zhang, Epitaxial films stabilized by long-range forces, *Phys. Rev. B* 58(8), 5116 (1998)

51. P. Liu, Y. W. Zhang, and C. Lu, Coarsening kinetics of heteroepitaxial islands in nucleationless Stranski–Krastanov growth, *Phys. Rev. B* 68(3), 035402 (2003)

52. J. N. Aqua, and T. Frisch, Influence of surface energy anisotropy on the dynamics of quantum dot growth, *Phys. Rev. B* 82(8), 085322 (2010)

53. S. P. A. Gill, An analytical model for the growth of quantum dots on ultrathin substrates, *Appl. Phys. Lett.* 98(16), 161910 (2011)

54. M. Khenner, W. T. Tekalign, and M. S. Levine, Stability of a strongly anisotropic thin epitaxial film in a wetting interaction with elastic substrate, *Europhys. Lett.* 93(2), 26001 (2011)

55. Y. W. Zhang and A. F. Bower, Three-dimensional analysis of shape transitions in strained-heteroepitaxial islands, *Appl. Phys. Lett.* 78(18), 2706 (2001)

56. F. Long, S. P. A. Gill, and A. C. Cocks, Effect of surface-energy anisotropy on the kinetics of quantum dot formation, *Phys. Rev. B* 64(12), 121307 (2001)

57. M. D. Korzec and P. L. Evans, From bell shapes to pyramids: A reduced continuum model for self-assembled quantum dot growth, *Physica D* 239(8), 465 (2010)

58. C. H. Chiu, Stable and uniform arrays of self-assembled nanocrystalline islands, *Phys. Rev. B* 69(16), 165413 (2004)

59. C. Herring, Effect of change of scale on sintering phenomena, *J. Appl. Phys.* 21(4), 301 (1950)

60. W. W. Mullins, Theory of thermal grooving, *J. Appl. Phys.* 28, 333 (1957)

61. J. W. Gibbs, The Collected Works, Thermodynamics Vol. 1, New York: Longmans Green, 1928

62. J. W. P. Schmelzer, On the determination of the kinetic prefactor in classical nucleation theory, *J. Non-Cryst. Solids* 356(52–54): 2901 (2010)

63. B.V. Derjaguin, Theory of homogeneous condensation upon moderate supersaturation, *Progress in Surface Science* 45(1–4), 1 (1994)

64. D. Kashchiev, Nucleation: Basic Theory with Applications, Oxford: Butterworth Heinemann, 2000

65. S. A. Kukushkin and A. V. Osipov, New phase formation on solid surfaces and thin film condensation, *Prog. Surf. Sci.* 51(1), 1 (1996)

66. T. P. Munt, D. E. Jesson, V. A. Shchukin, and D. Bimberg, Metastable states of surface nanostructure arrays studied using a Fokker–Planck equation, *Phys. Rev. B* 75(8), 085422 (2007)

67. I. M. Lifshitz and V. V. Slyozov, The kinetics of precipitation from supersaturated solid solutions, *J. Phys. Chem. Solids* 19(1–2), 35 (1961)

68. C. Wagner, Theorie der Alterung von Niederschlägen durch Umlösen (Ostwald-Reifung) [Theory of the aging of precipitates by dissolution-reprecipitation (Ostwald ripening)], *Zeitschrift für Elektrochemie* 65(7–8), 581 (1961)

69. A. V. Osipov, S. A. Kukushkin, F. Schmitt, and P. Hess, Kinetic model of coherent island formation in the case of self-limiting growth, *Phys. Rev. B* 64(20), 205421 (2001)

70. A. V. Osipov, F. Schmitt, S. A. Kukushkin, and P. Hess, Stress-driven nucleation of coherent islands: Theory and experiment, *Appl. Surf. Sci.* 188(1–2), 156 (2002)

71. V. G. Dubrovskii, G. E. Cirlin, and V. W. Ustinov, Kinetics of the initial stage of coherent island formation in heteroepitaxial systems, *Phys. Rev. B* 68(7), 075409 (2003)

72. V. G. Dubrovskii, G. E. Cirlin, Y. G. Musikhin, Y. B. Samsonenko, A. A. Tonkikh, N. K. Polyakov, V. A. Egorov, A. F. Tsatsul'nikov, N. A. Krizhanovskaya, V. M. Ustinov, and P. Werner, Effect of growth kinetics on the structural and optical properties of quantum dot ensembles, *J. Cryst. Growth* 267(1–2), 47 (2004)

73. V. G. Dubrovskii, Calculation of the size-distribution function for quantum dots at the kinetic stage of growth, *Semiconductors* 40(10), 1123 (2006)

74. J. Tersoff and F. K. LeGoues, Competing relaxation mechanisms in strained layers, *Phys. Rev. Lett.* 72, 3570 (1994)

75. T. Hanada, H. Totsuka, S. K. Hong, K. Godo, K. Miyajima, T. Goto, and T. Yao, Slowdown in development of self-assembled InAs/GaAs(001) dots near the critical thickness, *J. Vac. Sci. Technol. B* 24(4), 1886 (2006)

76. A. L. Giermann and C. V. Thompson, Solid-state dewetting for ordered arrays of crystallographically oriented metal particles, *Appl. Phys. Lett.* 86(12), 121903 (2005)

77. D. T. Danielson, D. K. Sparacin, J. Michel, and L. C. Kimerling, Surface-energy-driven dewetting theory of silicon-on-insulator agglomeration, *J. Appl. Phys.* 100(8), 083507 (2006)

78. E. Bussmann, F. Cheynis, F. Leroy, P. Müller, and O. Pierre-Louis, Dynamics of solid thin-film dewetting in the silicon-on-insulator system, *New J. Phys.* 13(4), 043017 (2011)

79. D. Wang and P. Schaaf, Solid-state dewetting for fabrication of metallic nanoparticles and influences of nanostructured substrates and dealloying, *Phys. Status Solidi A* 210(8), 1544 (2013)

80. F. Ruffino and M. G. Grimaldi, Dewetting of template-confined Au films on SiC surface: From patterned films to patterned arrays of nanoparticles, *Vacuum* 99, 28 (2014)

81. H. T. Dobbs, D. D. Vvedensky, A. Zangwill, J. Johansson, N. Carlsson, and W. Seifert, Mean-field theory of quantum dot formation, *Phys. Rev. Lett.* 79(5), 897 (1997)

82. Y. Chen and J. Washburn, Structural transition in large-lattice-mismatch heteroepitaxy, *Phys. Rev. Lett.* 77(19), 4046 (1996)

83. F. M. Ross, J. Tersoff, and R. M. Tromp, Coarsening of self-assembled Ge quantum dots on Si(001), *Phys. Rev. Lett.* 80(5), 984 (1998)
84. H. M. Koduvely and A. Zangwill, Epitaxial growth kinetics with interacting coherent islands, *Phys. Rev. Lett.* 60(4), R2204 (1999)
85. D. E. Jesson, T. P. Munt, V. A. Shchcukin, and D. Bimberg, Tunable metastability of surface nanostructure arrays, *Phys. Rev. Lett.* 92(11), 115503 (2004)
86. Y. Enomoto and M. Sawa, Simulation study on nanocluster growth deposited on a substrate, *Physica A* 331(1–2), 189 (2004)
87. M. Fanfoni and M. Tomellini, Film growth viewed as stochastic dot processes, *J. Phys.: Condens. Matter* 17(17), R571 (2005)
88. H. Z. Song, T. Usuki, Y. Nakata, N. Yokoyama, H. Sasakura, and S. Muto, Formation of InAs/GaAs quantum dots from a subcritical InAs wetting layer: A reflection high-energy electron diffraction and theoretical study, *Phys. Rev. B* 73(11), 115327 (2006)
89. M. Fanfoni, E. Placidi, F. Arciprete, E. Orsini, F. Patella, and A. Balzarotti, Sudden nucleation versus scale invariance of InAs quantum dots on GaAs, *Phys. Rev. B* 75(24), 245312 (2007)
90. K. A. Nevalainen, M. Rusanen, and I. T. Koponen, Size selected growth of nanodots: Effects of growth kinetics and energetics on the formation of stationary size distributions, *Eur. Phys. J. B* 56(4), 311 (2007)
91. F. Ratto and F. Rosei, Order and disorder in the heteroepitaxy of semiconductor nanostructures, *Mater. Sci. Eng. Rep.* 70(3–6), 243 (2010)
92. Ch. Heyn, Critical coverage for strain-induced formation of InAs quantum dots, *Phys. Rev. B* 64(16), 165306 (2001)
93. J. A. Venables, G. D. T. Spiller, and M. Hanbuchen, Nucleation and growth of thin films, *Rep. Prog. Phys.* 47(4), 399 (1984)
94. M. Itoh, Atomic-scale homoepitaxial growth simulations of reconstructed III–V surfaces, *Prog. Surf. Sci.* 66(3–5), 53 (2001)
95. J. W. Evans, P. A. Thiel, and M. C. Bartelt, Morphological evolution during epitaxial thin film growth: Formation of 2D islands and 3D mounds, *Surf. Sci. Rep.* 61(1–2), 1 (2006)
96. G. S. Bales and D. C. Chrzan, Dynamics of irreversible island growth during submonolayer epitaxy, *Phys. Rev. B* 50(9), 6057 (1994)
97. M. Körner, M. Einax, and P. Maass, Island size distributions in submonolayer growth: Prediction by mean field theory with coverage dependent capture number, *Phys. Rev. B* 82(20), 201401(R) (2010)
98. M. Körner, M. Einax, and P. Maass, Capture numbers and island size distributions in models of submonolayer surface growth, *Phys. Rev. B* 86(8), 085403 (2012)
99. J. G. Amar, F. Family, and P. M. Lam, Dynamic scaling of the island-size distribution and percolation in a model of submonolayer molecular-beam epitaxy, *Phys. Rev. B* 50(12), 8781 (1994)
100. D. R. Frankl and J. A. Venables, Nucleation on substrates from the vapour phase, *Adv. Phys.* 19(80), 409 (1970)
101. T. Witten and L. M. Sander, Diffusion-limited aggregation, a kinetic critical phenomenon, *Phys. Rev. Lett.* 47(19), 1400 (1981)
102. P. Meakin, Formation of fractal clusters and networks by irreversible diffusion-limited aggregation, *Phys. Rev. Lett.* 51(13), 1119 (1983)
103. M. Kolb, R. Botet, and R. Jullien, Scaling of kinetically growing clusters, *Phys. Rev. Lett.* 51(13), 1123 (1983)
104. A. Y. Menshutin and L. N. Shchur, Morphological diagram of diffusion driven aggregate growth in plane: Competition of anisotropy and adhesion, *Comput. Phys. Commun.* 182(9), 1819 (2011)
105. Z. Rácz and T. Vicsek, Diffusion-controlled deposition: Cluster statistics and scaling, *Phys. Rev. Lett.* 51(26), 2382 (1983)
106. T. Vicsek and F. Family, Dynamic scaling for aggregation of clusters, *Phys. Rev. Lett.* 52(19), 1669 (1983)
107. W. W. Mullins, The statistical self-similarity hypothesis in grain growth and particle coarsening, *J. Appl. Phys.* 59(4), 1341 (1986)
108. F. Family and P. Meakin, Scaling of the droplet-size distribution in vapor-deposited thin films, *Phys. Rev. Lett.* 61(4), 428 (1988)
109. F. Family and P. Meakin, Kinetics of droplet growth processes: Simulations, theory, and experiments, *Phys. Rev. A* 40(7), 3836 (1989)
110. M. Zinke-Allmang, L. C. Feldman, and W. van Saarloos, Experimental study of self-similarity in the coalescence growth regime, *Phys. Rev. Lett.* 68(15), 2358 (1992)
111. J. G. Amar, F. Family, and P. M. Lam, Dynamic scaling of the island-size distribution and percolation in a model of submonolayer molecular-beam epitaxy, *Phys. Rev. B* 50(12), 8781 (1994)
112. J. G. Amar and F. Family, Kinetics of submonolayer and multilayer epitaxial growth, *Thin Solid Films* 272(2), 208 (1996)
113. J. W. Evans and M. C. Bartelt, Nucleation, adatom capture, and island size distributions: Unified scaling analysis for submonolayer deposition, *Phys. Rev. B* 63(23), 235408 (2001)
114. J. W. Evans and M. C. Bartelt, Island sizes and capture zone areas in submonolayer deposition: Scaling and factorization of the joint probability distribution, *Phys. Rev. B* 66(23), 235410 (2002)
115. J. A. Stroscio and D. T. Pierce, Scaling of diffusion-mediated island growth in iron-on-iron homoepitaxy, *Phys. Rev. B* 49(12), 8522 (1994)
116. V. Bressler-Hill, S. Varma, A. Lorke, B. Z. Nosho, P. Petroff, and W. Weinberg, Island scaling in strained heteroepitaxy: InAs/GaAs(001), *Phys. Rev. Lett.* 74(16), 3209 (1995)

117. G. R. Bell, T. J. Krzyzewski, P. B. Joyce, and T. S. Jones, Island size scaling for submonolayer growth of InAs on GaAs(001)-(2×4): Strain and surface reconstruction effects, *Phys. Rev. B* 61(16), R10551 (2000)
118. C. Ratsch, A. Zangwill, P. Smilauer, and D. D. Vvedensky, Saturation and scaling of epitaxial island densities, *Phys. Rev. Lett.* 72(20), 3194 (1994)
119. J. G. Amar and F. Family, Critical cluster size: Island morphology and size distribution in submonolayer epitaxial growth, *Phys. Rev. Lett.* 74(11), 2066 (1995)
120. P. A. Mulheran and J. A. Blackman, The origins of island size scaling in heterogeneous film growth, *Philos. Mag. Lett.* 72(1), 55 (1995)
121. P. A. Mulheran and J. A. Blackman, Capture zones and scaling in homogeneous thin-film growth, *Phys. Rev. B* 53(15), 10261 (1996)
122. F. Ratto, A. Locatelli, S. Fontana, S. Kharrazi, S. Ashtaputre, S. Kulkarni, S. Heun, and F. Rosei, Diffusion dynamics during the nucleation and growth of Ge/Si nanostructures on Si(111), *Phys. Rev. Lett.* 96(9), 096103 (2006)
123. G. S. Solomon, J. A. Trezza, and J. S. Harris, Substrate temperature and monolayer coverage effects on epitaxial ordering of InAs and InGaAs islands on GaAs, *Appl. Phys. Lett.* 66(8), 991 (1995)
124. R. Leon, T. J. Senden, Y. Kim, C. Jagadish, and A. Clark, Nucleation transitions for InGaAs islands on vicinal (100) GaAs, *Phys. Rev. Lett.* 78(26), 4942 (1997)
125. K. Shiramine, T. Itoh, and S. Muto, Critical cluster size of InAs quantum dots formed by Stranski–Krastanow mode, *J. Vac. Sci. Technol. B* 22(2), 642 (2004)
126. F. Arciprete, E. Placidi, V. Sessi, M. Fanfoni, F. Patella, and A. Balzarotti, How kinetics drives the two- to three-dimensional transition in semiconductor strained heterostructures: The case of InAs/GaAs(001), *Appl. Phys. Lett.* 89(4), 041904 (2006)
127. Y. Ebiko, S. Muto, D. Suzuki, S. Itoh, K. Shiramine, T. Haga, Y. Nakata, and N. Yokoyama, Island size scaling in InAs/GaAs self-assembled quantum dots, *Phys. Rev. Lett.* 80(12), 2650 (1998)
128. T. J. Krzyzewski, P. B. Joyce, G. R. Bell, and T. S. Jones, Understanding the growth mode transition in InAs/GaAs(001) quantum dot formation, *Surf. Sci.* 532–535, 822 (2003)
129. T. P. Munt, D. E. Jesson, V. A. Shchukin, and D. Bimberg, Manipulating the size distributions of quantum dots associated with strain-renormalized surface energy, *Appl. Phys. Lett.* 85(10), 1784(2004)
130. K. Pirkkalainen, K. A. Riekki, and I. T. Koponen, Two computational methods for describing size selected nanocluster growth and obtaining accurate cluster size distributions, *Comput. Mater. Sci.* 43(2), 325 (2008)
131. K. Pirkkalainen, K. A. Nevalainen, and I. T. Koponen, Computational methods for mesoscopic modelling of size-selection in nanoisland growth, *J. Phys.: Conf. Ser.* 100(7), 072004 (2008)
132. K. A. Riekki, Size selected growth of nanodots: Analytical prediction for the selected size, *Eur. Phys. J. B* 85(6), 185, 2012
133. G. S. Bales and A. Zangwill, Self-consistent rate theory of submonolayer homoepitaxy with attachment/detachment kinetics, *Phys. Rev. B* 55(4), R1973 (1997)
134. H. A. Atwater and C. M. Yang, Island growth and coarsening in thin films — conservative and nonconservative systems, *J. Appl. Phys.* 67(10), 6202 (1990)
135. W. H. Press, S. A. Teukolsky, W. T. Vetterling, and B. P. Flannery, Numerical Recipes in Fortran 77, Cambridge: Cambridge University Press, 1992
136. J. W. Christian, The Theory of Transformations in Metals and Alloys, Part I, New York: Pergamon Press, 2002
137. E. M. Lifshitz and L. P. Pitaevskii, Physical Kinetics, Oxford: Butterworth-Heinemann, 1981
138. T. P. Munt, D. E. Jesson, V. A. Shchukin, and D. Bimberg, Manipulating the size distributions of quantum dots associated with strain-renormalized surface energy, *Appl. Phys. Lett.* 85(10), 1784 (2004)
139. D. J. Vine, D. E. Jesson, M. J. Morgan, V. Shchukin, and D. Bimberg, Shape transitions of metastable surface nanostructures, *Phys. Rev. B* 72(24), 241304 (2005)
140. R. Bergamaschini, M. Brehm, M. Grydlik, T. Fromherz, G. Bauer, and F. Montalenti, Temperature-dependent evolution of the wetting layer thickness during Ge deposition on Si(001), *Nanotechnology* 22(28), 285704 (2011)
141. C. Misbah, O. Pierre-Louis, and Y. Saito, Crystal surfaces in and out of equilibrium: A modern view, *Rev. Mod. Phys.* 82(1), 981, (2010)
142. T. Witten and L. M. Sander, Diffusion-limited aggregation, a kinetic critical phenomenon, *Phys. Rev. Lett.* 47(19), 1400 (1981)
143. G. H. Gilmer, M. H. Grabow, and A. F. Bakker, Modeling of epitaxial growth, *Mater. Sci. Eng. B* 6(2–3), 101 (1990)
144. D. D. Vvedensky, Epitaxial phenomena across length and time scales, *Surf. Interface Anal.* 31(7), 627 (2001)
145. R. E. Caflisch, Growth, structure and pattern formation for thin films, *J. Sci. Comput.* 37(1), 3 (2008)
146. K. Pirkkalainen and I. T. Koponen, Computational study on tuning the 2D self-assembly of metallic nanoclusters, *Surf. Sci.* 604(11–12), 951 (2010)
147. B. A. Joyce and D. D. Vvedensky, Self-organized growth on GaAs surfaces, *Mater. Sci. Eng. Rep.* 46(6), 127 (2004)
148. P. P. Petrov and W. Miller, Fast kinetic Monte Carlo simulation and statistics of quantum dot arrays, *Surf. Sci.* 621, 175 (2014)
149. E. Schöll and B. Bose, Kinetic Monte Carlo simulation of the nucleation stage of the self-organized growth of quantum dots, *Solid-State Electron.* 42(7–8), 1587 (1998)

150. G. Russo and P. Smereka, Computation of strained epitaxial growth in three dimensions by kinetic Monte Carlo, *J. Comput. Phys.* 214(2), 809 (2006)

151. T. P. Schulze and P. Smereka, An energy localization principle and its application to fast kinetic Monte Carlo simulation of heteroepitaxial growth, *J. Mech. Phys. Solids* 57(3), 521 (2009)

152. B. G. Orr, D. A. Kessler, C. W. Snyder, and L. M. Sander, A model for strain-induced roughening and coherent island growth, *Europhys. Lett.* 19(1), 33 (1992)

153. C. H. Lam, C. K. Lee, and L. M. Sander, Competing roughening mechanisms in strained heteroepitaxy: A fast kinetic Monte Carlo study, *Phys. Rev. Lett.* 89(21), 216102 (2002)

154. M. T. Lung, C. H. Lam, and L. M. Sander, Island, pit, and groove formation in strained heteroepitaxy, *Phys. Rev. Lett.* 95(8), 086102 (2005)

155. T. P. Schulze and P. Smereka, An energy localization principle and its application to fast kinetic Monte Carlo simulation of heteroepitaxial growth, *J. Mech. Phys. Solids* 57(3), 521 (2009)

156. F. Much and M. Biehl, Simulation of wetting-layer and island formation in heteroepitaxial growth, *Europhys. Lett.* 63, 14 (2003)

157. J. Y. Guo, Y. W. Zhang, and C. Lu, Effects of wetting and misfit strain on the pattern formation of heteroepitaxially grown thin films, *Comput. Mater. Sci.* 44(1), 174 (2008)

158. P. Gaillard, J. N. Aqua, and T. Frisch, Kinetic Monte Carlo simulations of the growth of silicon germanium pyramids, *Phys. Rev. B* 87(12), 125310 (2013)

159. G. Russo and P. Smereka, Computation of strained epitaxial growth in three dimensions by kinetic Monte Carlo, *J. Comput. Phys.* 214(2), 809 (2006)

160. J. N. Aqua and T. Frisch, Elastic interactions and kinetics during reversible submonolayer growth: Monte Carlo simulations, *Phys. Rev. B* 78(12), 121305 (2008)

161. R. Stumpf and M. Scheffler, Theory of self-diffusion at and growth of Al(111), *Phys. Rev. Lett.* 72(2), 254 (1994)

162. R. Stumpf and M. Scheffler, Ab initio calculations of energies and self-diffusion on flat and stepped surfaces of Al and their implications on crystal growth, *Phys. Rev. B* 53(8), 4958 (1996)

163. B. D. Yu and M. Scheffler, Anisotropy of growth of the close-packed surfaces of silver, *Phys. Rev. Lett.* 77(6), 1095 (1996)

164. A. Bogicevic, J. Strömquist, and B. Lundqvist, Low-symmetry diffusion barriers in homoepitaxial growth of Al(111), *Phys. Rev. Lett.* 81(3), 637 (1998)

165. A. La Magna, Nanoisland shape relaxation mechanism, *Surf. Sci.* 601(2), 308 (2007)

166. K. Thürmer, J. E. Reutt-Robey, and E. D. Williams, Nucleation limited crystal shape transformations, *Surf. Sci.* 537(1–3), 123 (2003)

167. C. Herring, in: Structure and Properties of Solid Surfaces, edited by R. Gomer and C. S. Smith, Chicago: The University of Chicago Press, 1952, pp 5–81

168. W. W. Mullins and G. S. Rohrer, Nucleation barrier for volume-conserving shape changes of faceted crystals, *J. Am. Ceram. Soc.* 83(1), 214 (2000)

169. G. S. Rohrer, C. L. Rohrer, and W. W. Mullins, Nucleation energy barriers for volume-conserving shape changes of crystals with nonequilibrium morphologies, *J. Am. Ceram. Soc.* 84(9), 2099 (2001)

170. N. Combe, P. Jensen, and A. Pimpinelli, Changing shapes in the nanoworld, *Phys. Rev. Lett.* 85(1), 110 (2000)

171. D. N. McCarthy and S. A. Brown, Evolution of neck radius and relaxation of coalescing nanoparticles, *Phys. Rev. B* 80, 064107 (2009)

172. F. Family and T. Vicsek, in: Dynamics of Fractal Surfaces, Singapore: World Scientific Press, 1991

173. A. L. Barabasi and H. E. Stanly, Fractal Concepts in Surface Growth, New York: Cambridge University Press, 1995

174. P. Meakin, Fractals, Scaling and Growth Far from Equilibrium, Cambridge: Cambridge University Press, 1998

175. F. Family and T. Vicsek, Scaling of the active zone in the Eden process on percolation networks and the ballistic deposition model, *J. Phys. Math. Gen.* 18(2), L75 (1985)

176. H. Brune, K. Bromann, H. Röder, K. Kern, J. Jacobsen, P. Stoltze, K. Jacobsen, and J. Nørskov, Effect of strain on surface diffusion and nucleation, *Phys. Rev. B* 52(20), R14380 (1995)

177. J. Krug, Four lectures on the physics of crystal growth, *Physica A* 313(1–2): 47, 2002

178. P. P. Chatraphorn, Z. Toroczkai, and S. Das Sarma, Epitaxial mounding in limited-mobility models of surface growth, *Phys. Rev. B* 64(20), 205407 (2001)

179. K. J. Caspersen, A. R. Layson, C. R. Stoldt, V. Fournee, P. Thiel, and J. Evans, Development and ordering of mounds during metal(100) homoepitaxy, *Phys. Rev. B* 65(19), 193407 (2002)

180. F. F. Leal, S. C. Ferreira, and S. O. Ferreira, Modelling of epitaxial film growth with an Ehrlich–Schwoebel barrier dependent on the step height, *J. Phys.: Condens. Matter* 23(29), 292201 (2011)

181. R. L. Schwoebel and E. J. Shipsey, Step motion on crystal surfaces, *J. Appl. Phys.* 37(10), 3682 (1966)

182. R. L. Schwoebel, Step motion on crystal surfaces (II), *J. Appl. Phys.* 40(2), 614 (1969)

183. J. Villain, Continuum models of crystal growth from atomic beams with and without desorption, *J. Phys. I* 1(1), 19 (1991)

184. J. G. Amar and F. Family, Step-adatom attraction as a new mechanism for instability in epitaxial growth, *Phys. Rev. Lett.* 77(22), 4584 (1996)

185. D. V. Brunev, I. G. Neizvestny, N. L. Shwartz, and Z. S. Yanovitskaja, Schwoebel barriers and quantum dot lateral size equalization during epitaxial growth, *Nanotechnology* 12(4), 413 (2001)

186. R. Zhu, E. Pan, and P. W. Chung, Fast multiscale kinetic Monte Carlo simulations of three-dimensional self-assembled quantum dot islands, *Phys. Rev. B* 75(20), 205339 (2007)
187. Z. Y. Zhang, J. Detch, and H. Metiu, Surface roughness in thin-film growth: The effect of mass transport between layers, *Phys. Rev. B* 48(7), 4972 (1993)
188. M. Kalff, P. Šmilauer, G. Comsa, and T. Michely, No coarsening in Pt(111) homoepitaxy, *Surf. Sci.* 426(3), L447 (1999)
189. B. Yang, Elastic energy release rate of quantum islands in Stranski–Krastanow growth, *J. Appl. Phys.* 92(7), 3704 (2002)
190. C. Ratsch, J. DeVita, and P. Smereka, Level-set simulation for the strain-driven sharpening of the island-size distribution during submonolayer heteroepitaxial growth, *Phys. Rev. B* 80(15), 155309 (2009)
191. A. C. Schindler, M. F. Gyure, G. D. Simms, D. Vvedensky, R. Caflisch, C. Connell, and E. Luo, Theory of strain relaxation in heteroepitaxial systems, *Phys. Rev. B* 67(7), 075316 (2003)
192. C. Ratsch, P. Smilauer, D. D. Vvedensky, and A. Zangwill, Mechanism for coherent island formation during heteroepitaxy, *J. Phys. I* 6, 575 (1996)
193. P. Nath and M. Ranganathan, Kinetic Monte Carlo simulations of heteroepitaxial growth with an atomistic model of elasticity, *Surf. Sci.* 606(17–18), 1450 (2012)
194. V. I. Tokar and H. Dreyssé, Nucleation of size calibrated three-dimensional nanodots in atomistic model of strained epitaxy: A Monte Carlo study, *J. Phys.: Condens. Matter* 25(4), 045001 (2013)
195. F. Buatier de Mongeot, W. Zhu, A. Molle, R. Buzio, C. Boragno, U. Valbusa, E. Wang, and Z. Zhang, Nanocrystal formation and faceting instability in Al(110) homoepitaxy: True upward adatom diffusion at step edges and island corners, *Phys. Rev. Lett.* 91(1), 016102 (2003)
196. K. Fichthorn and M. Scheffler, Nanophysics: A step up to self-assembly, *Nature* 429(6992), 617 (2004)
197. W. Zhu, F. Buatier de Mongeot, U. Valbusa, E. Wang, and Z. Zhang, Adatom ascending at step edges and faceting on fcc metal (110) surfaces, *Phys. Rev. Lett.* 92(10), 106102 (2004)
198. H. Yang, Q. Sun, Z. Zhang, and Y. Jia, Upward self-diffusion of adatoms and small clusters on facets of fcc metal (110) surfaces, *Phys. Rev. B* 76(11), 115417 (2007)
199. Z. Zhang, Q. Niu, and C. K. Shih, Electronic growth of metallic overlayers on semiconductor substrates, *Phys. Rev. Lett.* 80(24), 5381 (1998)
200. K. Budde, E. Abram, V. Yeh, and M. C. Tringides, Uniform, self-organized, seven-step height Pb/Si(111)-(7×7) islands at low temperatures, *Phys. Rev. B* 61(16), R10602 (2000)
201. K. L. Man, M. C. Tringides, M. M. T. Loy, and M. Altman, Superdiffusive motion of the Pb wetting layer on the Si(111) surface, *Phys. Rev. Lett.* 110(3), 036104 (2013)
202. M. Hupalo and M. C. Tringides, Ultrafast kinetics in Pb/Si(111) from the collective spreading of the wetting layer, *Phys. Rev. B* 75(23), 235443 (2007)
203. W. K. Burton, N. Cabrera, and F. C. Frank, The growth of crystals and the equilibrium structure of their surfaces, *Philos. Trans. R. Soc. London A* 243, 299 (1951)
204. H. C. Jeong and E. D. Williams, Steps on surfaces: Experiment and theory, *Surf. Sci. Rep.* 34(6–8): 171 (1999)
205. N. Israeli and D. Kandel, Profile of a decaying crystalline cone, *Phys. Rev. B* 60(8), 5946 (1999)
206. E. Korutcheva, A. M. Turiel, and I. Markov, Coherent Stranski–Krastanov growth in 1+1 dimensions with anharmonic interactions: An equilibrium study, *Phys. Rev. B* 61(24), 16890 (2000)
207. K. E. Khor and S. Das Sarma, Quantum dot self-assembly in growth of strained-layer thin films: A kinetic Monte Carlo study, *Phys. Rev. B* 62(24), 16657 (2000)
208. J. E. Prieto and I. Markov, Thermodynamic driving force of formation of coherent three-dimensional islands in Stranski–Krastanov growth, *Phys. Rev. B* 66(7), 073408 (2002)
209. J. E. Prieto and I. Markov, Quantum-dot nucleation in strained-layer epitaxy: Minimum-energy pathway in the stress-driven two-dimensional to three-dimensional transformation, *Phys. Rev. B* 72(20), 205412 (2005)
210. R. Xiang, M. T. Lung, and C. H. Lam, Layer-by-layer nucleation mechanism for quantum dot formation in strained heteroepitaxy, *Phys. Rev. E* 82(2), 021601 (2010)
211. J. E. Prieto and I. Markov, Second-layer nucleation in coherent Stranski–Krastanov growth of quantum dots, *Phys. Rev. B* 84(19), 195417 (2011)
212. K. M. Chen, D. Jesson, S. Pennycook, T. Thundat, and R. Warmack, Critical nuclei shapes in the stress-driven 2D-to-3D transition, *Phys. Rev. B* 56(4), R1700 (1997)
213. P. Sutter and M. G. Lagally, Nucleationless three-dimensional island formation in low-misfit heteroepitaxy, *Phys. Rev. Lett.* 84(20), 4637 (2000)
214. P. Kratzer, Q. K. K. Liu, P. Acosta-Diaz, C. Manzano, G. Costantini, R. Songmuang, A. Rastelli, O. Schmidt, and K. Kern, Shape transition during epitaxial growth of InAs quantum dots on GaAs(001): Theory and experiment, *Phys. Rev. B* 73(20), 205347 (2006)
215. D. J. Jesson, G. Chen, K. Chen, and S. Pennycook, Self-limiting growth of strained faceted islands, *Phys. Rev. Lett.* 80(23), 5156 (1998)
216. M. Kästner and B. Voigtländer, Kinetically self-limiting growth of Ge Islands on Si(001), *Phys. Rev. Lett.* 82(13), 2745 (1999)
217. J. Johansson and W. Seifert, Kinetics of self-assembled island formation: Part II – Island size, *J. Cryst. Growth* 234(1), 139 (2002)
218. F. Montalenti, P. Raiteri, D. B. Migas, H. von Känel, A. Rastelli, C. Manzano, G. Costantini, U. Denker, O. Schmidt, K. Kern, and L. Miglio, Atomic-scale pathway

of the pyramid-to-dome transition during Ge growth on Si(001), *Phys. Rev. Lett.* 93(21), 216102 (2004)

219. H. Eisele, A. Lenz, R. Heitz, R. Timm, M. Dähne, Y. Temko, T. Suzuki, and K. Jacobi, Change of InAs/GaAs quantum dot shape and composition during capping, *J. Appl. Phys.* 104(12), 124301 (2008)
220. A. Rastelli, H. Von Känel, B. Spencer, and J. Tersoff, Prepyramid-to-pyramid transition of SiGe islands on Si(001), *Phys. Rev. B* 68(11), 115301 (2003)
221. A. Vailionis, B. Cho, G. Glass, P. Desjardins, David G. Cahill, and J. E. Greene, Pathway for the strain-driven two-dimensional to three-dimensional transition during growth of Ge on Si(001), *Phys. Rev. Lett.* 85, 3672 (2000)
222. B. J. Spencer and J. Tersoff, Symmetry breaking in shape transitions of epitaxial quantum dots, *Phys. Rev. B* 87(16), 161301 (2013)
223. X. B. Niu, G. B. Stringfellow, and F. Liu, Nonequilibrium composition profiles of alloy quantum dots and their correlation with the growth mode, *Phys. Rev. Lett.* 107(7), 076101 (2011)
224. T. P. Schulze and P. Smereka, Kinetic Monte Carlo simulation of heteroepitaxial growth: Wetting layers, quantum dots, capping, and nanorings, *Phys. Rev. B* 86(23), 235313 (2012)
225. F. Watanabe, D. G. Cahill, and J. E. Greene, Roughening rates of strained-layer instabilities, *Phys. Rev. Lett.* 94(6), 066101 (2005)
226. M. A. Grinfeld, Instability of the separation boundry between a nonhydrostatically stressed elastic body and a melt, *Sov. Phys. Dokl.* 31, 831 (1986)
227. D. J. Srolovitz, On the stability of surfaces of stressed solids, *Acta Metall.* 37(2), 621 (1989)
228. O. Pierre-Louis, A. Chame, and Y. Saito, Dewetting of a solid monolayer, *Phys. Rev. Lett.* 99(13), 136101 (2007)
229. K. Thurmer and N. C. Bartelt, Nucleation-limited dewetting of ice films on Pt(111), *Phys. Rev. Lett.* 100(18), 186101 (2008)
230. K. Thürmer, J. E. Reutt-Robey, and E. D. Williams, Nucleation limited crystal shape transformations, *Surf. Sci.* 537(1–3), 123 (2003)
231. R. F. Strickland, Constable, Kinetics and Mechanism of Crystallization, New York: Academic Press, 1968
232. C. Herring, Some theorems on the free energies of crystal surfaces, *Phys. Rev.* 82(1), 87 (1951)
233. A. F. Andreev, Faceting phase transitions of crystals, *Sov. Phys. JETP* 53, 1063 (1981,
234. F. Cheynis, E. Bussmann, F. Leroy, T. Passanante, and P. Mülle, Dewetting dynamics of silicon-on-insulator thin films, *Phys. Rev. B* 84(24), 245439 (2011)
235. F. Leroy, F. Cheynis, T. Passante, and P. Müller, Dynamics, anisotropy, and stability of silicon-on-insulator dewetting fronts, *Phys. Rev. B* 85(19), 195414 (2012)
236. F. Baletto and R. Ferrando, Structural properties of nanoclusters: Energetic, thermodynamic, and kinetic effects, *Rev. Mod. Phys.* 77(1), 371 (2005)
237. W. Li, J. S. Lin, M. Karimi, C. Moses, and G. Vidali, Structural characterization of ultra-thin metal overlayers on Cu(001) by atom beam scattering, *Appl. Surf. Sci.* 48–49, 160 (1991)
238. W. Li, G. Vidali, and O. Biham, Scaling of island growth in Pb overlayers on Cu(001), *Phys. Rev. B* 48(11), 8336 (1993)
239. B. J. Siwick, J. R. Dwyer, R. E. Jordan, and R. J. D. Miller, An atomic-level view of melting using femtosecond electron diffraction, *Science* 302(5649), 1382 (2003)
240. C. V. Shank, R. Yen, and C. Hirlimann, Time-resolved reflectivity measurements of femtosecond-optical-pulse-induced phase transitions in silicon, *Phys. Rev. Lett.* 50(6), 454 (1983)
241. G. Sciaini and R. J. D. Miller, Femtosecond electron diffraction: heralding the era of atomically resolved dynamics, *Rep. Prog. Phys.* 74(9), 096101 (2011)
242. M. J. Aziz, Model for solute redistribution during rapid solidification, *J. Appl. Phys.* 53(2), 1158 (1982)
243. R. Willnecker, D. M. Herlach, and B. Feuerbacher, Grain refinement induced by a critical crystal growth velocity in undercooled melts, *Appl. Phys. Lett.* 56(4), 324 (1990)
244. W. G. Burgers, On the process of transition of the cubic-body-centered modification into the hexagonal-close-packed modification of zirconium, *Physica* 1(7–12), 561 (1934)
245. J. A. Hawreliak, B. El-Dasher, H. Lorenzana, G. Kimminau, A. Higginbotham, B. Nagler, S. M. Vinko, W. J. Murphy, T. Whitcher, J. S. Wark, S. Rothman, and N. Park, *In situ* X-ray diffraction measurements of the c/a ratio in the high-pressure ε phase of shock-compressed polycrystalline iron, *Phys. Rev. B* 83(14), 144114 (2011)
246. B. Dupé, B. Amadon, Y. P. Pellegrini, and C. Denoual, Mechanism for the $\alpha \rightarrow \varepsilon$ phase transition in iron, *Phys. Rev. B* 87(2), 024103 (2013)
247. T. Kudo, T. Inoue, T. Kita, and O. Wada, Real time analysis of self-assembled InAs/GaAs quantum dot growth by probing reflection high-energy electron diffraction chevron image, *J. Appl. Phys.* 104(7), 074305 (2008)
248. A. Feltrin and A. Freundlich, RHEED metrology of Stranski–Krastanov quantum dots, *J. Cryst. Growth* 301–302, 38 (2007)
249. A. Freundlich and C. Rajapaksha, Quantum dots and nanostructures: Synthesis, characterization, and modeling VIII, *Proc. SPIE* 7947, 79470P (2011)
250. M. Yakimov, V. Tokranov, G. Agnello, J. van Eisden, and S. Oktyabrsky, *In situ* monitoring of formation of InAs quantum dots and overgrowth by GaAs or AlAs, *J. Vac. Sci. Technol. B* 23(3), 1221 (2005)
251. K. Shimomura, T. Shirasaka, D. M. Tex, F. Yamada and I. Kamiya, RHEED transients during InAs quantum dot growth by MBE, *J. Vac. Sci. Technol. B* 30, 02B128 (2012)

252. J. M. Gérard, J. B. Genin, J. Lefebvre, J. M. Moison, N. Lebouché, and F. Barthe, Optical investigation of the self-organized growth of InAs/GaAs quantum boxes, *J. Cryst. Growth* 150, 351 (1995)

253. M. Takahasi, T. Kaizu, and J. Mizuki, *In situ* monitoring of internal strain and height of InAs nanoislands grown on GaAs(001), *Appl. Phys. Lett.* 88(10), 101917 (2006)

254. G. R. Bell, M. Pristovsek, T. Tsukamoto, B. G. Orr, Y. Arakawa, and N. Koguchi, *In situ* scanning tunneling microscopy of InAs quantum dots on GaAs(0 0 1) during molecular beam epitaxial growth, *Surf. Sci.* 544(2–3), 234 (2003)

255. S. Tsukamoto, T. Honma, G. R. Bell, A. Ishii, and Y. Arakawa, Atomistic insights for InAs quantum dot formation on GaAs(001) using STM within a MBE growth chamber, *Small* 2(3), 386 (2006)

256. H. R. Eisenberg and D. Kandel, Wetting layer thickness and early evolution of epitaxially strained thin films, *Phys. Rev. Lett.* 85(6), 1286 (2000)

257. P. Müller and R. Kern, The physical origin of the two-dimensional towards three-dimensional coherent epitaxial Stranski–Krastanov transition, *Appl. Surf. Sci.* 102, 6 (1996)

258. J. Tersoff, Stress-induced layer-by-layer growth of Ge on Si(100), *Phys. Rev. B* 43(11), 9377 (1991)

259. M. J. Beck, A. van de Walle, and M. Asta, Surface energetics and structure of the Ge wetting layer on Si(100), *Phys. Rev. B* 70(20), 205337 (2004)

260. M. Brehm, F. Montalenti, M. Grydlik, G. Vastola, H. Lichtenberger, N. Hrauda, M. J. Beck, T. Fromherz, F. Schäffler, L. Miglio, and G. Bauer, Key role of the wetting layer in revealing the hidden path of Ge/Si(001) Stranski–Krastanow growth onset, *Phys. Rev. B* 80(20), 205321 (2009)

261. I. Daruka and A. L. Barabási, Dislocation-free island formation in heteroepitaxial growth: A study at equilibrium, *Phys. Rev. Lett.* 79(19), 3708 (1997)

262. C. Chiu, Z. Huang, and C. T. Poh, Formation of nanostructures by the activated Stranski–Krastanow transition method, *Phys. Rev. Lett.* 93(13), 136105 (2004)

263. D. V. Yurasov and Y. N. Drozdov, Critical thickness for the Stranski–Krastanov transition treated with the effect of segregation, *Semiconductors* 42(5), 563 (2008)

264. H. R. Eisenberg and D. Kandel, Wetting layer thickness and early evolution of epitaxially strained thin films, *Phys. Rev. Lett.* 85(6), 1286 (2000)

265. C. H. Chiu and H. Gao, in: Thin Films: Stresses and Mechanical Properties V, edited by S. P. Baker, *et al.*, MRS Symposia Proceedings No. 356, Pittsburgh: Materials Research Society, 1995, page 33

266. R. V. Kukta and L. B. Freund, in: Thin Films: Stresses and Mechanical Properties VI, edited by W. W. Gerberich, *et al.*, MRS Symposia Proceedings No. 436, Pittsburgh: Materials Research Society, 1997, page 493

267. B. J. Spencer, Asymptotic derivation of the glued-wetting-layer model and contact-angle condition for Stranski–Krastanow islands, *Phys. Rev. B* 59(3), 2011 (1999)

268. S. M. Shivaprasad, S. Bera, and Y. Aparna, The epitaxial growth of Ag on Si(111)-(7×7) surface and its $(\sqrt{3}\times\sqrt{3})$-R30 surface phase transformation, *Bull. Mater. Sci.* 21(2), 111 (1998)

269. S. Äozkaya, M. Çakmak, and B. Alkan, Atomic and electronic structures of the group-IV elements on Si(111)-$(\sqrt{3}\times\sqrt{3})$ surface, *J. Phys. Conf. Ser.* 100, 072025 (2008)

270. H. W. Yeom, K. Yoo, and D. H. Oh, Electronic structures of Ga-induced incommensurate and commensurate overlayers on the Si(111) surface, *Surf. Sci.* 605(1–2), 146 (2011)

271. J. Čechal, M. Kolıbal, P. Kostelnık, and T. Šikola, Gallium structure on the Si(111)-(7×7) surface: Influence of Ga coverage and temperature, *J. Phys.: Condens. Matter* 19(1), 016011 (2007)

272. G. Meyer, M. Michailov, and M. Henzler, LEED studies of the epitaxy of Pb on Cu(111), *Surf. Sci.* 202(1–2), 125 (1988)

273. C. Nagl, O. Haller, E. Platzgummer, M. Schmid, and P. Varga, Submonolayer growth of Pb on Cu(111): surface alloying and de-alloying, *Surf. Sci.* 321(3), 237 (1994)

274. B. H. Müller, Th. Schmidt, and M. Henzler, Growth and melting of a Pb monolayer on Cu(111), *Surf. Sci.* 376(1–3), 123 (1997)

275. Y. Tu and J. Tersoff, Origin of apparent critical thickness for island formation in heteroepitaxy, *Phys. Rev. Lett.* 93(21), 216101 (2004)

276. T. Walther, A. G. Cullis, D. J. Norris, and M. Hopkinson, Nature of the Stranski–Krastanow transition during epitaxy of InGaAs on GaAs, *Phys. Rev. Lett.* 86(11), 2381 (2001)

277. J. G. Belk, J. L. Sudijono, D. M. Holmes, C. F. McConville, T. S. Jones, and B. A. Joyce, Spatial distribution of In during the initial stages of growth of InAs on GaAs(001)-c(4×4), *Surf. Sci.* 365(3), 735 (1996)

278. T. J. Krzyzewski, P. B. Joyce, G. R. Bell, and T. S. Jones, Surface morphology and reconstruction changes during heteroepitaxial growth of InAs on GaAs(001)- c(2×4), *Surf. Sci.* 482–485, 891 (2001)

279. J. Grabowski, C. Prohl, B. Höpfner, M. Dähne, and H. Eisele, Evolution of the InAs wetting layer on GaAs(001)-(4×4) on the atomic scale, *Appl. Phys. Lett.* 95(23), 233118 (2009)

280. C. Prohl, B. Höpfner, J. Grabowski, J. Grabowski, M. Dähne, and H. Eisele, Atomic structure and strain of the InAs wetting layer growing on GaAs(001)-c(4×4), *J. Vac. Sci. Tech. B* 28, C5E13 (2009)

281. M. Sauvage-Simkin, Y. Garreau, R. Pinchaux, M. Véron, J. Landesman, and J. Nagle, Commensurate and incommensurate phases at reconstructed (In,Ga)As(001) surfaces: X-ray diffraction evidence for a composition lock-in, *Phys. Rev. Lett.* 75(19), 3485 (1995)

282. C. Ratsch and A. Zangwill, Equilibrium theory of the Stranski–Krastanov epitaxial morphology, *Surf. Sci.* 293(1–2), 123 (1993)

283. V. I. Tokar and H. Dreyssé, Lattice gas model of coherent strained epitaxy, *Phys. Rev. B* 68(19), 195419 (2003)

284. V. I. Tokar and H. Dreysse, Size calibration of self-assembled nanoparticles in a model of strained epitaxy with passive substrate, *Phys. Rev. B* 72(3), 035438 (2005)

285. W. D. Knight, K. Clemenger, W. A. de Heer, W. Saunders, M. Chou, and M. Cohen, Electronic shell structure and abundances of sodium clusters, *Phys. Rev. Lett.* 52(24), 2141 (1984)

286. T. P. Martin, Shell of atoms, *Phys. Rep.* 273(4), 199 (1996)

287. S. Gwo, C. P. Chou, C. L. Wu, Y.J. Ye, S.J. Tsai, W.C. Lin, and M.T. Lin, Self-limiting size distribution of supported cobalt nanoclusters at room temperature, *Phys. Rev. Lett.* 90(18), 185506 (2003

288. M. Jałochowski, M. Hoffmann, and E. Bauer, Pb layer-by-layer growth at very low temperatures, *Phys. Rev. B* 51(11), 7231 (1995)

289. Y. L. Wang and M. Y. Lai, Formation of surface magic clusters: A pathway to monodispersed nanostructures on surfaces, *J. Phys.: Condens. Matter* 13(31), R589 (2001)

290. J. F. Jia, X. Liu, J. Z. Wang, J. L. Li, X. Wang, Q. K. Xue, Z. Q. Li, Z. Zhang, and S. Zhang, Fabrication and structural analysis of Al, Ga, and In nanocluster crystals, *Phys. Rev. B* 66(16), 165412 (2002)

291. C. Priester and M. Lannoo, Origin of self-assembled quantum dots in highly mismatched heteroepitaxy, *Phys. Rev. Lett.* 75(1), 93 (1995)

292. T. Kudo, T. Inoue, T. Kita, and O. Wada, Real time analysis of self-assembled InAs/GaAs quantum dot growth by probing reflection high-energy electron diffraction chevron image, *J. Appl. Phys.* 104(7), 074305 (2008)

293. M. Valden, X. Lai, and D. W. Goodman, Onset of catalytic activity of gold clusters on titania with the appearance of nonmetallic properties, *Science* 281(5383), 1647 (1998)

294. C. Xu, X. Lai, G.W. Zajac, and D.W. Goodman, Scanning tunneling microscopy studies of the TiO_2(110) surface: Structure and the nucleation growth of Pd, *Phys. Rev. B* 56(11), 13464 (1997)

295. F. Liu, Self-assembly of three-dimensional metal islands: Nonstrained versus strained islands, *Phys. Rev. Lett.* 89(24), 246105 (2002)

296. Z. Gai, B. Wu, J. P. Pierce, G. A. Farnan, D. Shu, M. Wang, Z. Zhang, and J. Shen, Self-assembly of nanometer-scale magnetic dots with narrow size distributions on an insulating substrate, *Phys. Rev. Lett.* 89(23), 235502 (2002

297. A. C. Levi and M. Kotrla, Theory and simulation of crystal growth, *J. Phys.: Condens. Matter* 9(2), 299 (1997)

298. J. Cleick, Chaos, Viking Penguin Inc., 1987

299. J. Wu, P. Jin, Y. H. Jiao, X. J. Lv, and Z. G. Wang, Evolution of InAs/GaAs(001) islands during the two- to three-dimensional growth mode transition in molecular-beam epitaxy, *Nanotechnology* 18(16), 165301 (2007)

300. J. A. Floro, M. B. Sinclair, E. Chason, L. Freund, R. Twesten, R. Hwang, and G. Lucadamo, Novel SiGe island coarsening kinetics: Ostwald ripening and elastic interactions, *Phys. Rev. Lett.* 84(4), 701 (2000)

301. M. Meixner, R. Kunert, and E. Scholl, Control of strain-mediated growth kinetics of self-assembled semiconductor quantum dots, *Phys. Rev. B* 67(19), 195301 (2003)

302. L. G. Wang, P. Kratzer, M. Scheffler, and N. Moll, Formation and Stability of Self-Assembled Coherent Islands in Highly Mismatched Heteroepitaxy, *Phys. Rev. Lett.* 82(20), 4042 (1999)

303. L. G. Wang, P. Kratzer, N. Moll, and M. Scheffler, Size, shape, and stability of InAs quantum dots on the GaAs(001) substrate, *Phys. Rev. B* 62(3), 1897 (2000)

304. A. Polimeni, A. Patane, M. Capizzi, F. Martelli, L. Nasi, and G. Salviati, Self-aggregation of quantum dots for very thin InAs layers grown on GaAs, *Phys. Rev. B* 53(8), R4213 (1996)

305. V. G. Dubrovskii, M. A. Kazansky, M. V. Nazarenko, and L. T. Adzhemyan, Numerical analysis of Ostwald ripening in two-dimensional systems, *J. Chem. Phys.* 134(9), 094507 (2011)

306. Y. S. Djikaev and E. Ruckenstein, Kinetic theory of nucleation based on a first passage time analysis: Improvement by the density-functional theory, *J. Chem. Phys.* 123(21), 214503 (2005)

307. N. P. Kobayashi, T. R. Ramachandran, P. Chen, and A. Madhukar, In situ, atomic force microscope studies of the evolution of InAs three-dimensional islands on GaAs(001), *Appl. Phys. Lett.* 68(23), 3299 (1996)

308. D. S. Guimard, H. Lee, M. Nishioka, and Y. Arakawa, Growth of high-uniformity InAs/GaAs quantum dots with ultralow density below $10^7 \mathrm{cm}^{-2}$ and emission above 1.3 μm, *Appl. Phys. Lett.* 92(16), 163101 (2008)

309. A. Rosenauer, D. Gerthsen, D. Dyck, M. Arzberger, G. Böhm, and G. Abstreiter, Quantification of segregation and mass transport in $In_xGa_{1-x}As$/GaAs Stranski–Krastanow layers, *Phys. Rev. B* 64(24), 245334 (2001)

310. M. Gsell, P. Jakob, and D. Menzel, Effect of substrate strain on adsorption, *Science* 280(5364), 717 (1998)

311. M. Mavrikakis, B. Hammer, and J. K. Nørskov, Effect of strain on the reactivity of metal surfaces, *Phys. Rev. Lett.* 81(13), 2819 (1998)

312. K. Muraki, S. Fukatsu, Y. Shiraki, and R. Ito, Surface segregation of In atoms during molecular beam epitaxy and its influence on the energy levels in InGaAs/GaAs quantum wells, *Appl. Phys. Lett.* 61(5), 557 (1992)

313. D. Litvinov, D. Gerthsen, A. Rosenauer, M. Schowalter, T. Passow, P. Feinäugle, and M. Hetterich, Transmission electron microscopy investigation of segregation and critical floating-layer content of indium for island formation in $In_xGa_{1-x}As$, *Phys. Rev. B* 74(16), 165306 (2006)

314. J. M. García, J. P. Silveira, and F. Briones, Strain relaxation and segregation effects during self-assembled InAs quantum dots formation on GaAs(001), *Appl. Phys. Lett.* 77(3), 409 (2000)
315. A. G. Cullis, D. J. Norris, T. Walther, M. A. Migliorato, and M. Hopkinson, Stranski–Krastanow transition and epitaxial island growth, *Phys. Rev. B* 66(8), 081305 (2002)
316. A. G. Cullis, D. J. Norris, M. A. Migliorato, and M. Hopkinson, Surface elemental segregation and the Stranski–Krastanow epitaxial islanding transition, *Appl. Surf. Sci.* 244(1–4), 65 (2005)
317. T. Honma, S. Tsukamoto, and Y. Arakawa, *In Situ* scanning tunneling microscope observation of InAs wetting layer formation on GaAs(001) during molecular beam epitaxy growth at 500°C, *Jpn. J. Appl. Phys.* 45(30), L777 (2006)
318. F. Patella, S. Nufris, F. Arciprete, M. Fanfoni, E. Placidi, A. Sgarlata, and A. Balzarotti, Tracing the two- to three-dimensional transition in the InAs/GaAs(001) heteroepitaxial growth, *Phys. Rev. B* 67(20), 205308 (2003)
319. J. M. Moison, C. Guille, F. Houzay, F. Barthe, and M. Van Rompay, Surface segregation of third-column atoms in group III-V arsenide compounds: Ternary alloys and heterostructures, *Phys. Rev. B* 40(9), 6149 (1989)
320. W. D. Xiao, Z. J. Yan, S. S. Kushvaha, M. J. Xu, and X. S. Wang, Different growth behavior of Ge, Al and Sb on graphite, *Surf. Rev. Lett.* 13(2–3), 287 (2006)
321. S. S. Kushvaha, Z. Yan, W. Xiao, M. J. Xu, Q. K. Xue, and X. S. Wang, Self-assembled Ge, Sb and Al nanostructures on graphite: comparative STM studies, *Nanotechnology* 18(14), 145501, (2007)
322. S. S. Kushvaha, H. Xu, W. Xiao, H. L. Zhang, A. T. S. Wee, and X.S. Wang, Scanning tunneling microscopy investigation of growth of self-assembled indium and aluminum nanostructures on inert substrates, *Thin Solid Films* 517(16), 4540 (2009)
323. S. S. Kushvaha, H. L. Zhang, Z. Yan, A. T. S. Wee, and X. S. Wang, Growth of self-assembled Mn, Sb and MnSb nanostructures on highly oriented pyrolytic graphite, *Thin Solid Films* 520(23), 6909 (2012)
324. A. Ohtake, M. Ozeki, M. Terauchi, F. Sato, and M. Tanaka, Strain-induced surface segregation in $In_{0.5}Ga_{0.5}As$/GaAs heteroepitaxy, *Appl. Phys. Lett.* 80(21), 3931 (2002)
325. A. Ohtake and M. Ozeki, Growth mode of $In_xGa_{1-x}As$ ($0 <\sim x <\sim 0.5$) on GaAs(001) under As-deficient conditions, *Phys. Rev. B* 65(15), 155318 (2002)
326. J. S. Kim and N. Koguchi, Near room temperature droplet epitaxy for fabrication of InAs quantum dots, *Appl. Phys. Lett.* 85(24), 5893 (2004)
327. A. Urbańczyk, G. J. Hamhuis, and R. Nötzel, In islands and their conversion to InAs quantum dots on GaAs (100): Structural and optical properties, *J. Appl. Phys.* 107(1), 014312 (2010)
328. K. Reyes, P. Smereka, D. Nothern, J. Millunchick, S. Bietti, C. Somaschini, S. Sanguinetti, and C. Frigeri, Unified model of droplet epitaxy for compound semiconductor nanostructures: Experiments and theory, *Phys. Rev. B* 87(16), 165406 (2013)
329. F. Bastiman, A. G. Cullis, and M. Hopkinson, InAs/GaAs(001) wetting layer formation observed in situ by concurrent MBE and STM, *Surf. Sci.* 603(24), 3439 (2009)
330. J. R. Arthur, Interaction of Ga and As_2 molecular beams with GaAs surfaces, *J. Appl. Phys.* 39(8), 4032 (1968)
331. J. R. Arthur, Surface stoichiometry and structure of GaAs, *Surf. Sci.* 43(2), 449 (1974)
332. J. R. Arthur, Gallium arsenide surface structure and reaction kinetics: Field emission microscopy, *J. Appl. Phys.* 37(8), 3057 (1966)
333. C. T. Foxon, M. R. Boudry, and B. A. Joyce, Evaluation of surface kinetic data by the transform analysis of modulated molecular beam measurements, *Surf. Sci.* 44(1), 69 (1974
334. C. T. Foxon and B. A. Joyce, Interaction kinetics of As_2 and Ga on 100 GaAs surfaces, *Surf. Sci.* 64(1), 293 (1977)
335. C. G. Morgan, P. Kratzer, and M. Scheffler, Arsenic dimer dynamics during MBE growth: Theoretical evidence for a novel chemisorption state of As_2 molecules on GaAs surfaces, *Phys. Rev. Lett.* 82(24), 4886 (1999)
336. M. Itoh, G. R. Bell, A. R. Avery, T. S. Jones, B. A. Joyce, and D. D. Vvedensky, Island nucleation and growth on reconstructed GaAs(001) surfaces,*Phys. Rev. Lett.* 81, 633 (1998)
337. S. V. Ghaisas and A. Madhukar, Monte Carlo simulations of MBE growth of III–V semiconductors: The growth kinetics, mechanism, and consequences for the dynamics of RHEED intensity, *J. Vac. Sci. Technol. B* 3(2), 540 (1985)
338. S. V. Ghaisas and A. Madhukar, Role of surface molecular reactions in influencing the growth mechanism and the nature of nonequilibrium surfaces: A Monte Carlo study of molecular-beam epitaxy, *Phys. Rev. Lett.* 56(10), 1066 (1986)
339. S. V. Ghaisas and A. Madhukar, Surface kinetics and growth interruption in molecular-beam epitaxy of compound semiconductors: A computer simulation study, *J. Appl. Phys.* 65(10), 3872 (1989)
340. T. Shitara, D. D. Vvedensky, M. R. Wilby, J. Zhang, J. Neave, and B. Joyce, Step-density variations and reflection high-energy electron-diffraction intensity oscillations during epitaxial growth on vicinal GaAs(001), *Phys. Rev. B* 46(11), 6815 (1992)
341. P. Šmilauer and D. D. Vvedensky, Step-edge barriers on GaAs(001), *Phys. Rev. B* 48(23), 17603 (1993)
342. K. Shiraishi and T. Ito, Theoretical investigation of adsorption behavior during molecular beam epitaxy growth of GaAs: ab initio based microscopic calculation, *J. Cryst. Growth* 150, 158 (1995)
343. G. Colayni and R. Venkat, Growth dynamics of InGaAs by MBE: Process simulation and theoretical analysis, *J. Cryst. Growth* 211(1–4), 21 (2000)

344. P. Kratzer, E. Penev, and M. Scheffler, Understanding the growth mechanisms of GaAs and InGaAs thin films by employing first-principles calculations, *Appl. Surf. Sci.* 216(1–4), 436 (2003)

345. J. Wu, Novel scenario for epitaxial growth process of quantum dots, *Micronanoelectronic Technology* 49, 141 (2012)

346. J. Wu and P. Jin, Epitaxial Growth Process of Quantum Dots, in: *Nanotechnology*, edited by S. Sinha, N. K. Navani, and J. N. Govil, Studium Press LLC, Volume 3, 2013, pp 335–368

347. A. Mujica, A. Rubio, A. Muñoz, and R. Needs, High-pressure phases of group-IV, III–V, and II–VI compounds, *Rev. Mod. Phys.* 75(3), 863 (2003)

348. N. E. Christensen, Calculated equation of state of InAs, *Phys. Rev. B* 33(7), 5096 (1986)

349. N. E. Christensen, High Pressure in Semiconductor Physics (I), edited by T Suski and W Paul, New York: Academic, 1998

350. L. Pedesseau, J. Even, A. Bondi, W. Guo, S. Richard, H. Folliot, C. Labbe, C. Cornet, O. Dehaese, A. Le Corre, O. Durand, and S. Loualiche, Theoretical study of highly strained InAs material from first-principles modelling: Application to an ideal QD, *J. Phys. D* 41(16), 165505 (2008)

351. Y. K. Vohra, S. T. Weir, and A. L. Ruoff, High-pressure phase transitions and equation of state of the III-V compound InAs up to 27 GPa, *Phys. Rev. B* 31(11), 7344 (1985)

352. M. Durandurdu, Structural phase transition of germanium under uniaxial stress: An ab initio study, *Phys. Rev. B* 71(5), 054112 (2005)

353. R. G. Hennig, A. Wadehra, K. P. Driver, W. D. Parker, C. J. Umrigar, and J. W. Wilkins, Phase transformation in Si from semiconducting diamond to metallic β-Sn phase in QMC and DFT under hydrostatic and anisotropic stress, *Phys. Rev. B* 82(1), 014101 (2010)

354. J. C. Jamieson, Crystal structures at high pressures of metallic modifications of silicon and germanium, *Science* 139(3556), 762 (1963)

355. K. Gaál-Nagy, A. Bauer, M. Schmitt, K. Karch, P. Pavone, and D. Strauch, Temperature and dynamical effects on the high-pressure cubic-diamond $\leftrightarrow$ β-Tin phase transition in Si and Ge, *Physica Status Solidi (b): Basic Res.* 211(1), 275 (1999)

356. C. Cheng, W. H. Huang, and H. J. Li, Thermodynamics of uniaxial phase transition: *Ab initio* study of the diamond-to-β-tin transition in Si and Ge, *Phys. Rev. B* 63(15), 153202 (2001)

357. K. H. Hellwege, Physics of Group IV Elements and III-V Elements, Landolt–Börnstein, New Series, Group III, Vol. 17, Part a, Berlin: Springer, 1982

358. A. Jayaraman, W. Klement, and G. C. Kennedy, Melting and polymorphism at high pressures in some group IV elements and III-V compounds with the diamond/zincblende structure, *Phys. Rev.* 130(2), 540 (1963)

359. F. P. Bundy, Phase diagrams of silicon and germanium to 200 kbar, 1000°C, *J. Chem. Phys.* 41(12), 3809 (1964)

360. D. J. Bottomley, The physical origin of InAs quantum dots on GaAs(001), *Appl. Phys. Lett.* 72(7), 783 (1998)

361. D. J. Bottomley, The free energy of condensed matter under stress, *Jpn. J. Appl. Phys.* 36(Part 2, No. 11A), L1464 (1997)

362. D. J. Bottomley, Formation and shape of InAs nanoparticles on GaAs surfaces, *J. Vac. Sci. Technol. B* 17(2), 259 (1999)

363. F. Rosei and P. Raiteri, Stress induced surface melting during the growth of the Ge wetting layer on Si(001) and Si(111), *Appl. Surf. Sci.* 195(1–4), 16 (2002)

364. D. K. Biegelsen, R. Bringans, J. Northrup, and L.E. Swartz, Surface reconstructions of GaAs(100) observed by scanning tunneling microscopy, *Phys. Rev. B* 41(9), 5701 (1990)

365. C. Ratsch, Strain induced change of surface reconstructions for InAs(001), *Phys. Rev. B* 63, 161306(R) (2001)

366. A. Ohtake, P. Kocan, J. Nakamura, A. Natori, and N. Koguchi, Kinetics in surface reconstructions on GaAs(001), *Phys. Rev. Lett.* 92(23), 236105 (2004)

367. M. Sauvage-Simkin, R. Pinchaux, J. Massies, P. Calverie, N. Jedrecy, J. Bonnet, and I. Robinson, Fractional stoichiometry of the GaAs(001)-$c(4\times4)$ surface: An *in-situ* X-ray scattering study, *Phys. Rev. Lett.* 62(5), 563 (1989)

368. F. Liu, F. Wu, and M. G. Lagally, Effect of strain on structure and morphology of ultrathin Ge films on Si(001), *Chem. Rev.* 97(4), 1045 (1997)

369. B. Voigtländer, Fundamental processes in Si/Si and Ge/Si epitaxy studied by scanning tunneling microscopy during growth, *Surf. Sci. Rep.* 43(5–8), 127 (2001)

370. J. Tersoff, Missing dimers and strain relief in Ge films on Si(100), *Phys. Rev. B* 45(15), 8833 (1992)

371. F. Liu and M. G. Lagally, Interplay of stress, structure, and stoichiometry in Ge-covered Si(001), *Phys. Rev. Lett.* 76(17), 3156 (1996)

372. T. Zhou, G. Renaud, C. Revenant, J. Issartel, T. U. Schülli, R. Felici, and A. Malachias, Atomic structure and composition of the $2 \times N$ reconstruction of the Ge wetting layer on Si(001) investigated by surface X-ray diffraction, *Phys. Rev. B* 83(19), 195426 (2011)

373. M. Tomitori, K. Watanabe, M. Kobayashi, and O. Nishikawa, STM study of the Ge growth mode on Si(001) substrates, *Appl. Surf. Sci.* 76–77, 322 (1994)

374. I. Goldfarb, J. H. G. Owen, P. T. Hayden, D. R. Bowler, K. Miki, and G. A. D. Briggs, Gas-source growth of group IV semiconductors (III): Nucleation and growth of Ge/Si(001), *Surf. Sci.* 394(1–3), 105 (1997)

375. P. W. Sutter, J. I. Flege, and E. I. Sutter, Epitaxial graphene on ruthenium, *Nature* 7(5), 406 (2008)

376. M. Henzler, Growth of epitaxial monolayers, *Surf. Sci.* 357–358, 809 (1996)

377. B. Lalmi, H. Oughaddou, H. Enriquez, A. Kara, S. Vizzini, B. Ealet, and B. Aufray, Epitaxial growth of a silicene sheet, *Appl. Phys. Lett.* 97(22), 223109 (2010)

378. A. Kara, H. Enriquez, A. P. Seitsonen, L. C. Lew Yan Voon, S. Vizzini, B. Aufray, and H. Oughaddou, A review on silicene — New candidate for electronics, *Surf. Sci. Rep.* 67(1), 1 (2012)
379. H. Jamgotchian, Y. Colignon, N. Hamzaoui, B. Ealet, J. Y. Hoarau, B. Aufray, and J. P. Bibérian, Growth of silicene layers on Ag(111): Unexpected effect of the substrate temperature, *J. Phys.: Condens. Matter* 24(17), 172001 (2012)
380. B. Feng, Z. Ding, S. Meng, Y. Yao, X. He, P. Cheng, L. Chen, and K. Wu, Evidence of silicene in honeycomb structures of silicon on Ag(111), *Nano Lett.* 12(7), 3507 (2012)
381. H. Şahin, S. Cahangirov, M. Topsakal, E. Bekaroglu, E. Akturk, R. Senger, and S. Ciraci, Monolayer honeycomb structures of group-IV elements and III-V binary compounds: First-principles calculations, *Phys. Rev. B* 80(15), 155453 (2009)
382. S. Scandolo, M. Bernasconi, G. L. Chiarotti, P. Focher, and E. Tosatti, Pressure-induced transformation path of graphite to diamond, *Phys. Rev. Lett.* 74(20), 4015 (1995)
383. D. T. Wang, N. Esser, M. Cardona, and J. Zegenhagen, Epitaxy of Sn on Si(111), *Surf. Sci.* 343(1–2), 31 (1995)
384. L. L. Wang, X. C. Ma, S. H. Ji, Y. Fu, Q. Shen, J. Jia, K. Kelly, and Q. Xue, Epitaxial growth and quantum well states study of Sn thin films on Sn induced Si(111)-(23×23) R30° surface, *Phys. Rev. B* 77(20), 205410 (2008)
385. Q. Shen, W. Li, G. Dong, G. F. Sun, Y. Sun, X. Ma, J. Jia, and Q. Xue, Self-assembled Sn nanoplatelets on Si(1 1 1)-$2\sqrt{3}\times 2\sqrt{3}$-Sn surfaces, *J. Phys. D* 42(1), 015305 (2009)
386. L. L. Wang, X. C. Ma, Y. X. Ning, S. H. Ji, Y. S. Fu, J. F. Jia, K. F. Kelly and Q. K. Xue, Atomic scale study of strain relaxation in Sn islands on Sn-induced Si(111)-($2\sqrt{3}\times 2\sqrt{3}$) surface, *Appl. Phys. Lett.* 94(15), 153111 (2009)
387. A. N'Diaye, S. Bleikamp, P. Feibelman, and T. Michely, Two-dimensional Ir cluster lattice on a graphene Moiré on Ir(111), *Phys. Rev. Lett.* 97(21), 215501 (2006)
388. J. P. Feibelman, Pinning of graphene to Ir(111) by flat Ir dots, *Phys. Rev. B* 77(16), 165419 (2008)
389. C. Busse, P. Lazic, R. Djemour, J. Coraux, T. Gerber, N. Atodiresei, V. Caciuc, R. Brako, A. T. N'Diaye, S. Blügel, J. Zegenhagen, and T. Michely, Graphene on Ir(111): Physisorption with chemical modulation, *Phys. Rev. Lett.* 107(3), 036101 (2011)
390. E. Loginova, S. Nie, K. Thurmer, N. C. Bartelt, and K. F. McCarty, Defects of graphene on Ir(111): Rotational domains and ridges, *Phys. Rev. B* 80(8), 085430 (2009)
391. D. C. Elias, R. R. Nair, T. M. G. Mohiuddin, S. V. Morozov, P. Blake, M. P. Halsall, A. C. Ferrari, D. W. Boukhvalov, M. I. Katsnelson, A. K. Geim, and K. S. Novoselov, Control of graphene's properties by reversible hydrogenation: Evidence for graphane, *Science* 323(5914), 610 (2009)
392. C. Freeman, F. Claeyssens, N. Allan, and J. Harding, Graphitic nanofilms as precursors to Wurtzite films: Theory, *Phys. Rev. Lett.* 96(6), 066102 (2006)
393. C. Tusche, H. L. Meyerheim, and J. Kirschner, Observation of depolarized ZnO(0001) monolayers: Formation of unreconstructed planar sheets, *Phys. Rev. Lett.* 99(2), 026102 (2007)
394. G. Weirum, G. Barcaro, A. Fortunelli, F. Weber, R. Schennach, S. Surnev, and F. P. Netzer, Growth and surface structure of zinc oxide layers on a Pd(111) surface, *J. Phys. Chem. C* 114(36), 15432 (2010)
395. M. F. Jarrold and V. A. Constant, Silicon cluster ions: Evidence for a structural transition, *Phys. Rev. Lett.* 67(21), 2994 (1991)
396. M. F. Jarrold, Nanosurface chemistry on size-selected silicon clusters, *Science* 252(5009), 1085 (1991)
397. M. F. Jarrold and J. E. Bower, Mobilities of silicon cluster ions: The reactivity of silicon sausages and spheres, *J. Chem. Phys.* 96(12), 9180 (1992)
398. R. R. Hudgins, M. Imai, M. F. Jarrold, and P. Dugourd, High-resolution ion mobility measurements for silicon cluster anions and cations, *J. Chem. Phys.* 111(17), 7865 (1999)
399. A. A. Shvartsburg, R. R. Hudgins, P. Dugourd, and M. F. Jarrold, Structural information from ion mobility measurements: Applications to semiconductor clusters, *Chem. Soc. Rev.* 30(1), 26 (2001)
400. D. F. Hagen, Characterization of isomeric compounds by gas and plasma chromatography, *Anal. Chem.* 51(7), 870 (1979)
401. G. von Helden, M. T. Hsu, P. R. Kemper, and M. T. Bowers, Structures of carbon cluster ions from 3 to 60 atoms: Linears to rings to fullerenes, *J. Chem. Phys.* 95(5), 3835 (1991)
402. S. Yoo, J. J. Zhao, J. L. Wang, and X. C. Zeng, Endohedral Silicon Fullerenes $Si_N (27 \leqslant N \leqslant 39)$, *J. Am. Chem. Soc.* 126(42), 13845 (2004)
403. J. Zhao, J. Wang, J. Jellinek, S. Yoo, and X. C. Zeng, Stuffed fullerene structures for medium-sized silicon clusters, *Eur. Phys. J. D* 34(1–3), 35 (2005)
404. O. Oña, V. E. Bazterra, M. C. Caputo, J. Facelli, P. Fuentealba, and M. Ferraro, Modified genetic algorithms to model cluster structures in medium-sized silicon clusters: Si_{18}–Si_{60}, *Phys. Rev. A* 73(5), 053203 (2006)
405. J. Zhao, L. Ma, and B. Wen, Lowest-energy endohedral fullerene structure of Si_{60} from a genetic algorithm and density-functional theory, *J. Phys.: Condens. Matter* 19(22), 226208 (2007)
406. R. L. Zhou and B. C. Pan, Structural features of silicon clusters $Si_n (n = 40–57, 60)$, *Phys. Lett. A* 368(5), 396 (2007)
407. M. Ehbrecht and F. Huisken, Gas-phase characterization of silicon nanoclusters produced by laser pyrolysis of silane, *Phys. Rev. B* 59(4), 2975 (1999)
408. D. K. Yu, R. Q. Zhang, and S. T. Lee, Structural transition in nanosized silicon clusters, *Phys. Rev. B* 65(24), 245417 (2002)
409. G. Ledoux, O. Guillois, D. Porterat, C. Reynaud, F. Huisken, B. Kohn, and V. Paillard, Photoluminescence prop-

erties of silicon nanocrystals as a function of their size, *Phys. Rev. B* 62(23), 15942 (2000)

410. P. Mélinon, P. Kéghélian, B. Prével, A. Perez, G. Guiraud, J. LeBrusq, J. Lermé, M. Pellarin, and M. Broyer, Nanostructured silicon films obtained by neutral cluster depositions, *J. Chem. Phys.* 107(23), 10278 (1997)
411. P. Mélinon, P. Kéghélian, B. Prével, V. Dupuis, A. Perez, B. Champagnon, Y. Guyot, M. Pellarin, J. Lermé, M. Broyer, J. L. Rousset, and P. Delichère, Structural, vibrational, and optical properties of silicon cluster assembled films, *J. Chem. Phys.* 108(11), 4607 (1998)
412. A. N. Goldstein, The melting of silicon nanocrystals: Submicron thin-film structures derived from nanocrystal precursors, *Appl. Phys. A* 62(1), 33 (1996)
413. U. Röthlisberger, W. Andreoni, and M. Parrinello, Structure of nanoscale silicon clusters, *Phys. Rev. Lett.* 72(5), 665 (1994)
414. D. Tománek and M. A. Schluter, Growth regimes of carbon clusters, *Phys. Rev. Lett.* 67(17), 2331 (1991)
415. P. R. C. Kent, M. D. Towler, R. J. Needs, and G. Rajagopal, Carbon clusters near the crossover to fullerene stability, *Phys. Rev. B* 62(23), 15394 (2000)
416. P. W. Fowler and D. E. Manolopoulos, An Atlas of Fullerenes, Oxford: Clarendon Press, 1995
417. E. Hernández, P. Ordejón, and H. Terrones, Fullerene growth and the role of nonclassical isomers, *Phys. Rev. B* 63(19), 193403 (2001)
418. J. R. Heath, in: Fullerenes: Synthesis, Properties and Chemistry of Large Carbon Clusters, edited by G. S. Hammond and V. J. Kuck, ACS Symposium Series No. 481, Washington: American Chemical Society, 1991, page 1
419. A. A. Shvartsburg, R. R. Hudgins, P. Dugourd, R. Gutierrez, T. Frauenheim, and M. Jarrold, Observation of “stick” and “handle” intermediates along the fullerene road, *Phys. Rev. Lett.* 84(11), 2421 (2000)
420. A. S. Barnard, Theory and modeling of nanocarbon phase stability, *Diamond Related Materials* 15(2–3), 285 (2006)
421. S. J. Kwon and J.G. Park, Theoretical analysis of the graphitization of a nanodiamond, *J. Phys.: Condens. Matter* 19(38), 386215 (2007)
422. H. W. Kroto, J. R. Heath, S. C. O’Brien, R. F. Curl, and R. E. Smalley, C_{60}: Buckminsterfullerene, *Nature* 318(6042), 162 (1985)
423. A. S. Barnard, Modelling of nanoparticles: Approaches to morphology and evolution, *Rep. Prog. Phys.* 73, 086502 (2010)
424. R. N. Kostoff, J. S. Murday, C. G. Y. Lau, and W. M. Tolles, The seminal literature of nanotechnology research, *J. Nanopart. Res.* 8, 193 (2006)
425. S. H. Tolbert and A. P. Alivisatos, The wurtzite to rock salt structural transformation in CdSe nanocrystals under high pressure, *J. Chem. Phys.* 102(11), 4642 (1995)